AD-A155 973 THE ROLE OF FINITE PARALLEL CONDUCTIVITY AND OTHER CLASSICAL PROCESSES ON . (U) JAYCOR SAN DIEGO CA J L SPERLING ET AL. 26 MAY 84 JAYCOR-J530-84-207/2308 1/2

UNCLASSIFIED DNA-TR-84-196 DNA001-83-C-0150 F/G 20/3 NL

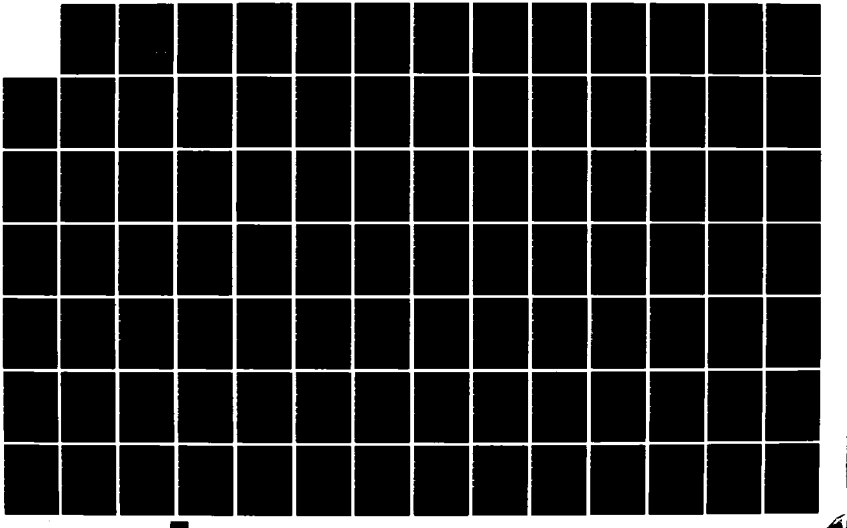

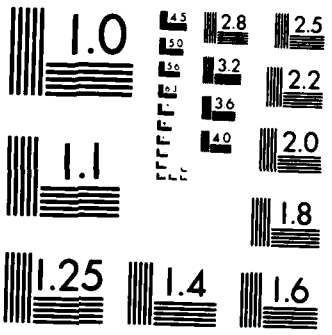

DNA-TR-84-196

THE ROLE OF FINITE PARALLEL CONDUCTIVITY AND OTHER CLASSICAL PROCESSES ON THE EVOLUTION OF HIGH-ALTITUDE PLASMAS

J.L. Sperling
A.J. Glassman
JAYCOR
P.O. Box 85154
San Diego, CA 92138-9259

26 May 1984

Technical Report

CONTRACT No. DNA 001-83-C-0150

THIS WORK WAS SPONSORED BY THE DEFENSE NUCLEAR AGENCY
UNDER RDT&E RMSS CODE B322083466 S99QMXBC00091 H2590D.

Prepared for
Director
DEFENSE NUCLEAR AGENCY
Washington,DC 20305-1000

Destroy this report when it is no longer needed. Do not return to sender.

PLEASE NOTIFY THE DEFENSE NUCLEAR AGENCY, ATTN: STTI, WASHINGTON, DC 20305-1000, IF YOUR ADDRESS IS INCORRECT, IF YOU WISH IT DELETED FROM THE DISTRIBUTION LIST, OR IF THE ADDRESSEE IS NO LONGER EMPLOYED BY YOUR ORGANIZATION.

UNCLASSIFIED

SECURITY CLASSIFICATION OF THIS PAGE (When Data Entered)

REPORT DOCUMENTATION PAGE		READ INSTRUCTIONS BEFORE COMPLETING FORM
1 REPORT NUMBER DNA-TR-84-196	2. GOVT ACCESSION NO. AD-A155973	3 RECIPIENT'S CATALOG NUMBER
4. TITLE (and Subtitle) THE ROLE OF FINITE PARALLEL CONDUCTIVITY AND OTHER CLASSICAL PROCESSES ON THE EVOLUTION OF HIGH-ALTITUDE PLASMAS		5 TYPE OF REPORT & PERIOD COVERED Technical Report 6. PERFORMING ORG. REPORT NUMBER J530-84-207/2308
7. AUTHOR(s) J. L. Sperling A. J. Glassman		8 CONTRACT OR GRANT NUMBER(s) DNA 001-83-C-0150
9. PERFORMING ORGANIZATION NAME AND ADDRESS JAYCOR P.O. Box 85154 San Diego, California 92138-9259		10. PROGRAM ELEMENT, PROJECT TASK AREA & WORK UNIT NUMBERS Task S99QMXBC-00091
11. CONTROLLING OFFICE NAME AND ADDRESS Director Defense Nuclear Agency Washington, DC 20305-1000		12. REPORT DATE 26 May 1984 13. NUMBER OF PAGES 134
14. MONITORING AGENCY NAME & ADDRESS(if different from Controlling Office)		15. SECURITY CLASS. (of this report) UNCLASSIFIED 15a. DECLASSIFICATION DOWNGRADING SCHEDULE N/A since UNCLASSIFIED

16 DISTRIBUTION STATEMENT (of this Report)

Approved for public release; distribution unlimited.

17. DISTRIBUTION STATEMENT (of the abstract entered in Block 20, if different from Report)

18 SUPPLEMENTARY NOTES

This work was sponsored by the Defense Nuclear Agency under RDT&E RMSS Code B322083466 S99QMXBC00091 H2590D.

19 KEY WORDS (Continue on reverse side if necessary and identify by block number)

Finite Parallel Conductivity	Electromagnetic Effects	SCENARIO
Ion Viscosity	Ion-Pedersen Currents	Striations
Ion-Neutral Diffusion	Ion-Polarization Currents	Outer Scale
U-Shaped Curve	MELT	Inner Scale

20 ABSTRACT (Continue on reverse side if necessary and identify by block number)

Theoretical and numerical analyses of high-altitude nuclear plasmas and ionospheric nonnuclear plasmas often make the assumption that the parallel plasma conductivity is infinite. Actually, electron-ion and electron-neutral collisions assure that the classical plasma conductivity is finite, albeit generally much larger than the perpendicular plasma conductivity. This report is divided into three independent chapters, each of which explicitly

DD FORM 1 JAN 73 1473 EDITION OF 1 NOV 65 IS OBSOLETE

UNCLASSIFIED

SECURITY CLASSIFICATION OF THIS PAGE (When Data Entered)

20. ABSTRACT (continued)

demonstrates that the reality of finite parallel conductivity can substantially impact the gross dynamics of high-altitude plasma clouds as well as the structuring of the clouds via Rayleigh-Taylor or gradient-drift mechanisms. Explicit quantitative demonstrations are given for the three-dimensional localization of electric field patterns around plasma clouds and the fact that perpendicular electric fields do not necessarily map between conjugate zones along the geomagnetic field. The results clearly point to the need for reconsidering the assumption of infinite parallel conductivity in theoretical and numerical models of the high-altitude nuclear environment. Although primarily concerned with the role of finite parallel conductivity in the evolution of high-altitude plasmas, the report also illustrates ways that ion-neutral diffusive currents and ion-viscosity can affect the evolution of high-altitude plasmas. The reader who is concerned with the modeling of the high-altitude nuclear environment, is especially referred to the third chapter which includes algebraic algorithms for describing striations in the high-altitude nuclear environment.

SUMMARY

In theoretical and numerical analyses of high-altitude nuclear plasmas and ionospheric nonnuclear plasmas, the assumptions are often made that the parallel plasma conductivity is infinite and that the electron dynamics perpendicular to the magnetic field are governed by E x B motion. These assumptions imply that perpendicular electric fields map perfectly along the magnetic field and that electrons always remain in the same flux tube.

Actually, electron-ion and electron-neutral collisions assure that the classical parallel plasma conductivity is finite, albeit generally much larger than the perpendicular plasma conductivity. This means that perpendicular electric fields do not map perfectly along the magnetic field and that electrons, which are originally in the same flux tube, do not always have to remain in the same flux tube.

The primary purpose of this report is to explicitly demonstrate that the reality of finite parallel conductivity can substantially impact the gross dynamics of high-altitude plasma clouds as well as the structuring of the clouds via Rayleigh-Taylor or gradient-drift mechanisms. Explicit quantitative demonstrations are given for the three-dimensional localization of electric field patterns around plasma clouds and for the fact that perpendicular electric fields do not necessarily map between conjugate points along the geomagnetic field. The results clearly point to the need for reconsidering the assumption of infinite parallel conductivity in theoretical and numerical models of the high-altitude nuclear environment.

A secondary purpose of this report is to illustrate ways that ion-neutral diffusive currents and ion-viscosity can affect the evolution of high-altitude plasmas.

This report is a compilation of three independent chapters, each of which demonstrates that finite parallel conductivity and associated parallel electron currents can directly contribute to the response of ionospheric and magnetospheric plasmas to an applied force. The third chapter should be of special interest to the reader who is concerned with the modeling of the high-altitude

nuclear environment, as the chapter includes algebraic algorithms for describing striations in the high-altitude nuclear environment.

Chapter 1, "On the Response of Three-Dimensional Plasma Clouds to an Applied Force," shows how a three-dimensional plasma cloud responds to an applied current-density field resulting from an applied force. Using a waterbag model for the plasma cloud, it is demonstrated that parallel electron currents reduce both the size of induced perpendicular electric fields and associated E x B velocities when the applied current-density field is perpendicular to the ambient magnetic field. It is suggested that anomalous resistive processes can contribute to the tendency of the backside of plasma clouds to steepen even if the plasma cloud and the surrounding plasma are uniform. Ion viscosity is explicitly demonstrated to create boundary layers near the edges of waterbag plasma clouds. These boundary layers are relatively thin at low altitudes but become increasingly broad at higher altitudes if ion-polarization currents are weak. It is demonstrated that the development of striations can be hindered when ion-neutral diffusive currents contribute to the overall, nondivergent, current-density field. Striation evolution is discussed in terms of a "U-shaped" curve (actually a straight line) which is indicative of the parameter regime when ion-neutral diffusive currents may play an appreciable role in the dynamics of striations and striation "freezing." A parameter, W, is defined as a measure of the size of induced electric fields. Ion-Pedersen, ion-polarization, and parallel-electron resistive currents all contribute to W.

Chapter 2, "The Role of Finite Parallel Length on the Onset of Striations," uses a simple plasma model to show that the finite parallel length of ionospheric plasma clouds plays a role in the delayed formation of striations by tending to reduce the growth rate of striation instabilities. Specifically, if the electron density in the plasma cloud is much larger than the electron density of the background electrons, the length of the plasma cloud enters through the field-line integrated electron density of the cloud. Taking into account the field-line integrated electron density, the onset of appreciable striations is assumed to occur when the growth rate of the striation instabilities is much faster than the rate of change of the bulk plasma. This point is quantified. The finite parallel length of plasma clouds tends to favor the growth of striations with finite rather than with zero perpendicular wave numbers.

Chapter 3, "Late-Time Striation Eigenmodes Along the Geomagnetic Field," derives a second-order linear differential equation for determining the linear eigenmodes of striation (i.e., gradient-drift and Rayleigh-Taylor) instabilities along the geomagnetic field. Eigenvalues (i.e., temporal frequencies in complex space) are determined along with the eigenmodes. The differential equation includes the contribution of two significant physical effects: ion-polarization currents, and inductive electric fields, and is solved for parameters and geometry appropriate to late-time HANE plasmas, as described by MELT. Ion-Pedersen, ion-gravity, and ion-curvature drifts are all considered as possible contributors to the formation of striations at late times. For a specified late-time plasma configuration, striations tend to have a larger scale size, perpendicular to the geomagnetic field, at higher altitudes than at lower altitudes. The ion-Pedersen drift becomes an especially important contributor to the formation of late-time striations with small perpendicular scale size. Electromagnetic effects are shown to be important for modes with smaller perpendicular wave numbers (i.e., $\lesssim 1\ km^{-1}$) and ion-viscosity is important for modes with larger perpendicular wave numbers (i.e., $\gtrsim 4\ km^{-1}$). Analytic criteria are given for the perpendicular wave numbers of the instability at which the real part of the frequency is equal to the growth rate and at which there is complete stabilization. It is argued that the equating of the real part of the frequency and the growth rate gives a meaningful estimate of the perpendicular wave number appropriate to striation "freezing." An algorithm, suitable for implementation in modeling codes, is given for determining the perpendicular wave number at "freezing." Simple empirical estimates for the parallel spatial extent of the striation density fluctuations are also described.

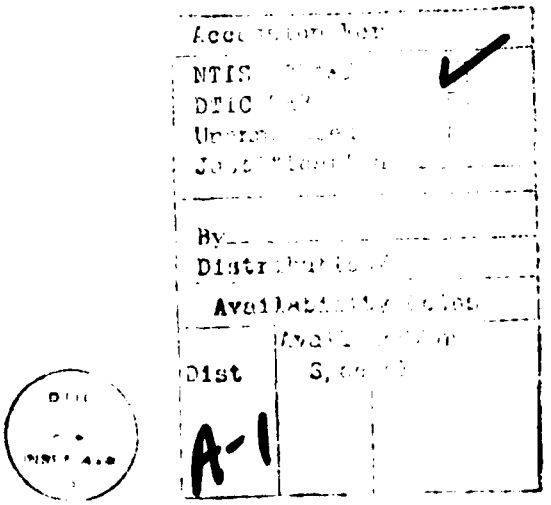

PREFACE

This work has benefitted from discussions with Dr. L. Wittwer of DNA, Dr. C. Prettie of BRA, Dr. R. Kilb and Dr. R. Stagat of MRC, and with Dr. S. Zalesak of NRL. The authors especially appreciate Dr. L. Wittwer's interest and support throughout the course of this work.

TABLE OF CONTENTS

LIST OF ILLUSTRATIONS

LIST OF TABLES

Table 1.2. Examples of expressions for the depolarization coefficients for several different limits.

	$\bar{h}_x(0)$	$\bar{h}_y(0)$	$\bar{h}_z(0)$	Notes
1. $c_t \gg a_t, b_t$ (elliptic cylinder)	$\frac{b_t}{a_t + b_t}$	$\frac{a_t}{a_t + b_t}$	0	
2. $c_t \gg a_t = b_t$ (circular cylinder)	0.5	0.5	0	
3. $b_t \gg a_t, c_t$ (elliptic disk)	$\frac{c_t}{a_t + c_t}$	0	$\frac{a_t}{a_t + c_t}$	
4. $c_t < a_t = b_t$ (oblate spheroid)	μ	μ	λ	$\lambda = \frac{1 + e^2}{e^3}\left[e - \tan^{-1}(e)\right]$; $\mu = 0.5\,(1 - \lambda)$; $e = (a_t^2/c_t^2 - 1)^{0.5}$
5. $c_t > a_t = b_t$ (prolate spheroid)	μ	μ	λ	$\lambda = \frac{1 - e^2}{2e^3}\left[\ln\left(\frac{1 + e}{1 - e}\right) - 2e\right]$; $\mu = 0.5\,(1 - \lambda)$; $e = (1 - a_t^2/c_t^2)^{0.5}$
6. $c_t = a_t = b_t$ (sphere)	1/3	1/3	1/3	

Appendix B uses (1.21a-b) to derive the total electrostatic potential for the case when the external applied force is completely electrostatic. The appendix demonstrates that the magnitude of the total electric field inside the ellipsoid is reduced relative to the value outside the ellipsoid if the appropriate conductivity inside the ellipsoid is larger than the corresponding conductivity outside the ellipsoid. For example, if the external applied electric field is purely x-directed, then $|\sigma_{x<}/\sigma_{x>}| > 1$ is required in order that the electric field inside the ellipsoid be smaller in magnitude than far from the ellipsoid.

The depolarization coefficients [i.e., $\bar{h}_x(0)$, $\bar{h}_y(0)$, and $\bar{h}_z(0)$] satisfy [Landau and Lifshitz, 1960]

$$0 < \bar{h}_x(0) < \bar{h}_y(0) < \bar{h}_z(0) \quad , \tag{1.24}$$

if $a_t > b_t > c_t$ and $s \geq 0$. Moreover [Landau and Lifshitz, 1960],

$$1 = \bar{h}_x(0) + \bar{h}_y(0) + \bar{h}_z(0) \quad , \tag{1.25}$$

and so

$$0 < \bar{h}_x(\xi), \bar{h}_y(\xi), \bar{h}_z(\xi) < 1 \quad . \tag{1.26}$$

It is clearly evident that the depolarization factors strongly affect the size of induced electric fields.

In general, the integrals determining the depolarization coefficients are elliptic and of the second kind [Stratton, 1941]. However, they can be evaluated in terms of more elementary functions in certain limits. Examples are given in Table 1.2.

The first two entries in Table 1.2 correspond to the ellipsoid becoming a long elliptical or circular cylinder u-, v-, w-coordinate system defined by (1.7). The entries agree with previous results for two-dimensional, infinitely long plasma clouds [Linson and Meltz, 1972]. These entries indicate that nonzero $\bar{j}_{oz\gtrless}$ do not generate nonzero electrostatic potentials, $\bar{\Phi}_{\gtrless}$. However, nonzero $\bar{j}_{ox\gtrless}$

In analogy with (1.18)

$$\bar{h}_y(\xi) = \frac{a_t b_t c_t}{2} \int_{\xi}^{\infty} \frac{dr}{(r + b_t^2)^{1.5}(r + a_t^2)^{0.5}(r + c_t^2)^{0.5}} \qquad (1.22a)$$

$$\bar{h}_z(\xi) = \frac{a_t b_t c_t}{2} \int_{\xi}^{\infty} \frac{dr}{(r + c_t^2)^{1.5}(r + a_t^2)^{0.5}(r + b_t^2)^{0.5}} \quad . \qquad (1.22b)$$

The current densities associated with $\bar{\phi}_{\gtrless}$ are

$$\vec{\bar{j}}_< = \frac{\bar{\sigma}_{\perp<}}{\bar{\sigma}_{\perp>}} \frac{(\bar{j}_{ox>} - \bar{j}_{ox<})\bar{h}_x(0)}{1 + \left(\frac{\bar{\sigma}_{\perp<}}{\bar{\sigma}_{\perp>}} - 1\right)\bar{h}_x(0)} + \frac{\bar{\sigma}_{\perp<}}{\bar{\sigma}_{\perp>}} \frac{(\bar{j}_{oy>} - \bar{j}_{oy<})\bar{h}_y(0)}{1 + \left(\frac{\bar{\sigma}_{\perp<}}{\bar{\sigma}_{\perp>}} - 1\right)\bar{h}_y(0)}$$

$$+ \frac{\bar{\sigma}_{z<}}{\bar{\sigma}_{z>}} \frac{(\bar{j}_{oz>} - \bar{j}_{oz<})\bar{h}_z(0)}{1 + \left(\frac{\bar{\sigma}_{z<}}{\bar{\sigma}_{z>}} - 1\right)\bar{h}_z(0)} \quad , \qquad (1.23a)$$

$$\vec{\bar{j}}_> = \frac{(\bar{j}_{ox>} - \bar{j}_{ox<})\bar{h}_x(\xi)}{1 + \left(\frac{\bar{\sigma}_{\perp<}}{\bar{\sigma}_{\perp>}} - 1\right)\bar{h}_x(0)} + \frac{(\bar{j}_{oy>} - \bar{j}_{oy<})\bar{h}_y(\xi)}{1 + \left(\frac{\bar{\sigma}_{\perp<}}{\bar{\sigma}_{\perp>}} - 1\right)\bar{h}_y(0)}$$

$$+ \frac{(\bar{j}_{oz>} - \bar{j}_{oz<})\bar{h}_z(\xi)}{1 + \left(\frac{\bar{\sigma}_{z<}}{\bar{\sigma}_{z>}} - 1\right)\bar{h}_z(0)} \quad . \qquad (1.23b)$$

For $j_{oy} = j_{oz} = 0$, (1.17)-(1.19) give

$$\bar{\phi}_< = \frac{x}{\bar{\sigma}_{\perp>}} \frac{(\bar{j}_{ox<} - \bar{j}_{ox>})\bar{h}_x(0)}{1 + \left(\frac{\bar{\sigma}_{\perp<}}{\bar{\sigma}_{\perp>}} - 1\right)\bar{h}_x(0)} \tag{1.20a}$$

$$\bar{\phi}_> = \frac{x}{\bar{\sigma}_{\perp>}} \frac{(\bar{j}_{ox<} - \bar{j}_{ox>})\bar{h}_x(\xi)}{1 + \left(\frac{\bar{\sigma}_{\perp<}}{\bar{\sigma}_{\perp>}} - 1\right)\bar{h}_x(0)} \quad . \tag{1.20b}$$

For the general case of j_{ox}, j_{oy}, and j_{oz} not equal to zero, symmetry arguments indicate that:

$$\bar{\phi}_< = \frac{x}{\bar{\sigma}_{\perp>}} \frac{(\bar{j}_{ox<} - \bar{j}_{ox>})\bar{h}_x(0)}{1 + \left(\frac{\bar{\sigma}_{\perp<}}{\bar{\sigma}_{\perp>}} - 1\right)\bar{h}_x(0)} + \frac{y}{\bar{\sigma}_{\perp>}} \frac{(\bar{j}_{oy<} - \bar{j}_{oy>})\bar{h}_y(0)}{1 + \left(\frac{\bar{\sigma}_{\perp<}}{\bar{\sigma}_{\perp>}} - 1\right)\bar{h}_y(0)}$$

$$+ \frac{z}{\bar{\sigma}_{z>}} \frac{(\bar{j}_{oz<} - \bar{j}_{oz>})\bar{h}_z(0)}{1 + \left(\frac{\bar{\sigma}_{z<}}{\bar{\sigma}_{z>}} - 1\right)\bar{h}_z(0)} \quad , \tag{1.21a}$$

$$\bar{\phi}_> = \frac{x}{\bar{\sigma}_{\perp>}} \frac{(\bar{j}_{ox<} - \bar{j}_{ox>})\bar{h}_x(\xi)}{1 + \left(\frac{\bar{\sigma}_{\perp<}}{\bar{\sigma}_{\perp>}} - 1\right)\bar{h}_x(0)} + \frac{y}{\bar{\sigma}_{\perp>}} \frac{(\bar{j}_{oy<} - \bar{j}_{oy>})\bar{h}_y(\xi)}{1 + \left(\frac{\bar{\sigma}_{\perp<}}{\bar{\sigma}_{\perp>}} - 1\right)\bar{h}_y(0)}$$

$$+ \frac{z}{\bar{\sigma}_{z>}} \frac{(\bar{j}_{oz<} - \bar{j}_{oz>})\bar{h}_z(\xi)}{1 + \left(\frac{\bar{\sigma}_{z<}}{\bar{\sigma}_{z>}} - 1\right)\bar{h}_z(0)} \quad . \tag{1.21b}$$

$$\bar{\psi}_{o\gtrless} = C_{\gtrless} F(\xi)F(\eta)F(\zeta) \tag{1.15}$$

with

$$C_{\gtrless} = \frac{-\bar{j}_{ox\gtrless}(\bar{\sigma}_{\perp>})^{1/2}}{[(b_t^2 - a_t^2)(c_t^2 - a_t^2)]^{1/2}} \quad , \quad F(\lambda) = (\lambda + a_t^2)^{1/2} \quad . \tag{1.16}$$

The electrostatic potential generated by the ellipsoid is

$$\overline{\phi_<} = C_1 \, F(\xi)F(\eta)F(\zeta) \quad , \tag{1.17a}$$

$$\overline{\phi_>} = C_2 \, F(\xi)F(\eta)F(\zeta)\bar{h}_x(\xi) \quad , \tag{1.17b}$$

with

$$\bar{h}_x(\xi) = \frac{a_t b_t c_t}{2} \int_{\xi}^{\infty} \frac{dr}{(r + a_t^2)^{1.5}(r + b_t^2)^{0.5}(r + c_t^2)^{0.5}} \quad . \tag{1.18}$$

At the surface of the ellipsoid (i.e., $\xi = 0$), the electrostatic potential and the normal component of the current density are both continuous [Stratton, 1941], i.e.,

$$\bar{\Phi}_> \Big|_{\xi=0} = \bar{\Phi}_< \Big|_{\xi=0} \tag{1.19a}$$

$$\left(\frac{\partial \bar{\Phi}_>}{\partial \xi} + \frac{1}{\bar{\sigma}_{\perp>}} \frac{\partial \bar{\psi}_{o>}}{\partial \xi}\right)_{\xi=0} = \left(\frac{\bar{\sigma}_{\perp<}}{\bar{\sigma}_{\perp>}} \frac{\partial \bar{\Phi}_<}{\partial \xi} + \frac{1}{\bar{\sigma}_{\perp>}} \frac{\partial \bar{\psi}_{o<}}{\partial \xi}\right)_{\xi=0} \quad . \tag{1.19b}$$

Equation (1.19b) uses the fact that the appropriate values for the external, applied, current-density field are $j_{ox\gtrless}/\bar{\sigma}_{\perp>}^{0.5}$ in the transformed space defined by the coordinates u, v, and w [Landau and Lifshitz, 1960].

For $\xi \geq -c_t^2$, (1.12) becomes an equation for an ellipsoid. For $-c_t^2 > \eta > -b_t^2$, (1.12) becomes an equation for a hyperboloid of one sheet. For $-b_t^2 > \zeta > -a_t^2$, (1.12) becomes an equation for a hyperboloid of two sheets. In terms of ξ, η, and ζ, the cartesian coordinates u, v, and w are:

$$u = \pm \left[\frac{(\xi + a_t^2)(\eta + a_t^2)(\zeta + a_t^2)}{(b_t^2 - a_t^2)(c_t^2 - a_t^2)} \right]^{1/2} , \tag{1.13a}$$

$$v = \pm \left[\frac{(\xi + b_t^2)(\eta + b_t^2)(\zeta + b_t^2)}{(c_t^2 - b_t^2)(a_t^2 - b_t^2)} \right]^{1/2} , \tag{1.13b}$$

$$w = \pm \left[\frac{(\xi + c_t^2)(\eta + c_t^2)(\zeta + c_t^2)}{(a_t^2 - c_t^2)(b_t^2 - c_t^2)} \right]^{1/2} . \tag{1.13c}$$

It is assumed that the external applied force drives a uniform current-density field, $\vec{j}_o$, both far from the ellipsoid and inside the ellipsoid [Stratton, 1941; Landau and Lifshitz, 1960]:

$$\vec{j}_{o\gtrless} = j_{ox\gtrless}\hat{x} + j_{oy\gtrless}\hat{y} + j_{oz\gtrless}\hat{z} = -\nabla\psi_{o\gtrless} \tag{1.14a}$$

$$\psi_{o\gtrless} = -j_{ox\gtrless}x - j_{oy\gtrless}y - j_{oz\gtrless}z . \tag{1.14b}$$

In (1.14a) the unit vectors in the x-, y-, and z-directions are represented by $\hat{x}$, $\hat{y}$, and $\hat{z}$, respectively. Laplace transformation, (1.5a), permits temporal variations of $\vec{j}_{o\gtrless}$ and $\psi_{o\gtrless}$ to be taken into account.

For the moment the special case, $\vec{j}_{o\gtrless} = j_{ox\gtrless}\hat{x}$ and $\psi_{o\gtrless} = -j_{ox\gtrless}x$, is considered. This simplification is subsequently relaxed using symmetry arguments. With the use of (1.5a) and (1.14a), it is then evident that [Stratton, 1941]

In the transformed coordinates the equation determining the potential for the external plasma is Laplace's equation which is appropriate for determining the electrostatic potential in a vacuum. Equation (1.8b) indicates that the conductivity tensor remains a diagonal tensor with the transformation (1.7), but the elements of the tensor have changed (i.e., $\bar{\sigma}_{x<} \rightarrow \bar{\sigma}_{x<}/\bar{\sigma}_{x>}$, $\bar{\sigma}_{y<} \rightarrow \bar{\sigma}_{y<}/\bar{\sigma}_{y>}$, and $\bar{\sigma}_{z<} \rightarrow \bar{\sigma}_{z<}/\bar{\sigma}_{z>}$).

The surface of the ellipsoid is determined by the equation [Stratton, 1941]:

$$\frac{x^2}{a_0^2} + \frac{y^2}{b_0^2} + \frac{z^2}{c_0^2} = 1 \quad . \tag{1.9}$$

The semiprincipal axes have length a_0, b_0, and c_0. Using (1.7) permits (1.9) to be rewritten as

$$\frac{u^2}{a_t^2} + \frac{v^2}{b_t^2} + \frac{w^2}{c_t^2} = 1 \quad , \tag{1.10}$$

with

$$a_t = a_0/(\bar{\sigma}_{x>})^{1/2} \quad , \quad b_t = b_0/(\bar{\sigma}_{y>})^{1/2} \quad , \quad c_t = c_0/(\bar{\sigma}_{z>})^{1/2} \quad . \tag{1.11}$$

Hence, in the transformed coordinates the plasma cloud is still an ellipsoid but the semiprincipal axes are now a_t, b_t, and c_t.

The exact functional forms for $\phi_<$ and $\phi_>$ can be most directly determined using the ellipsoidal coordinates ξ, η, and ζ [Stratton, 1941; Landau and Lifshitz, 1960]. If $r = \xi$, η, or ζ, then the ellipsoidal coordinates each satisfy the equation

$$\frac{(u)^2}{a_t^2 + r} + \frac{(v)^2}{b_t^2 + r} + \frac{(w)^2}{c_t^2 + r} = 1 \quad . \tag{1.12}$$

$$g = \frac{1}{2\pi i} \int_{s_0-i\infty}^{s_0+i\infty} ds\ \bar{g}\ \exp(st) \quad . \tag{1.5b}$$

In (1.5a-b), g is a function of time and $\bar{g}$ is the Laplace transform. The contour indicated by (1.5b) is to the right of all poles of $\bar{g}$ in the complex plane.

If $\phi_{\gtrless} = 0$ at t = 0, then the application of (1.5a) to (1.4a-b) results in:

$$0 = \left(\bar{\sigma}_{x>} \frac{\partial^2}{\partial x^2} + \bar{\sigma}_{y>} \frac{\partial^2}{\partial y^2} + \bar{\sigma}_{z>} \frac{\partial^2}{\partial z^2} \right) \bar{\phi}_{>} \tag{1.6a}$$

$$0 = \left(\bar{\sigma}_{x<} \frac{\partial^2}{\partial x^2} + \bar{\sigma}_{y<} \frac{\partial^2}{\partial y^2} + \bar{\sigma}_{z<} \frac{\partial^2}{\partial z^2} \right) \bar{\phi}_{<} \quad . \tag{1.6b}$$

Appendix A describes the mathematical forms for σ_x, σ_y, and σ_z used in this paper. The conductivities in the Laplace-transform space (i.e., $\bar{\sigma}_x$, $\bar{\sigma}_y$, and $\bar{\sigma}_z$) are also described in the appendix.

Consider the coordinate transformation on page 62 of Landau and Lifshitz [1960]:

$$u = x/(\bar{\sigma}_{x>})^{1/2} \quad , \quad v = y/(\bar{\sigma}_{y>})^{1/2} \quad , \quad w = z/(\bar{\sigma}_{z>})^{1/2} \quad . \tag{1.7}$$

With (1.7), (1.6a) and (1.6b) can be rewritten as

$$0 = \left(\frac{\partial^2}{\partial u^2} + \frac{\partial^2}{\partial v^2} + \frac{\partial^2}{\partial w^2} \right) \bar{\phi}_{>} \tag{1.8a}$$

$$0 = \left(\frac{\bar{\sigma}_{x<}}{\bar{\sigma}_{x>}} \frac{\partial^2}{\partial u^2} + \frac{\bar{\sigma}_{y<}}{\bar{\sigma}_{y>}} \frac{\partial^2}{\partial v^2} + \frac{\bar{\sigma}_{z<}}{\bar{\sigma}_{z>}} \frac{\partial^2}{\partial w^2} \right) \bar{\phi}_{<} \quad . \tag{1.8b}$$

The electrostatic fields can be determined from the potential, ϕ, through the relation,

$$\vec{E} = -\nabla \phi \quad . \tag{1.1}$$

The potential itself is determined from the constraint that the divergence of the current is equal to zero, i.e.,

$$0 = \nabla \cdot \overleftrightarrow{\sigma} \cdot \nabla \phi \quad , \tag{1.2}$$

where $\overleftrightarrow{\sigma}$ is the conductivity tensor. Throughout this paper, the conductivity tensor is assumed to be diagonal, i.e.,

$$\overleftrightarrow{\sigma} = \begin{pmatrix} \sigma_x & 0 & 0 \\ 0 & \sigma_y & 0 \\ 0 & 0 & \sigma_z \end{pmatrix} \quad . \tag{1.3}$$

Now using the subscript $>(<)$ to denote parameters outside (inside) the ellipsoid permits (1.2) to be written as:

$$0 = \left(\sigma_{x>} \frac{\partial^2}{\partial x^2} + \sigma_{y>} \frac{\partial^2}{\partial y^2} + \sigma_{z>} \frac{\partial^2}{\partial z^2} \right) \phi_> \quad , \tag{1.4a}$$

$$0 = \left(\sigma_{x<} \frac{\partial^2}{\partial x^2} + \sigma_{y<} \frac{\partial^2}{\partial y^2} + \sigma_{z<} \frac{\partial^2}{\partial z^2} \right) \phi_< \quad . \tag{1.4b}$$

The conductivities and potentials in (1.4a-b) may depend on time. The temporal variations can be accounted for by using the technique of Laplace transformation [Spiegel, 1965]:

$$\bar{g} = \int_0^\infty dt \; g \exp(-st) \tag{1.5a}$$

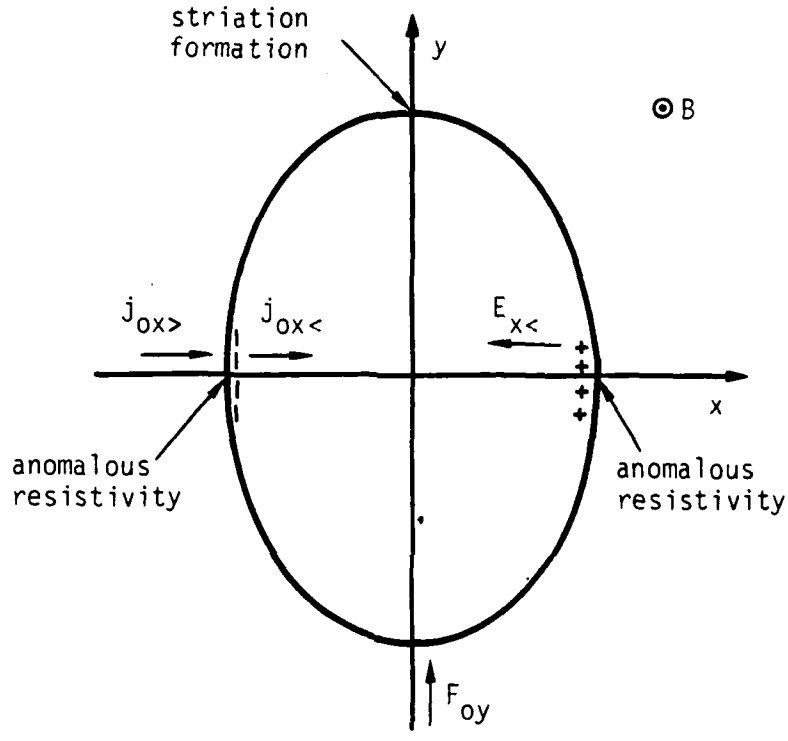

Figure 1.1. Illustration of a planar section of an ellipsoidal plasma cloud. The section is parallel to the x-y plane. The magnetic field is z-directed. For an applied y-directed force, F_{oy}, the associated plasma current densities are $j_{ox\gtrless}$. The induced electric field inside the cloud points in the negative x-direction. The most likely locations for anomalous resistivity and striation formation are also shown.

Table 1.1. Examples of external perpendicular forces appropriate to uniform magnetic fields. Symbols used are: m_i (ion mass), $\vec{g}_\perp$ (perpendicular component of the acceleration of gravity), $\vec{E}_{o\perp}$ (perpendicular electric field), d/dt (derivative with respect to time), ν_{in} (ion-neutral collision frequency), and $\vec{v}_n$ (neutral velocity).

		$\vec{F}_{o\perp}$
1.	Gravity	$m_i \vec{g}_\perp$
2.	Inertia	$m_i \frac{c}{B} \frac{d\vec{E}_{o\perp}}{dt}$
3.	Drag from neutral wind	$m_i \nu_{in} \vec{v}_n$

"freezing." From the mathematical standpoint, the curve is obtained by equating the real and imaginary part of the linear frequency associated with the striation instabilities [Sperling and Glassman, 1983; Sperling, 1983a]. It is shown that the curve obtained in this way is consistent with the observed perpendicular scale sizes of striations. A parameter, W, is defined as a measure of the size of induced electric fields. Striation evolution is discussed from the viewpoint that their existence must be indicative of the elongation and motion of a plasma-cloud material in the direction of an applied perpendicular force.

This chapter is divided in the following way. Using Laplace transforms, section 1.2 derives the induced three-dimensional electrostatic potential resulting from the application of an applied force to a plasma cloud and the surrounding plasma. Ion-Pedersen, ion-polarization, and parallel electron-resistive currents are all considered. Section 1.3 discusses the inverse Laplace transformation of certain equations in section 1.2. Section 1.4 discusses applications to the evolution of plasma clouds and the "U-shaped" curve. Section 1.5 is a summary. Six appendices clarify the discussion in the various sections.

1.2 CALCULATION OF INDUCED ELECTROSTATIC FIELDS

A relatively simple model is used to ascertain the role of three-dimensional effects on the electric fields generated by a plasma cloud in a uniform current field. The electric fields are assumed to be electrostatic and the current-density field is assumed to be the result of an external force (e.g., gravity, drag from neutral wind, ion inertia, curvature of magnetic field lines, etc.) imposed on the plasma cloud and the surrounding plasma. Examples of expressions for the current-densities due to external forces are found in Table 1.1, page 50 of Longmire [1963], and page 673 of Kilb [1977].

The plasma cloud is assumed to have the general configuration of an ellipsoid. All plane sections of an ellipsoid are ellipses or circles. Figure 1.1 is an illustration of a planar section of the ellipsoid parallel to the x-y plane. The plasmas in the interior and the exterior of the ellipsoidal cloud are assumed to both be uniform. The ambient magnetic field is uniform everywhere and z-directed.

Ion viscosity is quantitatively demonstrated to be a process which can affect the development of induced electric fields within plasma clouds when the applied force acts transverse to the magnetic field. Viscosity is an important consideration because the E x B velocities associated with the induced electric fields, can be nonuniform, particularly near the boundary of a plasma cloud. Specifically, it is demonstrated that viscous boundary layers develop near the edge of a waterbag model for a plasma cloud. Because the E x B velocity is nonuniform within the boundary layer, the boundary layer is effectively an ablation layer [Linson and Meltz, 1972]. For steady-state situations, the boundary layer is thinnest at low altitudes where the ion-neutral collision frequency is large, but at high altitudes, where the ion-neutral collision frequency is small, the boundary layer is broad. Hence, a waterbag model may not be appropriate for high-altitude plasma clouds near steady state. However, if ion-polarization currents are significant, thin boundary layers can form at high altitudes, even if the ion-neutral collision frequency is small.

Ion-neutral diffusion can reduce the tendency for induced perpendicular electric fields to form in the ionosphere, if the perpendicular density gradient is such that the ion-neutral diffusive current plays an essential role in the maintenance of *overall, nondivergent, current-density fields.* For the appropriate value of the perpendicular density gradient, it is not necessary to invoke induced electric fields and consequently the presence of an applied force correspondingly does not necessarily result in overall, E x B, plasma motion and elongation in the direction of the applied force. Since the formation of striations is a consequence of the tendency of a plasma cloud to move and elongate in the direction of a force, it can be expected that the development of striations is hindered by ion-neutral diffusion.

Striation evolution has been discussed in terms of the "U-shaped" curve [Linson and Meltz, 1972; McDonald, et al., 1981]. Previous analyses have considered the curve from the viewpoint of direct balance between striation growth and ambipolar diffusion, but this balance is not consistent with the observed perpendicular scale sizes for striations [McDonald, et al., 1981]. In this chapter, the appropriate curve (actually a straight line) is considered to indicate the parameter regime when ion-neutral diffusive currents play an appreciable role in the dynamics of striations and contribute to striation

1. ON THE RESPONSE OF THREE-DIMENSIONAL PLASMA CLOUDS TO AN APPLIED FORCE

1.1 INTRODUCTION

In a magnetized plasma, the application of a force (e.g., gravity, drag from neutral wind, ion inertia, etc.) transverse to the ambient magnetic field results in a current density transverse to both the ambient magnetic field and the force [Longmire, 1963]. Considered by itself, this current density may diverge as it flows through an inhomogeneous plasma. Concomitant charge accumulations result in induced electric fields transverse to the ambient magnetic field. Plasma motion and elongation in the direction of the force are a consequence of the induced electric fields. Indeed, the formation of striations is one way that plasma clouds tend to move and elongate in the direction of a force [Linson and Workman, 1970; Völk and Haerendel, 1971; Perkins, et al., 1973].

This chapter examines the significant contribution of parallel electron currents on the maintenance of overall quasineutrality when an applied force acts on both a plasma cloud and the surrounding plasma. It is explicitly demonstrated that parallel electron currents tend to short-circuit the electrostatic potential when the applied force is perpendicular to the magnetic field. Hence, the induced, perpendicular electric fields, within a plasma cloud, are correspondingly reduced when the self-consistent parallel electron currents are large.

When the self-consistent parallel currents are so large that the associated electron speed is larger than the ion thermal or electron thermal speed, turbulence processes or double layers may develop and tend to retard the currents [Block, 1972; Papadopoulos, 1977; Alfven, 1981]. Under such circumstances, the parallel electron currents are less effective in short-circuiting induced electrostatic potentials. It is demonstrated that the presence of anomalous resistive processes can contribute to the tendency of the backside of ionospheric barium clouds to steepen even if the plasma cloud and the surrounding plasma are initially uniform. The tendency of anomalous resistive processes to be important increases with altitude.

and $\bar{j}_{oy\gtrless}$ may generate nonzero electrostatic potentials, $\bar{\phi}_{\gtrless}$, depending on the precise geometry of the elliptical cylinder. For example, consider $b_t \gg a_t$ then the elliptic cylinder becomes a thin sheet with normal in the x-direction. In this case, $\bar{j}_{ox\gtrless}$ generates a substantial electrostatic field since $h_x(0) \approx 1$. However, $h_y(0) \approx 0$ and so $\bar{j}_{oy\gtrless}$ does not generate a substantial electrostatic field. Evidently, a relatively large surface area normal to the applied current is required for generating an appreciable electrostatic field.

In general, it can be expected that the finite extent of plasma clouds along the magnetic field should have a meaningful effect on the generation of perpendicular electrostatic potentials if $c_t \lesssim a_t, b_t$. Under such circumstances, the ellipsoid in the u-, v-, and w-coordinate system has a relatively short extent along the magnetic field. For $c_t \ll a_t, b_t$,

$$\bar{h}_z(0) \approx \frac{c_t}{2} \int_0^\infty \frac{dr}{(r + c_t^2)^{3/2}} = 1 \quad . \tag{1.27}$$

The combination of (1.25) and (1.27) gives

$$\bar{h}_x(0) = \bar{h}_y(0) = 0 \quad . \tag{1.28}$$

Equations (1.27) and (1.28) are in agreement with entry 3 of Table 1.2 if $c_t \ll a_t, b_t$. It then follows that if $c_t \ll a_t, b_t$, an appreciable electrostatic potential is not generated by nonzero $j_{ox\gtrless}$, $j_{oy\gtrless}$. This is because parallel electron currents play a central role in maintaining overall quasineutrality and tend to short-circuit the potential differences which would arise if perpendicular currents alone were important. However, the presence of nonzero $j_{oz\gtrless}$ may generate an electrostatic field.

In the limit when two of the semiprincipal axes are equal (i.e., $a_t = b_t$, $a_t = c_t$, or $b_t = c_t$) the ellipsoids become spheroids. Specifically, if $c_t < a_t = b_t$ the plasma cloud is an oblate spheroid but if $c_t > a_t = b_t$ the plasma cloud is a prolate spheroid.

Figure 1.2 is a plot of $\bar{h}_x(0)$ and $\bar{h}_z(0)$ for the case of $a_t = b_t$ and entries 4 and 5 in Table 1.2 [Stratton, 1941; Landau and Lifshitz, 1960]. In

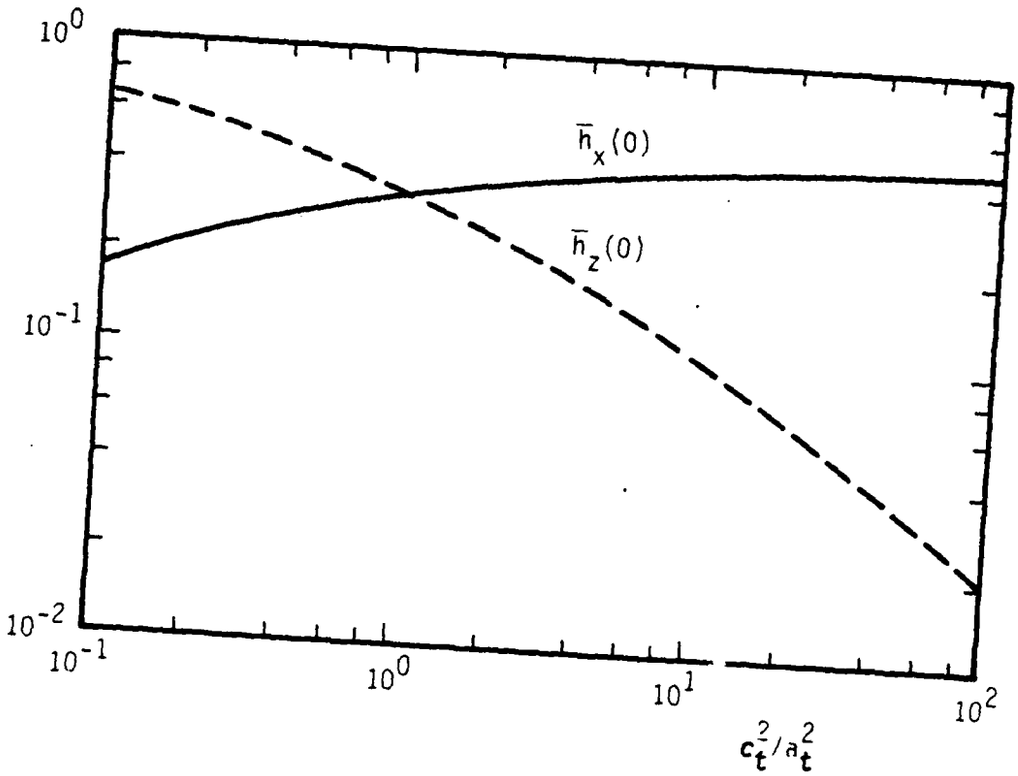

Figure 1.2. $\bar{h}_x(0)$ and $\bar{h}_z(0)$ versus c_t^2/a_t^2 for $a_t = b_t$.

agreement with entry 2 of Table 1.2, $\bar{h}_x(0) \to 0.5$ and $\bar{h}_z(0) \to 0$ as $c_t^2/a_t^2 \to \infty$. Similarly, if $c_t^2/a_t^2 \to 0$ then $\bar{h}_x(0) \to 0$ and $\bar{h}_z(0) \to 1$ in agreement with (1.27), (1.28), and entry 3 of Table 1.2. For $c_t = a_t = b_t$ the spheroid becomes a sphere and entry 6 in Table 1.2 follows directly from symmetry arguments.

Far from the ellipsoid (i.e., $\xi \gg a_t^2, b_t^2, c_t^2$),

$$\xi \to \rho^2 \equiv u^2 + v^2 + w^2 = \frac{x^2 + y^2}{\sigma_{\perp>}} + \frac{z^2}{\sigma_{z>}} \quad , \tag{1.29}$$

and

$$\bar{h}_x(\xi) \approx \bar{h}_y(\xi) \approx \bar{h}_z(\xi) \approx \frac{a_t b_t c_t}{2} \int_{\xi}^{\infty} \frac{dr}{r^{5/2}} \approx \frac{a_t b_t c_t}{3\xi^{3/2}} \quad . \tag{1.30}$$

The combination of (1.21b), (1.29), and (1.30) gives

$$\bar{\phi}_> \approx \frac{a_t b_t c_t}{3\rho^3} \left[\frac{x}{\bar{\sigma}_{\perp>}} \frac{(\bar{j}_{ox<} - \bar{j}_{ox>})}{1 + \left(\frac{\bar{\sigma}_{\perp<}}{\bar{\sigma}_{\perp>}} - 1 \right) \bar{h}_x(0)} + \frac{y}{\bar{\sigma}_{\perp>}} \frac{(\bar{j}_{oy<} - \bar{j}_{oy>})}{1 + \left(\frac{\bar{\sigma}_{\perp<}}{\bar{\sigma}_{\perp>}} - 1 \right) \bar{h}_y(0)} \right.$$

$$\left. + \frac{z}{\sigma_{z>}} \frac{(\bar{j}_{ox<} - \bar{j}_{ox>})}{1 + \left(\frac{\bar{\sigma}_{z<}}{\bar{\sigma}_{z>}} - 1 \right) \bar{h}_z(0)} \right] \quad . \tag{1.31}$$

It is evident from (1.31) that the electrostatic potential has a dipolar character sufficiently far from the ellipsoidal cloud [Landau and Lifshitz, 1960]. The ρ^{-3} dependence indicates a corresponding rapid spatial decay of the electric field.

1.3 INVERSE LAPLACE TRANSFORMATION

To determine the electrostatic potential in real space, the inverse Laplace transformation, (1.5b), can be applied to (1.21a-b). In general, an analytic expression for the inverse transformation cannot be obtained except in certain special limits. The special limits emphasized in this section are $c_t \gg a_t, b_t$ and $c_t \ll a_t = b_t$. It is assumed that $j_{oy\gtrless} = j_{oz\gtrless} = 0$. It is also assumed that $j_{ox\gtrless}$ is constant in time so that

$$\bar{j}_{ox\gtrless} = j_{ox\gtrless} s^{-1} \quad . \tag{1.32}$$

With (1.21a), (1.23a), (1.32), and (A4) of Appendix A, the final-value theorem for Laplace transformations gives [Spiegel, 1965]

$$\phi_< (t \to \infty) = \lim_{s \to 0} (s\bar{\phi}_<) = \frac{x(j_{ox<} - j_{ox>})h_x(0)}{\alpha_> \nu_{in>} + (\alpha_< \nu_{in<} - \alpha_> \nu_{in>})h_x(0)} \quad , \tag{1.33a}$$

$$j_{x<}(t \to \infty) = \lim_{s \to 0} (s\bar{j}_<) = \frac{(j_{ox>} - j_{ox<})\alpha_< \nu_{in<} h_x(0)}{\alpha_> \nu_{in>} + (\alpha_< \nu_{in<} - \alpha_> \nu_{in>})h_x(0)} \quad , \tag{1.33b}$$

with

$$h_x(0) = \int_0^\infty \frac{dr}{\left(r + \frac{a_0^2}{\alpha_> \nu_{in>}}\right)^{3/2} \left(r + \frac{b_0^2}{\alpha_> \nu_{in>}}\right)^{1/2} \left(r + \frac{c_0^2}{\sigma_{z>}}\right)^{1/2}} \quad . \tag{1.34}$$

If $c_t \gg a_t, b_t$, then the ellipsoid becomes a very long elliptical cylinder in the transformed coordinates specified by (1.7). Parallel electron currents do not play a major role in maintaining overall quasineutrality. The combination of (1.21a), (1.32), (A4) of Appendix A, and entry 1 of Table 1.2 gives

$$\bar{\phi}_< = \frac{x}{s} \frac{(j_{ox<} - j_{ox>})b_0}{a_0 \alpha_> (s + \nu_{in>}) + b_0 \alpha_< (s + \nu_{in<})} \quad , \tag{1.35}$$

with $\alpha_{\gtrless}$ determined from (A5) of Appendix A. The combination of (1.5b) and (1.34) gives

$$\phi_< = \frac{xb_0(j_{ox<} - j_{ox>})}{a_0\alpha_>\nu_{in>} + b_0\alpha_<\nu_{in<}}\left[1 - \exp\left(-t\,\frac{\alpha_>\nu_{in>}a_0 + \alpha_<\nu_{in<}b_0}{\alpha_>a_0 + \alpha_<b_0}\right)\right]. \quad (1.36)$$

It follows from (1.36) that

$$\phi_< \xrightarrow[t\to\infty]{} \frac{xb_0(j_{ox<} - j_{ox>})}{a_0\alpha_>\nu_{in>} + b_0\alpha_<\nu_{in<}} \quad . \quad (1.37)$$

If $c_t \ll a_t = b_t$, then the ellipsoid becomes a thin circular disk in the transformed coordinates specified by (1.7). Parallel electron currents play an essential role in maintaining overall quasineutrality and impede the tendency for substantial electrostatic potentials to form. The combination of (1.21a), (1.31), (A4) of Appendix A, and entry 4 of Table 1.2 gives

$$\bar{\phi}_< = \frac{x}{s}\,\frac{(j_{ox<} - j_{ox>})k(s + \nu_{in>})^{1/2}}{\alpha_>(s + \nu_{in>})[1 - k(s + \nu_{in>})^{1/2}] + \alpha_<(s + \nu_{in<})k(s + \nu_{in>})^{1/2}} \quad , (1.38)$$

with

$$k = \frac{\pi}{4}\,\frac{c_0}{a_0}\left(\frac{\alpha_>}{\sigma_{z>}}\right)^{0.5} \quad . \quad (1.39)$$

Equation (1.38) may be rewritten as

$$\bar{\phi}_< = \frac{x}{s}\,\frac{(j_{ox<} - j_{ox>})}{(\alpha_< - \alpha_>)(\lambda_+ - \lambda_-)}\left[\frac{1}{(s + \nu_{in>})^{1/2} - \lambda_+} - \frac{1}{(s + \nu_{in>})^{1/2} - \lambda_-}\right] \quad , \quad (1.40)$$

with

$$\lambda_{\pm} = -\frac{\omega_b}{2} \pm \left(\frac{\omega_b^2}{4} - \omega_c\right) \quad ,$$

$$\omega_b = \frac{1}{k(\alpha_< / \alpha_> - 1)} \quad , \quad \omega_c = \frac{\nu_{in<} - \nu_{in>}}{\alpha_< - \alpha_>} \quad . \tag{1.41}$$

The combination of (1.5b), (1.32), and (1.40) gives [Spiegel, 1965]

$$\Phi_< = \frac{x(j_{ox<} - j_{ox>})}{\alpha_< - \alpha_>} \frac{1}{\lambda_+ - \lambda_-} \left\{ \frac{1}{\lambda_-^2 - \nu_{in>}} \left[\lambda_- + \nu_{in}^{0.5} \operatorname{erf}(\nu_{in}^{0.5} t^{0.5}) \right.\right.$$

$$\left. - \lambda_- \exp(\lambda_-^2 t - \nu_{in>} t) \operatorname{erfc}(-\lambda_- t^{0.5}) \right]$$

$$- \frac{1}{\lambda_+^2 - \nu_{in>}} \left[\lambda_+ + \nu_{in>}^{0.5} \operatorname{erf}(\nu_{in}^{0.5} t^{0.5}) \right.$$

$$\left.\left. - \lambda_+ \exp(\lambda_+^2 t - \nu_{in>} t) \operatorname{erfc}(-\lambda_+ t^{0.5}) \right] \right\} \quad . \tag{1.42}$$

Now if $\nu_{in\gtrless} \ll \sigma_{z>}$ then

$$\lambda_+ \approx \frac{\pi}{4} \frac{(\nu_{in>} - \nu_{in<})}{(\alpha_> \sigma_{z>})^{0.5}} \quad , \tag{1.43a}$$

$$\lambda_- \approx \frac{4}{\pi} \frac{a_0}{c_0} \left(\frac{\sigma_{z>}}{\alpha_>}\right)^{0.5} \frac{1}{1 - \alpha_< / \alpha_>} \quad . \tag{1.43b}$$

Furthermore, if $|\lambda_+| \ll \nu_{in>}$ and $\alpha_</\alpha_> > 1$ then $\lambda_- < 0$. It then follows that $\phi_<$ has the following form for $t \gg \nu_{in>}$:

$$\phi_< \sim \frac{\pi}{4} \frac{c_0}{a_0} \frac{x(j_{ox<} - j_{ox>})}{(\alpha_> \sigma_{z>} \nu_{in>})^{0.5}} \quad . \tag{1.44}$$

When neutrals are sparse and $\nu_{in>}$ becomes very small, then $|\phi_<|$ can tend to become large. However, a large value for the parallel conductivity counteracts the formation of large electrostatic potentials by providing a mechanism for short-circuiting.

For $c_t \ll a_t = b_t$, the maximum magnitude for the steady-state parallel electron current on the surface of the ellipsoid is determined from Appendix C to be

$$|j_{z>,max}| \approx \frac{|j_{ox<} - j_{ox>}|}{2} \left(\frac{\sigma_{z>}}{\alpha_> \nu_{in>}}\right)^{0.5} \quad . \tag{1.45}$$

This expression assumes that $j_{oy\gtrless} = j_{oz\gtrless} = 0$. The maximum parallel electron speed corresponding to (1.45) is

$$|v_{z>,max}| \equiv \left|\frac{j_{z>,max}}{en_>}\right| \approx \frac{|j_{ox<} - j_{ox>}|}{2en_>} \left(\frac{\sigma_{z>}}{\alpha_> \nu_{in>}}\right)^{0.5} \quad . \tag{1.46}$$

It is evident from (1.46) that $|v_{z>,max}|$ diverges for $\sigma_{z>} \to \infty$ and $\nu_{in>} \to 0$.

If $c_t \ll a_t, b_t$ then parallel electron currents are important and tend to reduce the effective value of $|\phi_{\gtrless}|$. However, it follows that if parallel electron currents are an essential component of the total current system, including the plasma cloud, then the parallel currents may be sufficiently large to generate turbulence or double layers [Block, 1972; Papadopoulos, 1977; Alfven, 1981]. Since parallel conductivity is effectively decreased by turbulence and double layers, it follows that parallel currents are correspondingly decreased and less able to contribute to the overall current systems. An increase in the magnitude of $|\phi_{\gtrless}|$ is also implied.

If the effective parallel conductivity is reduced by plasma processes (e.g., turbulence or double layers), (1.46) correctly demonstrates that there is a corresponding reduction in the parallel electron velocity, the free-energy source responsible for the turbulence and double layers. Equations (1.45) and (1.46) also show that small values for the magnitude of the perpendicular conductivity tend to increase the likelihood of large parallel electron current densities and velocities. This is a consequence of perpendicular current densities being unable to maintain nondivergent current-density fields by themselves. Hence, parallel currents must contribute in a substantial way to the maintenance of overall quasineutrality. The tendency for large parallel electron velocities to occur is clearly increased if $|j_{ox<}| \gg |j_{ox>}|$ and if the electron density is much larger inside the plasma cloud than outside the cloud.

Up to now it has been assumed that perpendicular current densities, associated with a plasma cloud and divergent $\vec{j}_o$, are of the ion-Pedersen or ion-polarization types. However, ion viscosity (cf. Appendix D) and ion-neutral diffusion (cf. Appendix E) may also contribute to the maintenance of overall current-density fields which are nondivergent. Appendix D points out that ion viscosity permits large perpendicular gradients, at lower altitudes in the ionosphere where ion-neutral collisions occur at a relatively rapid rate. At higher altitudes where ion-neutral collisions are negligible, ion viscosity still permits the formation of sharp perpendicular density gradients if ion-polarization currents are sufficiently strong. Appendix E shows that a particular value for the perpendicular density profile within a one-dimensional plasma cloud permits ion-neutral diffusive currents to contribute to overall nondivergent current-density fields without requiring the formation of electric fields. Appendix E also shows that the required scale size of the perpendicular density gradient is consistent with the observed scale size of "frozen" striations.

1.4 APPLICATION TO THE EVOLUTION OF PLASMA CLOUDS AND THE "U-SHAPED" CURVE

With the application of a force, a plasma cloud responds in two ways. First, the cloud tends to polarize in such a way that the motion of the cloud minimizes the force in the cloud frame of reference. For example, in the ionosphere, a plasma cloud would try to move at the neutral velocity as a result

of ion-neutral drag. Analogously, in a nondissipative medium, a plasma cloud would tend to accelerate in accordance with the gravitational force. Second, plasma clouds deform through elongation in the direction of an applied force. In this way the surface area projecting in the direction of a force is minimized and the cloud becomes aligned in the direction of the applied force.

Figure 1.1 illustrates a planar section of a three-dimensional ellipsoidal plasma cloud parallel to the z = 0 plane. Assume that the electron density within the plasma cloud is constant and that a force is applied in the y-direction. As shown in Figure 1.1, the associated current-density field is in the x-direction for ambient magnetic field pointing out of the paper. The induced electric field within the plasma cloud points in the negative x-direction and so the reasonable result is obtained that the associated E x B velocity and the applied force both point in the positive y-direction.

If the volume of the plasma cloud remains fixed, it is evident from the discussion in section 1.3 and the entries in Table 1.2, that an increase in the ratio, b_t/a_t, implies elongation in the direction of an applied, y-directed force. Moreover, larger values for the ratios, c_t/a_t and c_t/b_t, indicate a reduction in the short-circuiting involving parallel electron currents and also indicate that a larger surface area projects in the direction of the current-density field associated with an applied, y-directed force. Elongation of a plasma cloud along the magnetic field or anomalous resistivity both can contribute to larger values for c_t. As b_t and c_t increase relative to a_t, larger values for $h_x(0)$ are implied and so both the induced electric field inside the plasma cloud as well as the associated y-directed E x B velocity both correspondingly increase. If the volume of the plasma cloud remains fixed and the electron density remains uniform, continued acceleration of the plasma cloud in the direction of an applied force can be expected to continue until $\bar{h}_x(0) = 1$ (i.e., $c_t \gg b_t \gg a_t$). When $\bar{h}_x(0) \approx 1$ further elongation and acceleration of material in a plasma cloud can occur only if local density enhancements develop which effectively increase the local value of the perpendicular conductivity within the cloud material. Induced electric fields should be correspondingly larger at the locations of these density enhancements.

In order for the overall current-density field to be nondivergent, it is immediately evident from Figure 1.1 that the induced parallel electron current

density must be largest near the two points where the surface of the ellipsoid intersects the x-axis. For $c_t^2/a_t^2 \ll 1$ [e.g., c_0 = 10 km, a_0 = 2 km, and $(\sigma_{z>}/\alpha_{>}\nu_{in>})$ = 1 x 10^6], (1.45) provides an estimate for the magnitude of this parallel electron current and (1.46) provides the corresponding estimate for the parallel electron speed. For representative ionospheric conditions at 200 km and 400 km altitude as illustrated by Goldman et al. [1976], Table 1.3 quantifies (1.46). The table shows that the parallel electron speed can exceed the ion thermal speed both at 200 km and 400 km altitude. In fact, the parallel electron speed is especially large at an altitude of 200 km where it may even exceed the electron thermal velocity. This suggests that anomalous resistive effects (e.g., turbulence and double layers) [Block, 1972; Papadopoulos, 1977; Alfven, 1981] can play an important role in the dynamics of the plasma cloud by effectively decreasing the parallel electron conductivity of the external plasma near the locations where the plasma cloud intersects the x-axis in Figure 1.1. At these locations, parallel electron current densities are less able to contribute to overall nondivergent current-density fields than locations away from the x-axis. (By contrast the discussion of sections 1.2 and 1.3 assumed that the parallel conductivity is the same everywhere outside the plasma cloud.) Consequently, inside the cloud, the induced electric fields and the associated induced current densities must be larger near y = 0 than away from y = 0. The attendant E x B velocity is also largest near y = 0. It follows that the density of the cloud cannot remain constant but must tend to become larger for y > 0 rather than y < 0. There is steepening of the density profile for y > 0, the backside of the cloud, and the density profile becomes less steep for y < 0, the frontside of the cloud. In short, turbulence and double layers can contribute to observed steepening and accumulations of density on the backside of plasma clouds (and also striations) by permitting inhomogeneous E x B velocities within the plasma cloud. Localized anomalous resistivity is a mechanism for breaking symmetry in a plasma cloud and permitting an initially uniform plasma cloud to become nonuniform.

The formation of striations is the oft observed way that plasma clouds tend to accelerate and elongate in the direction of an applied force. The approximate location where striations form is illustrated in Figure 1.1. When striations form, it can be expected that their perpendicular surfaces would tend to be tangent to an applied perpendicular force so that the surface area

Table 1.3. $|v_{z>,max}|$ as determined from (1.46) for altitudes of 200 and 400 km. It is assumed that the applied force is electrostatic and that $cE_{ox}/B = 1 \times 10^4$ cm/s. All perpendicular plasma currents are of the ion-Pedersen type. Plasma and neutral parameters are determined from Figures 2-4 of Goldman et al. [1976] for solar minimum and solar maximum conditions. For an ion atomic mass of 16 and $T_i = T_e = 0.1$ eV, the ion and electron thermal speeds are 7.7×10^4 cm/s and 1.3×10^7 cm/s, respectively. It is assumed that $n_</n_>$ is 1×10^3 and 10 for altitudes of 200 km and 400 km, respectively.

Altitude (km)	200	400
$\|v_{z>,max}\|$ (cm/s) solar minimum	1.6×10^8	8.5×10^4
$\|v_{z>,max}\|$ (cm/s) solar maximum	1.5×10^8	1.6×10^5

projecting in the direction of the force is minimized (see Figure 1.3). Striations tend to be aligned in the direction of the applied force. A completely consistent picture is obtained if the induced electric fields tend to be normal to the applied force and to the perpendicular surfaces of the striations. With this configuration bulk plasma motion occurs in the direction of the applied force in agreement with Prettie et al. [1983] and not in the direction of the induced electric fields. Hence, striations cannot easily separate from one another and they appear to move in unison in the E x B direction [McDonald et al., 1981]. If the direction of the applied force should change, from the initial form indicated in Figure 1.3, then the plasma would tend to change from the configuration shown in Figure 1.3 to a new configuration which is aligned in the new direction of the applied force. New striations may develop as the new configuration is attained.

The purpose of the rest of this section is to explicitly demonstrate additional ways that three-dimensional effects contribute to the evolution of plasma clouds and the interpretation of the evolution using the "U-shaped" curve [Linson and Meltz, 1972; McDonald et al, 1981]. Steady-state and temporally varying situations are discussed consecutively. For simplicity, it is assumed that $j_{oy\gtrless} = j_{oz\gtrless} = 0$.

a. Steady State

If j_{ox} is a result of ion-Pedersen drifts, then

$$\frac{j_{ox>}}{\alpha_{>}\nu_{in>}} = \frac{j_{ox<}}{\alpha_{<}\nu_{in<}} \quad . \tag{1.47}$$

The combination of (1.33b) and (1.47) gives the total x-directed plasma current within the ellipsoidal plasma cloud:

$$j_{x<,tot} = j_{x<} + j_{ox<} = \frac{j_{ox<}}{1 + (M_0 - 1)h_x(0)} \quad , \tag{1.48}$$

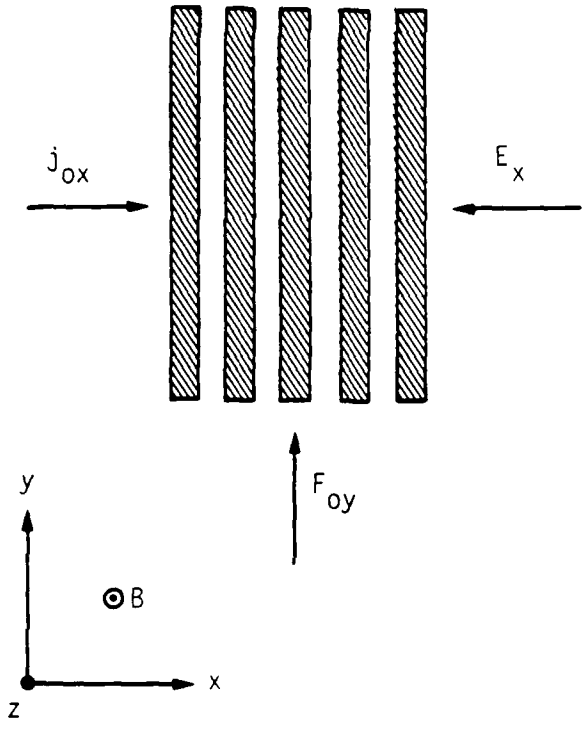

Figure 1.3. Schematic illustrating the tendency of striation sheets to be aligned in the direction of the applied force, F_{oy}. The induced electric field points in the negative x-direction. E x B motion neither directly alters the thickness of striations nor their separation.

with M_0 being the ratio of local plasma conductivities, i.e.,

$$M_0 = \frac{\alpha_< \nu_{in<}}{\alpha_> \nu_{in>}} \quad . \tag{1.49}$$

The geometry of the plasma cloud contributes to (1.48) through the depolarization factor, $h_x(0)$.

Two-dimensional analyses of striation evolution in barium clouds often use field-line integration of Pedersen conductivity to take the distribution of plasma, along the geomagnetic field, into account [Linson and Meltz, 1972; McDonald et al., 1981; Prettie et al., 1983]. Appendix F shows that the concept of field-line integration is appropriate, to within a factor of order unity, when c_t, $a_t \ll b_t$ or $c_t \ll a_t = b_t$ but is not appropriate to $c_t \sim a_t$ or b_t.

Now two-dimensional studies and entry 2 of Table 1.2 give [Linson and Meltz, 1972; Overman et al., 1983]

$$\frac{j_{x<,tot}}{j_{ox}} = \frac{2}{1 + M_0} \quad , \tag{1.50}$$

for an infinitely long circular cylinder. By analogy define a parameter W such that

$$\frac{j_{x<,tot}}{j_{ox<}} = \frac{2}{1 + W} = \frac{1}{1 + (M_0 - 1)h_x(0)} \quad . \tag{1.51}$$

It then follows that

$$W = 1 + 2(M_0 - 1)h_x(0) \quad . \tag{1.52}$$

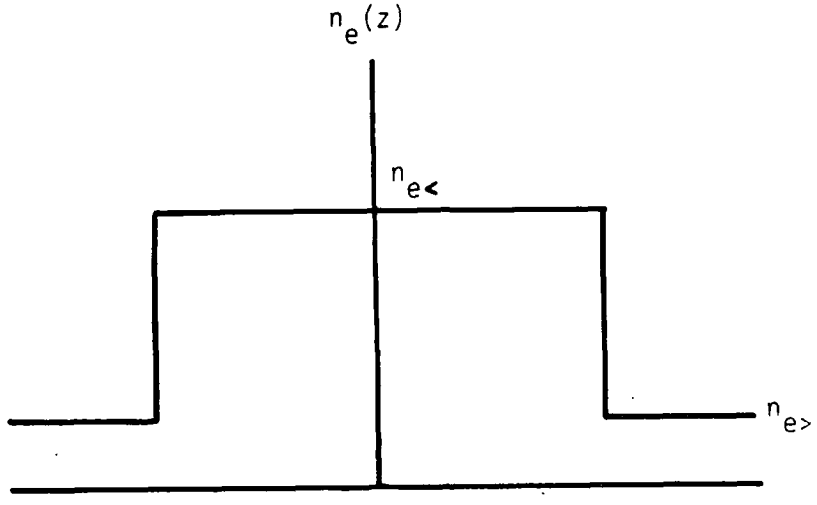

Figure 2.1. Model for plasma density used in the calculation of eigenmodes.

the case in the ionosphere [Goldman and Sperling, 1982]. Third, parallel electric fields can be mainly inductive, mainly electrostatic, or both inductive and electrostatic. The inductive contribution to the electric fields implies modal magnetic fields orthogonal to the ambient magnetic field.

Artificial plasma clouds in the ionosphere have a finite spatial extent that can influence the development and properties of plasma instabilities. In this chapter, particular emphasis is placed on determining certain effects on the Rayleigh-Taylor and E x B-gradient-drift class of instabilities resulting from the finite length of plasma clouds along the geomagnetic field. The theory is applied to the onset of striations in barium clouds.

It is demonstrated, with a rather simple plasma geometry, that finite plasma length implies parallel modal currents and parallel modal electric fields which contribute to the development of eigenmode structure along the geomagnetic field. Specifically, the finite field-line integrated electron density of ionospheric plasma clouds plays a role in the delayed formation of striations by tending to reduce the growth rate of striation instabilities. Taking into account the field-line integrated electron density, the onset of appreciable striations is assumed to occur when the growth rate of the striation instabilities is much faster than the rate of change of the bulk plasma. This point is subsequently quantified. The finite parallel length of ionospheric plasma clouds tends to favor the growth of striations with finite rather than with zero perpendicular wave numbers.

In section 2.2, the calculation model and its implications are detailed. Section 2.3 describes the quantitative evaluation of the model for parameters appropriate to barium releases. Concluding remarks are given in section 2.4.

2.2 CALCULATION MODEL

The plasma model is very similar to the one used in Sperling [1983c] to study the effect of finite parallel length on the loss-cone instability hypothesized to be responsible for prompt striations. The finite extent of the unstable plasma cloud is approximated by assuming that it is localized to $|z| \leq z_0$ (see Figure 2.1). Here z is the coordinate along the constant magnetic field, $\vec{B}$, and z_0 is a positive constant. The plasma for $|z| \leq z_0$ has a perpendicular density-gradient scale length, $L_\perp$, but the plasma for $|z| > z_0$ is

2. THE ROLE OF FINITE PARALLEL LENGTH ON THE ONSET OF STRIATIONS

2.1 INTRODUCTION

In the disturbed ionosphere, Rayleigh-Taylor [Scannapieco and Ossakow, 1976; Ott, 1978; Ossakow et al., 1979; Zalesak and Ossakow, 1980] and E x B gradient drift instabilities [Simon, 1963; Linson and Workman, 1970; McDonald et al., 1980, 1981] are considered to be primary sources for fluid structuring. These instabilities are predicted to be aligned along magnetic field lines with the result that analysis and numerical simulation has emphasized the flute approximation, which neglects the explicit dependence of modes on the coordinate parallel to the ambient magnetic field. Plasma and magnetic field variations in the direction of the magnetic field, when considered, have been taken into account, in a gross sense, by averaging plasma parameters over magnetic field lines, but without considering the implications on the ionosphere of accompanying modal variation along magnetic field lines. One exception to this generality is the paper by Goldman et al. [1976], which calculates eigenmodes in the electrostatic approximation, recognizing that modes must vary along the magnetic field lines as one moves away from the source of instability, an artificial plasma cloud.

The zero electron mass approximation is often made in the theoretical analysis of plasma oscillations for frequencies below the lower-hybrid frequency because it is both convenient and simplifying. In combination with the electrostatic approximation, the zero electron-mass approximation implies that magnetic field lines are equipotentials and that modes have a flutelike character. However, the approximation of zero electron mass is inconsistent with the observation of parallel electric fields in many plasmas, and precludes consideration of a number of associated possible effects. First, although often much smaller than other electric field components, parallel electric fields can contribute in a most significant way to the properties and structure of eigenmodes [Allis et al., 1963; Paoloni, 1975; Sperling, 1982a]. Second, parallel electric fields can result in the transfer of energy and momentum between the mode and parallel electron or ion motion. Depending on circumstances, this coupling can be collisionless [Stix, 1962] or collisional, as often

turbulence or double layers may develop [Block, 1972; Papadopoulos, 1977; Alfven, 1981]. As a result, the tendency of parallel electron currents to contribute overall current patterns can then be reduced. It is suggested that this anomalous resistivity contributes to the breaking of symmetry, even in the idealized plasma model considered in section 1.2. As a result, the anomalous resistivity contributes to the steepening of the backside of plasma clouds.

Ion viscosity and ion-neutral diffusion can effect the formation of induced electric fields when an applied perpendicular force acts on both a plasma cloud and the surrounding plasma. For steady-state situations and when the ion-neutral collision frequency is large, viscous boundary layers develop near the edge of the plasma cloud. For a barium cloud at an altitude of 200 km, the boundary layer can be approximately 2×10^3 cm thick. Ion-neutral diffusive currents can reduce the size of the induced electric fields required to maintain overall nondivergent current-density fields. Indeed, no induced electric fields are required if the density profile inside a plasma cloud has the form indicated in Appendix E.

Striation evolution has been discussed in terms of the "U-shaped" curve [Linson and Meltz, 1972; McDonald et al., 1981]. In the present chapter, the curve (actually a straight line) is considered to indicate the parameter regime when ion-neutral diffusive currents can play an appreciable role in the dynamics of striations and contribute to striation "freezing" [Sperling and Glassman, 1983; Sperling, 1983a]. A parameter, W, is defined as a measure of the size of induced electric field. Striation evolution is discussed from the premise that their existence must represent the means whereby a plasma cloud elongates and moves in the direction of an applied force.

the combination of (1.62)-(1.64) gives

$$W = 2\left\{1 + \frac{b_0 M_0(\lambda_1 - 1)}{a_0 + b_0 M_0}\left[1 - \exp\left(-t\nu_{in>}\frac{a_0 + b_0 M_0}{a_0 + b_0\lambda_2}\right)\right]\right.$$

$$\left. + \frac{b_0\lambda_2(\lambda_1 - 1)}{a_0 + b_0\lambda_2}\exp\left(-t\nu_{in>}\frac{a_0 + b_0 M_0}{a_0 + b_0\lambda_2}\right)\right\}^{-1} - 1 \quad . \qquad (1.65)$$

If (1.47) is valid then $\lambda_1 = M_0^{-1}$. It is evident from (1.65) that steady-state values for W are attained after several ion-neutral collision times (i.e., $\nu_{in>}t$ and $\nu_{in<}t \gtrsim 1$).

As altitude increases, the ion-neutral collision frequency decreases and so discrete plasma structures should be able to accelerate for longer periods of time at higher altitudes than at lower altitudes where ion-neutral collisions can rapidly retard plasma motion [Scholer, 1970; Sperling, 1983b]. Indeed, during a magnetospheric barium release striations were observed to accelerate over periods of several minutes [Mende, 1973]. It was suggested by Mende [1973] that electromagnetic effects, not considered in this chapter, can contribute to the eventual breaking of the acceleration at high altitude.

1.5 SUMMARY

A very general, three-dimensional ellipsoidal model for plasma clouds has been used to explicitly determine the significant role of parallel conductivity and self-consistent parallel electron currents on the formation of induced electric fields when an applied force acts upon the plasma cloud and the surrounding plasma. Field-line integration is not required for the analysis but the results (see Appendix F) do indicate the parameter regime where field-line integration is approximately appropriate.

Self-consistent parallel electron currents in the three-dimensional configuration may tend to be so large that the associated parallel electron velocities may exceed the ion-thermal or even the electron-thermal speed and so

Both ion-Pedersen and ion-polarization currents contribute to (1.59). The total x-directed current density in the plasma cloud is

$$j_{x<,tot} = j_{ox<} + j_{x<} \quad . \tag{1.60}$$

If in analogy to (1.51) a parameter W is defined such that

$$\frac{j_{x<,tot}}{j_{ox<}} \equiv \frac{2}{1 + W} \quad , \tag{1.61}$$

then the combination of (1.59) and (1.60) gives

$$W = \frac{2}{1 + \frac{\alpha_<}{2\pi i}(\nu_{in<} + \frac{\partial}{\partial t}) \int_{s_0-i\infty}^{s_0+i\infty} ds \frac{\left[(\bar{j}_{ox>}/\bar{j}_{ox<}) - 1\right]\bar{h}_x(0)}{\bar{\sigma}_{\perp>} + (\bar{\sigma}_{\perp<} - \bar{\sigma}_{\perp>})\bar{h}_x(0)}} - 1 \quad . \tag{1.62}$$

By permitting temporal variations, the parameter W has been given a more general form than indicated by (1.52).

The limit of two-dimensional plasma clouds (i.e., $c_t \gg a_t, b_t$) yields the simplest example for the application of (1.62). Equations (1.36) and (1.59) then give

$$j_{x<} = \frac{-b_0\alpha_<\nu_{in<}(j_{ox<} - j_{ox>})}{a_0\alpha_>\nu_{in>} + b_0\alpha_<\nu_{in<}} \left[1 - \exp\left(-t\,\frac{a_0\alpha_>\nu_{in>} + b_0\alpha_<\nu_{in<}}{a_0\alpha_> + b_0\alpha_<}\right)\right]$$

$$- \frac{b_0\alpha_<(j_{ox<} - j_{ox>})}{a_0\alpha_> + b_0\alpha_<} \exp\left(-t\,\frac{a_0\alpha_>\nu_{in>} + b_0\alpha_<\nu_{in<}}{a_0\alpha_> + b_0\alpha_<}\right) \quad . \tag{1.63}$$

Equation (1.63) implies (1.48) in the limit of $t \to \infty$ and $h_x(0) = b_0/(a_0 + b_0)$ as suggested by entry 1 of Table 1.2. With the definitions

$$\lambda_1 \equiv \frac{j_{ox>}}{j_{ox<}} \quad , \quad \lambda_2 \equiv \frac{\alpha_<}{\alpha_>} \quad , \tag{1.64}$$

Table 1.4. W and $2/(W + 1)$ for $c/a = 5$, $\sigma_{z>}/\alpha_{>}\nu_{in>} = 1 \times 10^6$, and various values of M_0. The plasma cloud is assumed to be a spheroid with symmetry transverse to the magnetic field.

M_0	W	$\frac{2}{W + 1}$
1	1.00	1.00
5	1.03	0.99
10	1.07	0.97
100	1.77	0.72
1000	8.79	0.20

calculated. The results are shown in Table 1.4. It is evident from the table that parallel electron currents substantially contribute to overall quasi-neutrality and reduce the contribution of induced Pedersen currents to the total perpendicular current in the ellipsoidal plasma cloud. For $M_0 = 100$, $cE_{ox}/B = 1 \times 10^4$ cm/s, and T_i (ion temperature) = 0.1 eV, then (1.55) and Table 1.4 give $k_t = 0.2$ km. The corresponding wavelength is $2\pi/k_t = 0.3$ km. This wavelength is consistent with the perpendicular scale sizes of "frozen" striations [Linson and Meltz, 1972].

Now Linson and Meltz [1972] invoke parallel electron currents and coupling to conjugate zones in order to account for the observed motion of unstriated barium-ion clouds. Effectively, this permits N_c/N_0 (i.e., the ratio of height-integrated cloud to ambient electron densities) to be decreased relative to the situation when parallel electron currents and coupling to conjugate zones is neglected. Now $N_c/N_0 \lesssim 10$ when parallel electron currents and coupling are considered by Linson and Meltz [1972]. If N_c/N_0 is identified with W in (1.53) then good qualitative agreement is obtained between Linson and Meltz [1972] and Table 1.4 (i.e., $W \lesssim 10$) even though Linson and Meltz [1972] do not explicitly include finite parallel conductivity in their expressions and this present paper does not consider an inhomogeneous background ionosphere. Evidently, parallel electron currents play an essential role in the dynamics of ionospheric barium clouds by substantially reducing the magnitude of induced perpendicular electric fields in the clouds.

b. Temporal Variations

In the most general sense, including temporal variations of external currents and induced electric fields, the induced x-directed current within the plasma cloud is determined from (1.5b), (1.23a), and (A4) of Appendix A to be

$$j_{x<} = \frac{\alpha_<}{2\pi i}\left(\nu_{in<} + \frac{d}{dt}\right)\int_{s_0-i\infty}^{s_0+i\infty} ds\, \frac{(\bar{j}_{ox>} - \bar{j}_{ox<})\bar{h}_x(0)}{\bar{\sigma}_{\perp>} + (\bar{\sigma}_{\perp<} - \bar{\sigma}_{\perp>})\bar{h}_x(0)} \quad . \quad (1.59)$$

ambient ions. Equation (1.58) differs from the previously hypothesized view that striation "freezing" indicates the balance between bifurcation and cross-field diffusion [McDonald, et al., 1981; Vesecky, et al., 1980]. In contrast to the earlier hypothesis, enhancements in the cross-field diffusion need not be invoked in the derivation of (1.58) and so with (1.58) one can easily account for the long-term persistence of striations. Moreover, when (1.58) is satisfied, ion velocities and ion-viscous forces are both minimized within the bulk of a striation.

Figure 1.5 suggests that the formation of striations can proceed if plasma condition corresponds to points above the curve. This is illustrated by trajectory a in the figure. Conversely, the formation of striations is not likely to proceed for plasma conditions corresponding to points below the curve in Figure 1.5. However, for these plasma conditions it still can be hypothesized that plasma processes like ion-neutral diffusion may tend to move the total plasma condition along trajectory b. A key point regarding both trajectories a and b is that the value of W, attained once the curve is reached, must be larger than the initial value for W. This is consistent with the idea that the formation of striations must be a manifestation of the elongation and deformation of a plasma cloud in response to an applied force. Once the conditions of the plasma cloud are such that a point on the curve in Figure 1.5 is reached, it is assumed that the plasma condition is such as to remain on the curve. Further bifurcation is not possible since an increase in W is inconsistent with a smaller value of $\bar{L}$, as indicated by trajectory c in Figure 1.5. Hence, striations are "frozen." Ambipolar diffusion, ablation, recombination, and etc. decrease W over the long term and consequently slowly cause the plasma state to go along trajectory d in Figure 1.5. The perpendicular scale size of striations slowly decreases along this trajectory. From the standpoint of power spectral densities, the outer scale length (i.e., k_t^{-1}) approaches the inner scale length [e.g., κ_z^{-1} in (D9) of Appendix D] [Vesecky et al., 1980].

At a time of roughly ten minutes after release at approximately 200 km altitude might reasonably be expected to have a length ~ 20 km along the magnetic field and a radius ~ 2 km transverse to the magnetic field [Linson and Baxter, 1977]. Hence, $c/a \sim 5$. If $\sigma_{z>}/\alpha_{>}\nu_{in>} \sim 1 \times 10^6$ then $c_t^2/a_t^2 = 2.5 \times 10^{-5}$. For a spheroidal plasma cloud, entry 4 of Table 1.2 then permits W and $2/(W + 1)$ to be

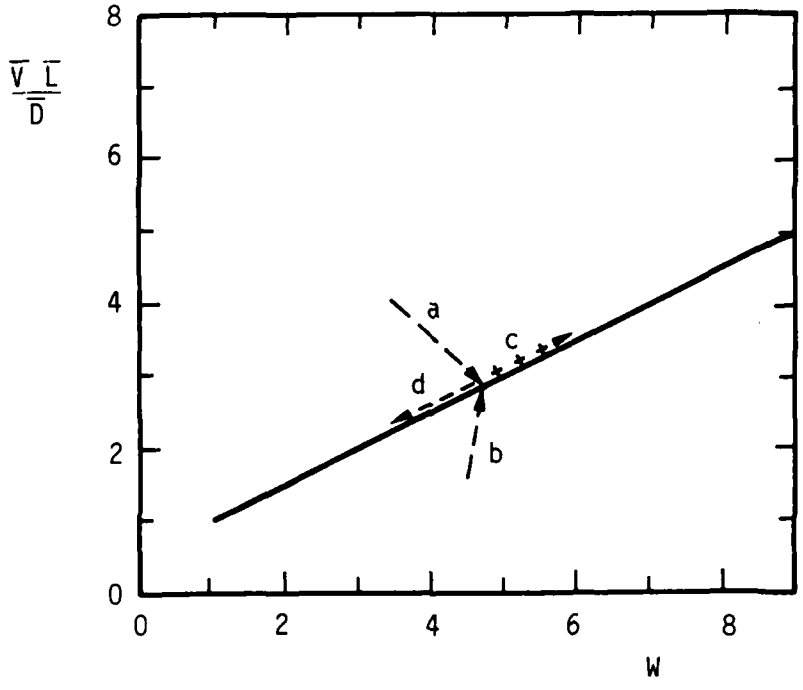

Figure 1.5. $R = \bar{V}\,\bar{L}/\bar{D}$ versus $(W + 1)/2$. Possible trajectories for cloud evolution may be a, b, and d but trajectory c is not permitted.

The curve illustrating the marginal condition for the formation of striations can be determined as a function of W and the effective Reynold's number

$$R = \frac{\bar{V}\,\bar{L}}{\bar{D}} \quad . \tag{1.56}$$

In (1.56) the following symbols are used: $\bar{V}$ (effective plasma velocity), $\bar{L}$ (effective perpendicular scale length), and $\bar{D}$ (effective cross-field diffusivity). If in (1.54)-(1.56) the following identifications are made

$$\bar{V} = \frac{M_0 - 1}{M_0 + 1}\frac{cE_{ox}}{B} \quad , \quad \bar{L} = k_t^{-1} \quad , \quad \bar{D} = \frac{M_0 - 1}{M_0 + 1}\rho_i^2\Omega_i \quad , \tag{1.57}$$

then

$$R = \frac{W + 1}{2} \quad , \tag{1.58}$$

is the condition for marginal stability. This expression, which is plotted in Figure 1.5, does not have an explicit dependence on M_0 but is nevertheless valid only for $M_0 > 1$. Equation (1.58) is appropriate to lower values of the plasma density for which ion viscosity is unimportant.

For a static situation, $2E_{ox}/(W + 1)$ in (1.55) can be interpreted to be the ambipolar electric field consistent with ion-neutral diffusion and the scale length k_t^{-1}. This suggests a physically meaningful interpretation for (1.58) and the curve in Figure 1.5. The equation and figure indicate the balance of two effects: bifurcation and the attainment of thermodynamic equilibrium for ions. Consider an ionospheric barium cloud. By thermodynamic equilibrium, we mean that (1.55) is satisfied so that the applied electric-field force acting on cloud ions is exactly balanced by the pressure forces associated with the cloud ions [cf, (E6) in Appendix E]. Hence, the presence of the cloud does not result in additional ion currents within the frame of reference where the effective electric field, $2E_{ox}/(W + 1)$, is zero. Stated another way, the current carriers in the indicated frame of reference can be conceptualized to be electrons and

strongly coupled [Perkins et al., 1973] and undoubtedly have complicated three-dimensional dependences. Indeed, (1.21a-b) demonstrate that induced electric fields can have strong spatial variations for even the relatively simple case of a uniform ellipsoidal, plasma cloud surrounded by a uniform plasma. Furthermore, plasma "equilibrium" is not an obvious nor proven requirement for the formation of striations L. Wittwer, private communication, 1983 . An important unresolved issue is the understanding of how three-dimensional effects impact the basic plasma state upon which striations evolve.

The real part of the frequency in (1.54) is a direct consequence of the contribution of ion-neutral diffusive currents to overall quasineutrality and the neglect of ambipolar electric fields in the basic plasma model upon which the striations develop. Now if ion-neutral diffusive currents are important, Appendix E demonstrates that the contribution of electric fields, with associated Pedersen currents, to the maintenance of quasineutrality is correspondingly reduced. Consequently, elongation and bulk plasma motion in the direction of the force is also inhibited. Although ion-neutral diffusion has not been considered in the quantitative evaluation of W in (1.52), it is evident from a qualitative standpoint that ion-neutral diffusion can effectively result in larger values of W in (1.53).

It is assumed that bifurcation can proceed only if $\mathrm{Re}(\omega) < \mathrm{Im}(\omega)$ [Sperling and Glassman, 1983; Sperling, 1983a]. Presumably, for $\mathrm{Re}(\omega) > \mathrm{Im}(\omega)$ ion-neutral diffusion plays a dominant role in maintaining quasineutrality and electric fields are not strongly induced in the nonlinear striations. Hence, the tendency of striations with $\mathrm{Re}(\omega) > \mathrm{Im}(\omega)$ to elongate a plasma cloud and cause plasma motion in the direction of the applied force is reduced.

If striations can only develop for perpendicular wave numbers such that $\mathrm{Re}(\omega) \lesssim \mathrm{Im}(\omega)$, the permissible perpendicular wave numbers for striations satisfy

$$k_y \lesssim k_t \equiv \frac{2}{W+1} \frac{cE_{ox}}{B} \frac{1}{\Omega_i \rho_i^2} \quad . \tag{1.55}$$

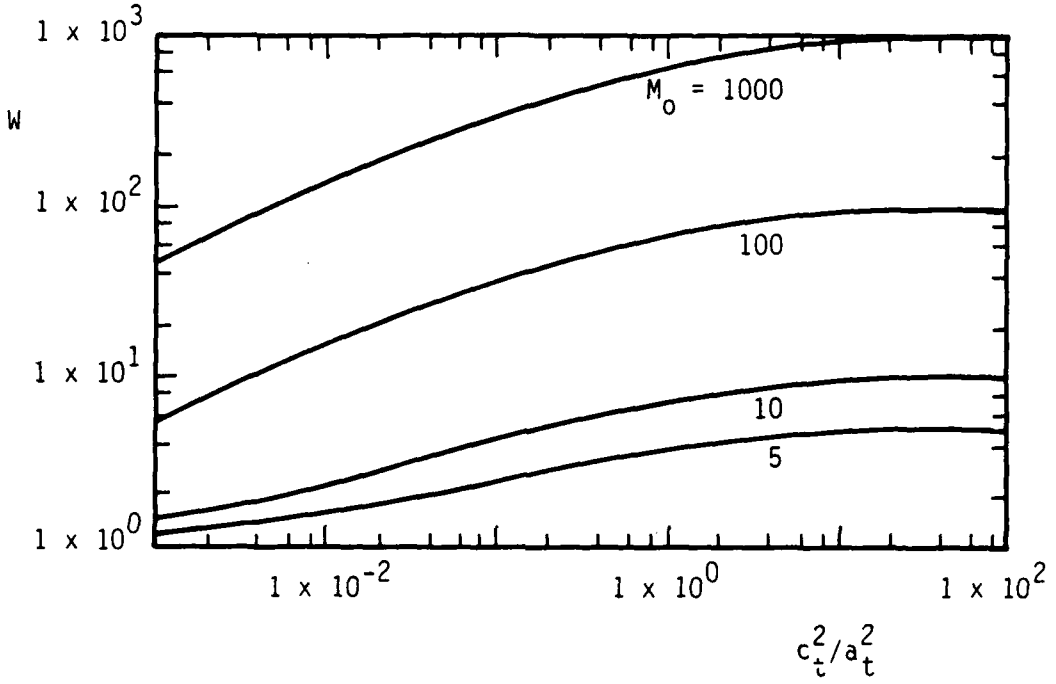

Figure 1.4. W versus c_t^2/a_t^2 for $a_t^2 = b_t^2$. $j_{ox\gtrless} \neq 0$ and $j_{oy\gtrless} = j_{oz\gtrless} = 0$.

For $|j_{x<,tot}| \ll |j_{ox<}|$ it is necessary that $W \gg 1$ or equivalently $M_0 h_x(0) \gg 1$. Clearly $M_0 \gg 1$ is not a sufficient condition for the total x-directed current in the ellipsoid to be much smaller than $|j_{ox<}|$. This is clearly demonstrated by Figure 1.4 which is a plot of W versus c_t^2/a_t^2 for a spheroid. The figure shows that $W \to 1$ for $c_t^2/a_t^2 \to 0$, but $W \to M_0$ for $c_t^2/a_t^2 \to \infty$.

If $j_{x<,tot}$ and $j_{ox<}$ are ion-Pedersen current densities then

$$\frac{E_{x<,tot}}{E_{ox}} = \frac{2}{1 + W} \quad . \tag{1.53}$$

In (1.53) the total x-directed electric field in the ellipsoid is represented by $E_{x<,tot}$.

The formation of striations is a manifestation of the tendency of plasma clouds to elongate and move in the direction of an applied force. It follows that with the development of striations the effective overall value of W for a plasma cloud must increase. Under such circumstances, (1.51) and (1.53) indicate that $j_{x<,tot}$ and $E_{x<,tot}$ are appropriately reduced.

The linear frequency of collisional E x B or Rayleigh-Taylor instabilities is determined by combination of (1.21) of Sperling [1983a] and (1.51) or (1.53). Specifically,

$$\omega = \min(k_y, L_\perp) \frac{M_0 - 1}{M_0 + 1} \left(i \frac{2}{W + 1} \frac{cE_{ox}}{B} + k_y \rho_i^2 \Omega_i \right) \quad . \tag{1.54}$$

In (1.54) the following symbols are used: ω (frequency), k_y (wave number transverse to the ambient magnetic field and the density gradient), $L_\perp$ (scale length of the perpendicular density gradient), and ρ_i (ion-gyroradius). The expression assumes $\nu_{in>}/\Omega_{i>} = \nu_{in<}/\Omega_{i<}$ and $T_{i>} = T_{i<}$. To account for other sources of current, besides electric fields, E_{ox} in (1.54) may be more generally replaced by $j_{ox<}/\sigma_{\perp<}$.

The plasma model used to derive (1.54) includes neither ambipolar electric fields nor parallel electron currents as both these phenomenon can be

assumed to be uniform in the perpendicular direction. Plasma properties are constant for $|z| \leq z_0$ and $|z| > z_0$. The only discontinuity in plasma properties occurs at $|z| = z_0$. For simplicity, it is assumed here that the plasma geometry is completely symmetric about $z = 0$.

The modes are assumed to have the plane wave form, $\exp[i(k_\perp y + k_{>(<)} z) + \gamma t]$ with $k_\perp$, y, γ, and t being the perpendicular wave number, coordinate in the y-direction, growth rate, and time, respectively. Throughout it is assumed that the subscripts, >(<), represent quantities appropriate to $|z| >(<) z_0$, and so $k_{>(<)}$ represent the parallel wave number outside (inside) the unstable plasma.

In general, ionospheric plasma clouds evolve dynamically as a result of external forces and diffusion processes, and so it is assumed that $\gamma \gg 1/\bar{t}$, where $\bar{t}$ is the time scale for bulk plasma parameters to change.

Sperling [1983d] derives a dispersion relation for the Rayleigh-Taylor and E x B instabilities which includes the contributions of parallel currents, parallel electric fields, and electromagnetic effects in a medium which is uniform along the magnetic field. This dispersion relation, (15) of Sperling [1983d], is

$$0 = \frac{i}{T_i} \left\{ \frac{(\omega - \omega_0 + i\nu_i)[1 - \Gamma_0(\lambda_i)] + \omega_i^* \Gamma_0(\lambda_i)}{\omega - \omega_0 + i\nu_i [1 - \Gamma_0(\lambda_i)]} - \frac{\omega_i^*}{\omega} \right\}$$

$$\left(\frac{i\omega_e^2}{\omega\nu_e} \frac{\omega_e^* - \omega}{\omega + i\delta} + \frac{k_\perp^2 c^2}{\omega^2} \right) - \frac{1}{T_e} \frac{\delta}{\omega + i\delta} \frac{k_\perp^2 c^2}{\omega^2} \left(1 - \frac{\omega_e^*}{\omega} \right) \quad , \qquad (2.1)$$

with

$$\Gamma_0(\lambda_i) = I_0(\lambda_i) \exp(-\lambda_i) \quad , \quad \omega_0 = k_\perp v_0 \quad , \quad \omega_i^* = \frac{\lambda_i \Omega_i}{k_\perp L_\perp} \quad ,$$

$$\omega_e^* = - \frac{T_e}{T_i} \omega_i^* \quad , \quad \lambda_i = \frac{k_\perp^2 \kappa_B T_i}{m_i \Omega_i^2} \quad , \quad \Omega_i = \frac{eB}{m_i c} \quad ,$$

$$\omega_e^2 = \frac{4\pi n_e e^2}{m_e} \quad , \quad \delta = \frac{k_\parallel^2 \kappa_B T_e}{m_e \nu_e} \quad . \qquad (2.2)$$

The following symbols are also used in writing (2.1) and (2.2): ν_i (ion collision frequency), I_0 (modified Bessel function of the first kind and order zero), T_e (electron temperature), T_i (ion temperature), κ_B (Boltzmann constant), m_i (ion mass), m_e (electron mass), e (electron charge), n_e (electron density), $k_\parallel (= k_{>(<)}$, parallel wave number), ω (= $i\gamma$, frequency), and ν_e (effective collision frequency for electron motion along the geomagnetic field). Ions are assumed to be singly ionized.

The parameter v_0 is the zero-order, y-directed velocity of individual ions. For example, v_0 is the ion-Pedersen drift for E x B gradient drift modes [Ossakow et al., 1979], the ion-polarization drift for Rayleigh-Taylor modes driven by ion inertia [Sperling, 1982b], and the ion-gravity drift for Rayleigh-Taylor modes driven by gravity [Kadomtsev, 1965]. Expressions for v_0 are explicitly written and described in the references.

We now consider the limit of collisional modes with relatively long wavelength, i.e.,

$$\nu_i \gg |\omega| \gg |\omega_i^*|, |\omega_e^*|, |\omega_0|, |\delta|; \lambda_i \ll 1 \quad . \tag{2.3}$$

Equation (2.1) becomes

$$0 = \frac{i}{T_i} \frac{i\nu_i\lambda_i\omega + \omega_i^*\omega_0}{\omega} \left(\frac{k_\perp^2 c^2}{\omega^2} - \frac{i\omega_e^2}{\omega\nu_e} \right) - \frac{\delta}{T_e} \frac{k_\perp^2 c^2}{\omega^2} \quad . \tag{2.4}$$

With the replacement of ω by $i\gamma$, (2.4) can be solved for δ. The result is

$$\delta = \frac{T_e}{T_i} \nu_i\lambda_i \left(\frac{\gamma_0}{\gamma} - 1 \right) \left(\frac{\omega_e^2\gamma}{k_\perp^2 c^2 \nu_e} + 1 \right) \tag{2.5}$$

with

$$\gamma_0 = \frac{v_0\Omega_i}{L_\perp \nu_i} \quad , \tag{2.6}$$

the maximum growth rate for the pure flute instability. Equation (2.5) implies forms for the parallel wave numbers in the interior and exterior regions specified in Figure 2.1. Specifically,

$$k_<^2 = \frac{\nu_{i<}\gamma\beta_<}{v_{A<}^2}\left(\frac{\gamma_0}{\gamma} - 1\right) \tag{2.7a}$$

$$k_>^2 = -\frac{\nu_{i>}\gamma\beta_>}{v_{A>}^2} \tag{2.7b}$$

with

$$v_{A>(<)}^2 = \frac{B^2}{4\pi n_{e>(<)} m_{i>(<)}} \quad , \quad \beta_{>(<)} = 1 + \frac{k_\perp^2 c^2 \nu_{e>(<)}}{\omega_{e>(<)}^2 \gamma} \quad . \tag{2.8}$$

Here v_A is the Alfven speed. Because of the use of (2.3), (2.7b) does not depend upon v_0 in the external region with $|z| > z_0$.

Equation (13b) of Sperling [1983d], (2.3), and Faraday's law imply that

$$B_{1x>(<)} = \frac{k_{>(<)}c}{\gamma\beta_{>(<)}} E_{1y>(<)} \quad , \tag{2.9a}$$

$$E_{1z>(<)} = \frac{k_{>(<)}}{k_\perp} \frac{k_\perp^2 c^2 \nu_{e>(<)}}{\omega_{e>(<)}^2 \gamma\beta_{>(<)}} E_{1y>(<)} \quad . \tag{2.9b}$$

In (2.9) modal fields are represented in the following way: B_{1x} (x-directed magnetic field), E_{1z} (z-directed electric field), and E_{1y} (y-directed electric field).

The assumed plasma model is symmetric about $z = 0$ and (2.7b) implies that evanescence away from the plasma cloud is the appropriate boundary condition for $|z| > z_0$. The following explicit forms are suggested for the modal electric and magnetic fields:

$$E_{1y}(y,z,t) = E_{1y<}[\exp(ik_< z) \pm \exp(-ik_< z)]$$

$$H(z_0 - |z|) + E_{1y>} \exp[-|k_>|(z - z_0)]$$

$$H(z - z_0) \pm E_{1y>} \exp[|k_>|(z + z_0)]$$

$$H(-z - z_0) \exp(ik_\perp y + \gamma t) \qquad (2.10a)$$

$$E_{1z}(y,z,t) = \Big\{E_{1z<}[\exp(ik_< z) \mp \exp(-ik_< z)]$$

$$H(z_0 - |z|) + E_{1z>} \exp[-|k_>|(z - z_0)]$$

$$H(z - z_0) \mp E_{1z>} \exp[|k_>|(z + z_0)]$$

$$H(-z - z_0)\Big\} \exp(ik_\perp y + \gamma t) \qquad (2.10b)$$

$$B_{1x}(y,z,t) = \Big\{B_{1x<}[\exp(ik_< z) \mp \exp(-ik_< z)]$$

$$H(z_0 - |z|) + B_{1x>} \exp[-|k_>|(z - z_0)]$$

$$H(z - z_0) \mp B_{1x>} \exp[|k_>|(z + z_0)]$$

$$H(-z - z_0)\Big\} \exp(ik_\perp y + \gamma t) \quad . \qquad (2.10c)$$

In (2.10a-c) the Heaviside function, H, is equal to 1 for positive argument and 0 for negative argument. Consistent with (2.9a-b), the form of (2.10a-c) indicates

that $E_{1z}(y,z,t)$ and $B_{1x}(y,z,t)$ are odd (even) about $z = 0$ if $E_{1y}(y,z,t)$ is even (odd) about $z = 0$.

To complete the specification of the eigenmodes, it is necessary to invoke boundary conditions at $|z| = z_0$. In particular, tangential electric and magnetic fields are continuous across a discontinuity in dielectric properties [Jackson, 1962; Allis et al., 1963; Paoloni, 1975; Sperling, 1983c]. For the eigenmodes with $E_{1y}(y,z,t)$ even about $z = 0$, it follows from (2.9)-(2.10) that

$$E_{1y>} = 2E_{1y<} \cos(k_< z_0) \tag{2.11a}$$

$$\frac{|k_>|}{\beta_>} E_{1y>} = 2 \frac{k_<}{\beta_<} E_{1y<} \sin(k_< z_0) \quad . \tag{2.11b}$$

Hence,

$$k_< z_0 = \tan^{-1}(|k_>|\beta_</k_<\beta_>) + p\pi \tag{2.12}$$

with p a nonnegative integer for positive $k_<$. Similarly for the eigenmodes with $E_{1y}(y,z,t)$ odd about $z = 0$,

$$E_{1y>} = 2iE_{1y<} \sin(k_< z_0) \tag{2.13a}$$

$$- \frac{|k_>|}{\beta_>} E_{1y>} = 2i \frac{k_<}{\beta_<} E_{1y<} \cos(k_< z_0) \quad , \tag{2.13b}$$

and so

$$k_< z_0 = - \tan^{-1}(k_<\beta_>/|k_>|\beta_<) + p\pi \tag{2.14}$$

with p a positive integer for positive $k_<$. For a specified value of z_0, the parallel wave numbers, growth rates, and modal fields are completely specified by (2.7), (2.9), and (2.12) or (2.14).

Now $\tan^{-1}$ is bounded by 0 and $\pi/2$ and so the lowest order eigenmode is determined by (2.12) with p = 0. In particular,

$$k_< z_0 = \tan^{-1}(|k_>| \beta_< / k_< \beta_>) \quad . \tag{2.15}$$

If $|k_> \beta_< / k_< \beta_>| \ll 1$ then it follows that $|k_< z_0|$ is also much smaller than 1. Equation (2.7) indicates that the inequality has a tendency to be better satisfied if the density of an unstable plasma cloud is much larger than the density of the stable background. The examples presented in the subsequent section satisfy the inequality. Equations (2.7), (2.8), and (2.15) now give

$$\frac{(\nu_{i>} \gamma \beta_>)^{1/2}}{v_{A>}} = z_0 \frac{\nu_{i<} \gamma \beta_>}{v_{A<}^2} \left(\frac{\gamma_0}{\gamma} - 1 \right) \quad . \tag{2.16}$$

For γ real it is evident from (2.16) that $0 < \gamma < \gamma_0$. By squaring both sides of (2.16) it is possible to obtain a cubic equation of the form

$$0 = bu^3 + (1 - a - 2b)\, u^2 + (b - 2)\, u + 1 \tag{2.17}$$

with

$$u = \gamma/\gamma_0 \quad , \quad a = 4 \frac{\nu_{i>}}{\nu_{e>}} \frac{m_{i>}}{m_e} \frac{\Omega_{i<}^2}{\nu_{i<}^2} \frac{n_{e>}^2}{N_c^2} \frac{1}{k_\perp^2} \quad , \quad b = \frac{\omega_{e>}^2 \gamma_0}{k_\perp^2 c^2 \nu_{e>}} \quad . \tag{2.18}$$

The parameter "a" indicates that the total integrated electron density in the unstable cloud (i.e., $N_c \equiv 2 n_{e<} z_0$) is a significant quantity [S. Zalesak, private communication, 1983].

It is instructive to examine (2.17) in several limits. For $b \to 0$, (2.7)-(2.9) indicate that the modal electric fields are becoming increasingly electrostatic while the modal magnetic fields are becoming smaller. Equation (2.17) then can be reduced to

$$0 \cong (1 - a)u^2 - 2u + 1 \tag{2.19}$$

with appropriate solution

$$u = \frac{1 - a^{1/2}}{1 - a} \quad . \tag{2.20}$$

The asymptotic forms for (2.20) are

$$u \approx a^{-1/2} \quad , \qquad \text{for } a \gg 1 \tag{2.21a}$$

$$u \approx 1 - a^{1/2} \quad , \qquad \text{for } a \ll 1 \quad . \tag{2.21b}$$

Equations (2.20) and (2.21) have the physically attractive feature that $u \to 0$ for very short plasma clouds but approaches 1 for long plasma clouds. In the electrostatic limit (2.7) becomes

$$k_<^2 = k_\perp^2 \frac{\nu_{i<}\nu_{e<}}{\Omega_{i<}^2} \frac{m_e}{m_{i<}} \left(\frac{\gamma_0}{\gamma} - 1\right) \quad , \tag{2.22a}$$

$$k_>^2 = - k_\perp^2 \frac{\nu_{i>}\nu_{e>}}{\Omega_{i>}^2} \frac{m_e}{m_{i>}} \quad . \tag{2.22b}$$

In the electrostatic limit both the growth rates and the parallel wave numbers depend on $k_\perp$. Note that (2.22b), which is independent of γ, implies that eigenmodes must become increasingly localized along the magnetic field as $k_\perp$ increases.

In the inductive limit with $b \to \infty$, (2.17) can be rewritten in the approximate form

$$0 = u^2 - (2 + a/b)\, u + 1 \tag{2.23}$$

with appropriate solution

$$u = 1 + \frac{a}{2b} - \left(\frac{a}{b} + \frac{a^2}{4b^2}\right)^{1/2} \quad . \tag{2.24}$$

Asymptotic forms for this expression are

$$u \approx b/a \quad , \qquad \text{for } a/b \gg 1 \tag{2.25a}$$

$$u \approx 1 - (a/b)^{1/2} \quad , \qquad \text{for } a/b \ll 1 \quad . \tag{2.25b}$$

Again the asymptotic expressions for u have the pleasing form of being very small for sufficiently short clouds and approaching 1 for sufficiently long clouds. In the inductive limit, (2.7a-b) become

$$k_<^2 = \frac{\nu_{i<}\gamma}{v_{A<}^2}\left(\frac{\gamma_0}{\gamma} - 1\right) \tag{2.26a}$$

$$k_>^2 = -\frac{\nu_{i>}\gamma}{v_{A>}^2} \quad . \tag{2.26b}$$

Growth rates and eigenmodes do not depend on $k_\perp$ in the inductive limit. Also, (2.9a-b) indicate that consistent with $|b| \to \infty$, $|E_{1z}| \to 0$ while $|B_{1x}|$ becomes independent of $k_\perp$.

2.3 RESULTS

The plasma model outlined in section 2.2 is rather simple and admittedly does not include all the intricacies and complicated inhomogeneities of the real ionosphere. Nevertheless, the model does show that growth rate is a function of the field-line electron density of the plasma cloud (i.e., N_c). In the inductive limit, growth rates and parallel wave numbers are not a function of the perpendicular wave number. In the electrostatic limit, growth rates and parallel wave numbers are strong functions of the perpendicular wave number.

As quantitative examples, consider Figures 2.2a-b which are plots of $k_\perp$ (km^{-1}) versus γ/γ_0 for different values of N_c (10^{12} cm^{-2}). Figures 2.2a-b assume $\gamma_0 = 0.01\ s^{-1}$ and $\gamma_0 = 0.1\ s^{-1}$, respectively. The plots assume $n_{e>} = 1 \times 10^5\ cm^{-3}$, $T_{i<} = T_{i>} = T_{e<} = T_{e>} = 0.1$ eV, and B = 0.4 G. The ions for $|z| < z_0$ are assumed to be barium (i.e., $m_{i<} = 137\ m_p$, with m_p the proton mass) and the ions for $|z| > z_0$ are assumed to be air with $m_{i>} = 20\ m_p$. The mass of an atmospheric neutral particle, $m_{0<(>)}$, is also assumed to be 20 m_p. The neutral density, $n_{0<} = n_{0>} = 8.3 \times 10^9\ cm^{-3}$, is appropriate to an altitude of $\sim$200 km [Knapp and Schwartz, 1975]. The collision frequencies are determined from [Braginskii, 1965; Kilb, 1977]

$$\nu_{i<} = 2.5 \times 10^{12}\ m_0 n_0 \tag{2.27a}$$

$$\nu_{i>} = 2.5 \times 10^{13}\ m_0 n_0 \tag{2.27b}$$

$$\nu_{e<(>)} = 0.51\ \nu_{ei<(>)} + 1.9 \times 10^{-8}\ n_0 \tag{2.27c}$$

$$\nu_{e<} = 0.51\ \nu_{ei<} + 1.9 \times 10^{-8}\ n_0 \tag{2.27d}$$

$$\nu_{ei<(>)} = 1.1 \times 10^{-3}\ n_{e<(>)} \quad . \tag{2.27e}$$

In (2.27) all parameters are in cgs units.

Figures 2.2a-b show the following general tendencies. The growth rate, γ, becomes larger as the perpendicular wave number, $k_\perp$, increases and as N_c increases. The modes become more inductive with $|\partial\gamma/\partial k_\perp| \to 0$ as N_c increases and $k_\perp$ becomes smaller. The inductive nature of modes is enhanced if the maximum possible growth rate for instability, γ_0, increases. For larger values of $k_\perp$ (i.e., $k_\perp \to 10\ km^{-1}$), modes become highly electrostatic. In accordance with (2.20), γ/γ_0 then is independent of γ_0 and so the corresponding curves in Figures 2.2a-b become essentially the same. Equation (2.16) is a good approximation to (2.15) for $\gamma/\gamma_0 < 0.95$.

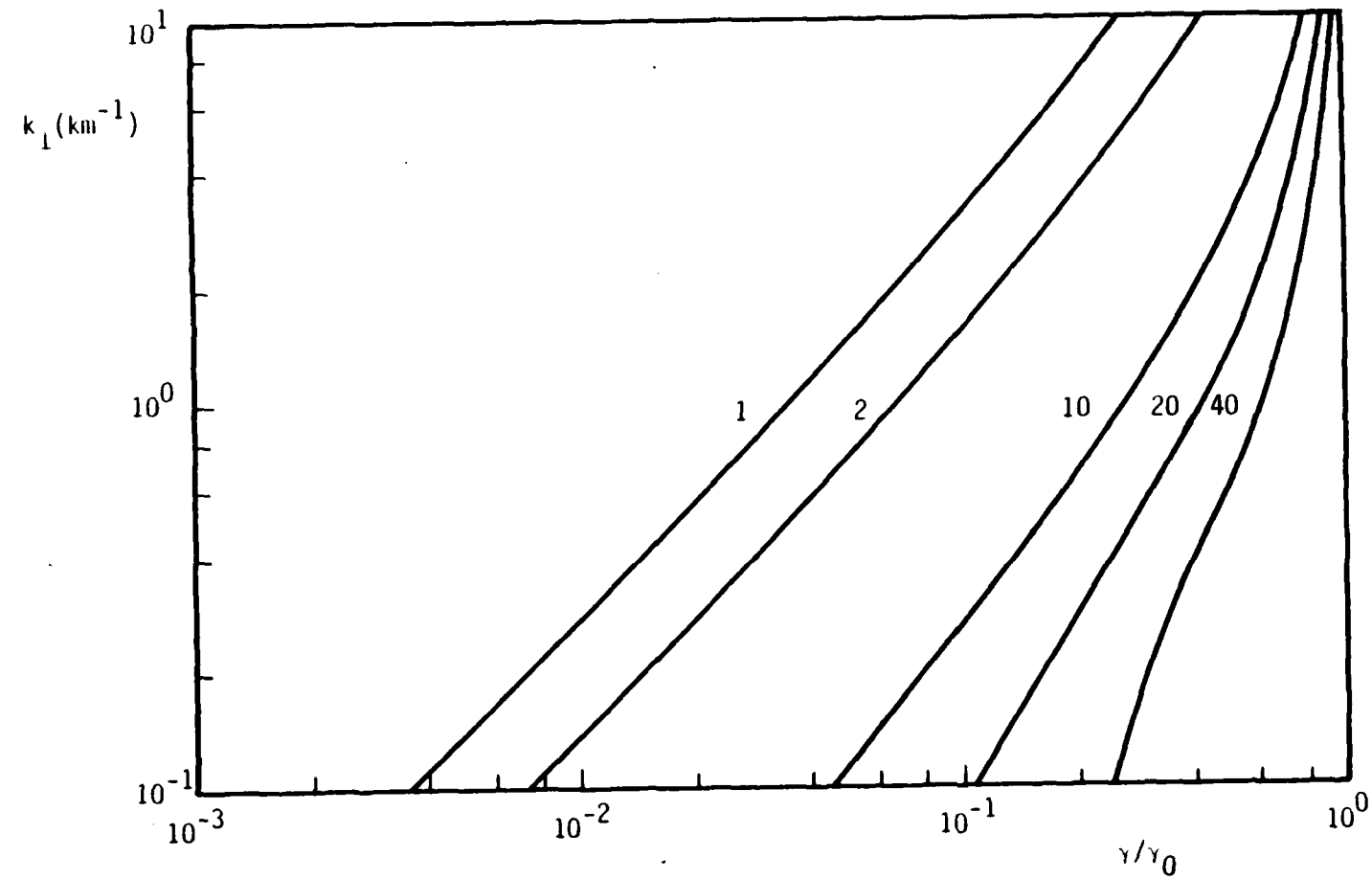

Figure 2.2a. $k_\perp$ (km^{-1}) versus γ/γ_0 for different values of N_c (10^{12} cm^{-2}) as determined from (2.17). $n_{0<} = n_{0>} = 8.3 \times 10^9$ cm^{-3}, $n_{e>} = 1 \times 10^5$ cm^{-3}, $m_{0<} = m_{0>} = 20\ m_p$, $m_{i<} = 137\ m_p$, $m_{i>} = 20\ m_p$, $T_{e>} = T_{e<} = T_{i>} = T_{i<} = 0.1$ eV, and B = 0.4 G. $\gamma_0 = 0.01\ s^{-1}$.

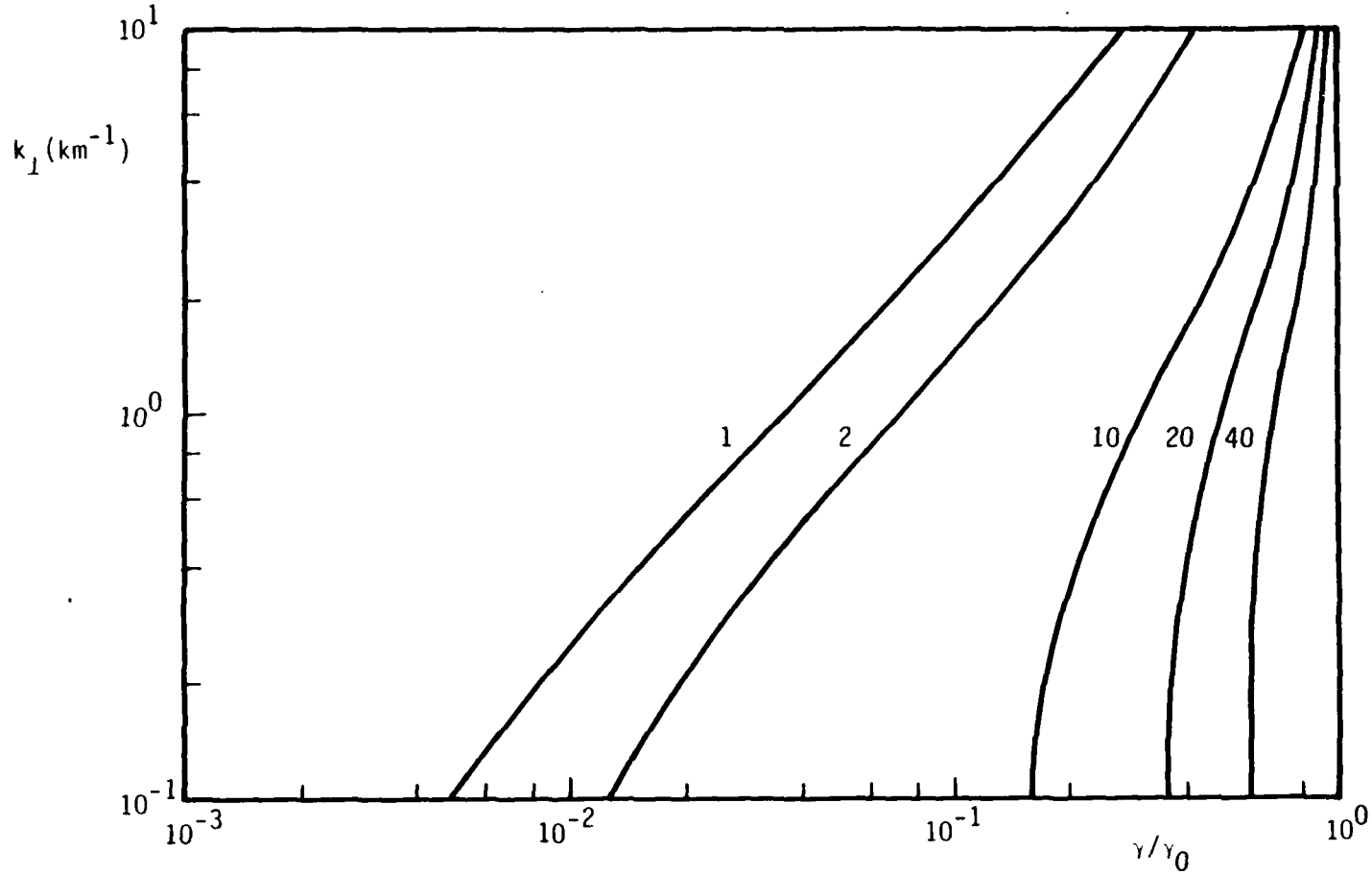

Figure 2.2b. $k_\perp$ (km^{-1}) versus γ/γ_0 for different values of N_c (10^{12} cm^{-2}) as determined from (2.17). $n_{0<} = n_{0>} = 8.3 \times 10^9$ cm^{-3}, $n_{e>} = 1 \times 10^5$ cm^{-3}, $m_{0<} = m_{0>} = 20\ m_p$, $m_{i<} = 137\ m_p$, $m_{i>} = 20\ m_p$, $T_{e>} = T_{e<} = T_{i>} = T_{i<} = 0.1$ eV, and $B = 0.4$ G. $\gamma_0 = 0.1\ s^{-1}$.

Consider a plasma which is simultaneously steepening perpendicular to the magnetic field and elongating along the magnetic field. If ionization, recombination, diffusion, and convection can be neglected, a reasonable assumption is that N_c is a constant as the unstable plasma cloud elongates [S. Zalesak, private communication, 1983]. Earlier in the steepening, γ_0 might be 0.01 s^{-1} and Figure 2.2a is appropriate. The figure clearly shows the tendency for growth rate to be a strong function of $k_\perp$, particularly for smaller values of N_c. Parallel currents and parallel electric fields tend to most strongly short-circuit perpendicular electric fields associated with the unstable modes when $k_\perp$ is small. It is evident that preferential growth occurs at larger wave numbers. At later times, when γ_0 might be ~ 0.1 s^{-1}, the same basic tendencies still remain, but growth rates are a somewhat weaker function of $k_\perp$ since inductive effects are more important.

When E x B gradient drift instabilities are the primary cause of striations in barium clouds, the onset of striations in barium clouds occurs several minutes after the detonation of the barium release. Specifically for larger barium clouds, like Spruce [Linson and Meltz, 1972], the onset time for striations is estimated to be generally greater than approximately 5 minutes [McDonald et al., 1980]. Now Linson and Meltz [1972] have estimated that the Spruce and Olive ion clouds had an approximately 30-40 km extent along the magnetic field at approximately 5 minutes. This parallel extent corresponds to $z_0 \approx$ 15-20 km for Figures 2.2a-b. If $n_{e<} = 1 \times 10^7$ cm^{-3}, then $N_c \approx 3\text{-}4 \times 10^{13}$ cm^{-2}. For the growth of striations to be significant, it is assumed that the growth rate for striations must be greater than the rate at which the bulk parameters of the cloud change, but finite N_c implies a growth rate which is smaller than γ_0. Now if the typical time scale for bulk plasma parameters to change is $\bar{t} = 300$ s, then $\gamma \gg 1/\bar{t}$ implies $\gamma/\gamma_0 \gg 0.3$ and 0.03 in Figures 2.2a and 2.2b, respectively. Figure 2.2a indeed shows that clouds with $N_c \gtrsim 2 \times 10^{13}$ cm^{-2} have a substantial range of finite perpendicular wave numbers with sufficiently rapid growth rates. Figure 2.2b, which is appropriate to the case of more substantial steepening than Figure 2.2a, indicates that $\gamma \gg 1/300$ s is easily satisfied for $N_c > 2 \times 10^{13}$ cm^{-2}. Examination of Figures 2.2a and 2.2b suggests, that in evolving plasma clouds, preferential striation growth should occur for k_y finite rather than for $k_y = 0$.

2.4 CONCLUDING REMARKS

A simple plasma geometry is used to show that the finite field-line integrated electron density of ionospheric plasma clouds plays a role in the delayed formation of striations by tending to reduce the growth rate of striation instabilities. Taking into account the field-line integrated electron density, the onset of appreciable striations is assumed to occur when the growth rate of the striation instabilities is much faster than the rate of change of the bulk plasma. This point is quantified by examination of Figures 2.2a and 2.2b. The finite parallel length of plasma clouds tends to favor the growth of striations with finite rather than with zero perpendicular wave numbers.

The results presented in this chapter are not qualitatively changed by considering more complicated and realistic plasma geometries than the one used here. However, it should be noted that warm plasma effects (e.g., ambipolar diffusion), not considered in the present chapter, tend to reduce growth rates for sufficiently large $k_\perp$ [McDonald et al., 1981]. Indeed, the combination of parallel inhomogeneities and warm plasma effects generally causes a maximizing of the growth rate for $k_\perp$ in the range of $1 \sim 10\ km^{-1}$ [J. L. Sperling and A. J. Glassman, 1983].

3. LATE-TIME STRIATION EIGENMODES ALONG THE GEOMAGNETIC FIELD

3.1 INTRODUCTION

Following a high-altitude nuclear burst, plasma is injected at high speed along the geomagnetic field into the upper ionosphere and the magnetosphere. The resulting nuclear plumes can have densities orders of magnitude larger than under normal ambient conditions. In fact, in view of their large overall spatial extent and high density, nuclear plumes represent a markedly different medium than spread-F plasmas or barium clouds for the formation of striations. For example, it has been reported that collisional striation instabilities, associated with ion-neutral collisions, can be expected to have a much shorter extent along the geomagnetic field in the high-altitude nuclear environment than in the barium-cloud environment [Sperling, 1983e].

The large parallel extent and high density of nuclear plumes offers the possibility that collisionless fluid instabilities, driven at high altitude, may play a very substantial role in structuring at later times [Kilb, 1977]. Of course, because nuclear plumes extend well into the ionosphere, the possibility remains that collisional instabilities, associated with ion-neutral collision, can also still provide impetus for structuring. By contrast, the smaller mass and parallel extent of barium clouds, likely limits their structuring to solely collisionless or collisional processes depending on the altitude of the barium release. For barium releases at an altitude of approximately 200 km, structuring is probably a result of collisional instabilities.

In nuclear plumes, the curvature of the geomagnetic field and the high velocity (e.g., $\sim$ 5 km/s) at which plasma is ejected along the geomagnetic field suggests that centrifugal forces might contribute to the "effective gravity," necessary for structuring by a collisionless Rayleigh-Taylor mechanism [Kilb, 1977]. Assuming a dipolar model for the geomagnetic field, an appropriate expression for $\vec{g}_c$ is [Kilb, 1977]:

$$\vec{g}_c = \frac{3w_{\parallel}^2}{R} \frac{[1 + \cos^2(\theta)]\sin(\theta)}{[1 + 3\cos^2(\theta)]^{3/2}} \hat{e}_\phi \times \frac{\vec{B}_o}{B_o} \quad . \tag{3.1}$$

(3.21). In particular, $\psi(z)$ is required to decay far from the source of free energy responsible for instability, i.e.,

$$|\psi(z \to \pm\infty)| \to 0 \quad . \tag{3.30}$$

The appropriateness of this boundary condition is shown in great detail in Sperling [1983e] to mainly result from the tendency of striation fields to become more electrostatic at lower altitudes. Indeed, the numerical results presented in Section 3.4 demonstrate the correctness of (3.30).

3.3 APPLICATIONS TO MODELING

The ability to bifurcate requires that the relative phases of parameters (e.g., density, electric field, etc.) in the parent structures be identical to the relative phases in the daughter structures [Vesecky et al., 1980]. However, for $k_\perp \gtrsim k_t$ our numerical results, using the assumed plasma models, indicate that the modes become highly dispersive and the relative phases of parameters become sensitive functions of the perpendicular wave number. Here k_t is the perpendicular wave number at which the real part of the frequency is equal to the growth rate. Moreover, since the eigenmodes become more localized along the geomagnetic field as perpendicular wave number increases and concomitantly, eigenvalues become insensitive to parallel variations of the plasma, the density of eigenmodes and eigenvalues in phase space increases along with the real frequency. This suggests that striations are limited to scale sizes larger than the wavelength for which the real frequency is equal to the growth rate.

The coefficient for ion diffusion, resulting from ion-neutral collisions, can play an important role in determining k_t, especially when unstable plasmas are not too dense. This is demonstrated in Appendix G which determines k_t in various important limits. The ion-neutral diffusion does not directly stabilize the instability because electrons tend to diffuse across the magnetic field at a much slower rate than ions, but it does cause the instability to acquire a significant real frequency for the assumed plasma model.

Although the real part of the frequency may be sensitive to the assumed theoretical plasma models [S. Zalesak, private communication, 1984], the perpendicular wave number determined by equating the real and imaginary parts of the frequency can be interpreted in a way which is independent of the models. In particular, at least for the collisional gradient-drift instability, it can be

For $\omega \approx i\gamma$ with γ real and $\gamma \gg |\omega_e^*|$, the effective resistivity is increased by the ratio $1 + (\omega_e^2\gamma/k_\perp^2c^2\nu_e)$ from the purely classical electrostatic value. Since

$$1 \ll P \equiv \left| \frac{\omega_e^2}{k_\perp^2 c^2} \frac{\omega - \omega_e^*}{\nu_e} \right| \quad , \tag{3.26}$$

implies an important contribution from the electromagnetic correction, it is evident that for fixed $k_\perp^2$, c^2, ω, and ω_e^* the electromagnetic correction has the greatest impact at higher altitudes where ω_e^2/ν_e is maximum. At lower altitudes ω_e^2/ν_e is reduced by electron-neutral collisions [Goldman et al., 1976] and the electromagnetic correction is less significant. It is interesting to note that turbulence and double layers, which increase the effective value of ν_e, would also reduce the importance of electromagnetic effects [Block, 1972; Papadopoulos, 1977; Sperling, 1982b].

Consider the neglect of ion-viscosity, ambipolar-diffusion, and ion-polarization corrections in (3.21) and (3.22). If in addition,

$$1 \gg \left| \frac{k_\perp \alpha \kappa_B T_{eo}}{e} \right| \quad , \tag{3.27}$$

and asymptotically electrostatic modes are assumed, i.e.,

$$1 \gg \left| \frac{\omega_e^2}{k_\perp^2 c^2} \frac{\omega - \omega_e^*}{\nu_e} \right| \quad , \tag{3.28}$$

then (3.21) and (3.22) reduce to (13) of Goldman et al. [1976]. Equation (3.27) is generally easily satisfied for:

$$|\nu_i \lambda_i| \quad , \quad |\omega_i^*| \ll |\omega| \, (T_{io}/T_{eo}) \quad . \tag{3.29}$$

To completely determine Ψ and the other associated striation parameters, it is necessary to specify the boundary conditions imposed on the solution

In (3.21)

$$A(z) = \frac{en_{eo}}{m_e} \frac{1}{i \frac{\omega_e^2}{k_\perp^2 c^2} (\omega - \omega_e^2) - \nu_e} \quad , \quad B(z) = \frac{dA(z)}{dz} \quad ,$$

$$C(z) = n_{eo} \frac{(\nu_c - i\omega)\alpha + \frac{c}{B_o L}}{\frac{\alpha \kappa_B T_{eo}}{e} - \frac{i}{k_\perp}} \quad . \tag{3.22}$$

Equation (3.21) is the dispersion relation solved in this work.

With the form of Ψ determined from (3.21), n_{el}, n_{il}, B_{lx}, E_{lz}, and v_{elz} are determined from (3.16), (3.17a), and (3.17c-e). In addition, the parallel current associated with the modes, j_{elz}, is determined from:

$$j_{elz} = en_{eo} v_{elz} \quad . \tag{3.23}$$

If ion-ion diffusion is neglected, (3.21) can be easily generalized to multiple ion species by redefining α such that:

$$\alpha = - \frac{ie}{k_\perp \kappa_B n_{eo}} \sum_i \frac{n_{io}}{T_{io}} \frac{(\omega - \omega_{io} + i\nu_i)\lambda_i + \omega_i^*}{a_i(\omega - \omega_{io}) + i\nu_i \lambda_i} \quad , \tag{3.24}$$

with the summation over ion species and

$$n_{eo} = \sum_i n_{io} \quad . \tag{3.25}$$

The electromagnetic correction to (3.21) is localized to $\omega_e^2(\omega - \omega_e^*)/k_\perp^2 c^2$ in the denominator of A(z) in (3.22). From the mathematical standpoint, the electromagnetic correction acts to effectively modify the plasma resistivity.

In (3.17a-f),

$$\lambda_i = \frac{k_\perp^2 \kappa_B T_{io}}{m_i \Omega_i^2} \quad , \quad \omega_e^2 = \frac{4\pi n_{eo} e^2}{m_e} \quad , \quad \omega_e^* = - \frac{T_{eo}}{T_{io}} \omega_i^* \quad , \quad n_{eo} = n_{io} \quad ,$$

$$\nu_c = k_\perp^2 D_c \quad , \quad D_c = \frac{\kappa_B (T_{io} + T_{eo})}{m_i \Omega_i^2} \frac{m_e}{m_i} \nu_{ei} \quad ,$$

$$\bar{\nu}_c = \frac{k_\perp^2 \kappa_B T_{eo}}{m_i \Omega_i^2} \frac{m_e}{m_i} \nu_{en} \quad . \tag{3.18}$$

The second-order differential equation can be written in a somewhat simpler form with the definition:

$$\psi \equiv \left(\frac{\alpha \kappa_B T_{eo}}{e} - \frac{i}{k_\perp} \right) E_{1y} \quad . \tag{3.19}$$

Hence,

$$E_{1y} = \frac{\psi}{\frac{\alpha \kappa_B T_{eo}}{e} - \frac{i}{k_\perp}} \tag{3.20}$$

and

$$0 = \left[A(z) \frac{d^2}{dz^2} + B(z) \frac{d}{dz} + C(z) \right] \psi \quad . \tag{3.21}$$

In writing (3.15d), the displacement current has been neglected. This assumption is equivalent to quasi-neutrality, i.e.,

$$n_{el} = n_{il} \quad . \tag{3.16}$$

The combination of (3.12) and (3.15a-d) gives:

$$n_{el} = \alpha n_{eo} E_{ly} \quad , \tag{3.17a}$$

$$\alpha = - \frac{ie}{k_\perp \kappa_B T_{io}} \frac{(\omega - \omega_o + i\nu_i)\lambda_i + \omega_i^*}{a(\omega - \omega_o) + i\nu_i\lambda_i + i\nu_c} \quad , \tag{3.17b}$$

$$B_{lx} = - \frac{4\pi i}{ck_\perp} en_{eo} v_{elz} \quad , \tag{3.17c}$$

$$E_{lz} = - \frac{4\pi i\omega e n_{eo} v_{elz}}{k_\perp^2 c^2} - \frac{i}{k_\perp} \frac{\partial E_{ly}}{\partial z} \quad , \tag{3.17d}$$

$$v_{elz} = \frac{\kappa_B T_{eo} \frac{\partial}{\partial z} (\alpha E_{ly}) - i \frac{e}{k_\perp} \frac{\partial E_{ly}}{\partial z}}{i \frac{m_e \omega_e^2}{k_\perp^2 c^2} (\omega - \omega_e^*) - m_e \nu_e} \quad , \tag{3.17e}$$

$$0 = (\nu_c + \bar{\nu}_c - i\omega)\alpha n_{eo} E_{ly} + \frac{c n_{eo}}{B_o L_\perp} E_{ly}$$

$$+ \frac{d}{dz} \left[\frac{n_{eo}}{m_e} \frac{\kappa_B T_{eo} \frac{d}{dz} (\alpha E_{ly}) - \frac{ie}{k_\perp} \frac{d}{dz} (E_{ly})}{i \frac{\omega_e^2}{k_\perp^2 c^2} (\omega - \omega_e^*) - \nu_e} \right] \quad . \tag{3.17f}$$

velocity v_{elz} in response to the modes, is determined from the linearized momentum equation:

$$0 = - \kappa_B T_{eo} n_{eo} \frac{d}{dz}\left(\frac{n_{el}}{n_{eo}}\right) - e n_{eo} E_{lz} - m_e \nu_e n_{eo} v_{elz}$$

$$+ e n_{eo} v_{eoy} B_{lx}/c \quad , \tag{3.12}$$

with [Braginskii, 1965]:

$$\nu_e = \nu_{en} + 0.51\, \nu_{ei} \quad , \quad v_{eoy} = - \frac{c\, \kappa_B T_{eo}}{e B_o} \frac{dn_{eo}}{dx} \frac{1}{n_{eo}} \quad . \tag{3.13}$$

Here v_{eoy} is the zero order electron diamagnetic drift and B_{lx} is the x-directed, modal, magnetic field. Hence,

$$v_{elz} = - \frac{e}{m_e \nu_e}\left[\frac{\kappa_B T_{eo}}{e} \frac{d}{dz}\left(\frac{n_{el}}{n_{eo}}\right) + E_{lz} - \frac{v_{eoy}}{c} B_{lx}\right] \quad . \tag{3.14}$$

Next we consider the ion and electron continuity equations, Faraday's law, and Ampere's law:

$$0 = -i\omega n_{il} + i k_\perp n_{il} u_{ioy} + \frac{\partial}{\partial x}\left(n_{io} v_{ilx}\right) + i k_\perp n_{io} v_{ily} \quad , \tag{3.15a}$$

$$0 = -i\omega n_{el} + \frac{\partial}{\partial x}\left(n_{eo} v_{elx}\right) + i k_\perp n_{eo} v_{ely} + \frac{d}{dz}\left(n_{eo} v_{elz}\right) \quad , \tag{3.15b}$$

$$\frac{\omega}{c} B_{lx} = k_\perp E_{lz} + i \frac{d}{dz}\left(E_{ly}\right) \quad , \tag{3.15c}$$

$$i k_\perp B_{lx} = \frac{4\pi}{c} e n_{eo} v_{elz} \quad . \tag{3.15d}$$

In (3.9), ω_i^* is the ion-diamagnetic drift frequency. It follows that:

$$v_{i1x} = \frac{c}{aB_o}\left(E_{1y} - \frac{\kappa_B T_{io} ik_\perp n_{i1}}{en_{io}}\right) , \tag{3.10a}$$

$$v_{i1y} = \frac{(\nu_i - i\omega + i\omega_o)}{\Omega_i}\frac{c}{aB_o}\left(E_{1y} - \frac{\kappa_B T_{io} ik_\perp n_{i1}}{en_{io}}\right) - \frac{m_e}{m_i}\frac{\nu_{ei}}{\Omega_i}\frac{c}{aB_o}$$

$$x \frac{\kappa_B(T_{io}n_{i1} + T_{eo}n_{e1})}{en_{io}} ik_\perp , \tag{3.10b}$$

$$v_{e1x} = \frac{c}{B_o}\left(E_{1y} + \frac{\kappa_B T_{eo} ik_\perp n_{e1}}{en_{eo}}\right) , \tag{3.10c}$$

$$v_{e1y} = -\frac{m_e}{m_i}\frac{\nu_{ei}}{\Omega_i}\frac{c}{B_o}\frac{\kappa_B(T_{io}n_{i1} + T_{eo}n_{e1})}{en_{io}} ik_\perp$$

$$-\frac{m_e}{m_i}\frac{\nu_{en}}{\Omega_i}\frac{c}{B_o}\left(E_{1y} + \frac{\kappa_B T_{eo} ik_\perp n_{e1}}{en_{eo}}\right) . \tag{3.10d}$$

In (3.10a-b):

$$a \equiv 1 + \nu_i^2/\Omega_i^2 . \tag{3.11}$$

The second term in (3.10b) is an approximation which is reasonable provided $\nu_{en} \gg \nu_{ei}$ when $a \gg 1$. Under such circumstances, the contribution from diffusion due to electron-neutral and ion-neutral collisions is much larger than the diffusion resulting from electron-ion collisions.

In addition to the perpendicular electron currents, parallel electron currents contribute to the growth of modes. Parallel ion currents are much less important and are neglected here [Sperling, 1983d]. The parallel electron

$$\Omega_i = eB_o/m_i c \quad , \quad \nu_{ii} = \frac{\alpha'}{3 \times 10^7} \left(\frac{2}{A}\right)^{1/2} \frac{n_{eo}}{T_{io}^{3/2}} \quad ,$$

$$\nu_{ei} = \frac{\alpha'}{3.5 \times 10^5} \frac{n_{eo}}{T_{eo}^{3/2}} \quad ,$$

$$\alpha' = 23.4 - 1.15 \log_{10}(n_{eo}) + 3.45 \log_{10}(T_{eo}) \quad ,$$

$$\nu_{en} = 8.1 \times 10^{-8} T_e^{0.64} n_{no} \quad ,$$

$$\nu_{in} = 2.5 \times 10^{13} m_n n_{no} \qquad \text{for air ions} \quad . \tag{3.7}$$

All parameters are in cgs units except for temperatures which are in units of eV. The Boltzmann constant is $\kappa_B \approx 1.6 \times 10^{-12}$ ergs/eV. In (3.7), A, m_n, and n_{no} represent the ion atomic mass, neutral particle mass, and the neutral number density, respectively. The expression for ν_i includes contributions from both the ion-neutral collisions and ion-ion viscosity. In sufficiently dense ionospheric clouds, the ion-ion collision frequency, ν_{ii}, can be larger than the ion-gyrofrequency.

In (3.6a-b),

$$\omega_o = k_\perp u_{ioy} \quad , \quad u_{ioy} = \frac{c g_{ey}}{\nu_{in} B_o} \frac{\eta_{in}}{1 + \eta_{in}^2} \quad , \quad \eta_{in} = \frac{\nu_{in}}{\Omega_i} \quad , \tag{3.8}$$

and u_{ioy} is the y-directed drift velocity of individual ions. The y-component of the effective gravity is written as g_{ey}. Here, $\hat{z}$ and $\hat{y}$ are the unit vectors in the z- and y-directions, respectively.

Equations (3.6a-d) are solved with the assumption that:

$$\Omega_i \gg |\omega| \ , \ |\omega_o| \ , \ |\omega_i^*| \ , \ m_e \nu_{en}/m_i \ , \ m_e \nu_{ei}/m_i$$

$$\omega_i^* = k_\perp \frac{\kappa_B T_{io}}{m_i \Omega_i L_\perp} \quad . \tag{3.9}$$

The linear ion and electron velocities perpendicular to the background magnetic field and in response to the modes can be determined from the fluid equations:

$$-im_i n_{io}(\omega - \omega_o)v_{ily} = -\kappa_B T_{io} ik_\perp n_{il} + en_{io}E_{ly} - en_{io}v_{ilx}B_o/c$$
$$- m_i n_{io}\nu_i v_{ily} - m_e n_{eo}\nu_{ei}(v_{ily} - v_{ely}) \quad , \quad (3.6a)$$

$$-im_i n_{io}(\omega - \omega_o)v_{ilx} = q_i n_{io}v_{ily}B_o/c - m_i n_{io}\nu_i v_{ilx}$$
$$- m_e n_{eo}\nu_{ei}(v_{ilx} - v_{elx}) \quad , \quad (3.6b)$$

$$0 = -\kappa_B T_{eo} ik_\perp n_{el} - en_{eo}E_{ly} + en_{eo}v_{elx}B_o/c$$
$$- m_e n_{eo}\nu_{ei}(v_{ely} - v_{ily}) - m_e n_{eo}\nu_{en}v_{ely} \quad , \quad (3.6c)$$

$$0 = -en_{eo}v_{ely}B_o/c - m_e n_{eo}\nu_{ei}(v_{elx} - v_{ilx}) - m_e n_{eo}\nu_{en}v_{elx} \quad . \quad (3.6d)$$

In (3.6a-d) the subscript, o, indicates background parameters while the subscript, 1, indicates the response to the modes. Ion quantities are represented by the subscript, i, and the subscript, e, is used for electron quantities. The x- (y-) directed components of vectors are represented by the subscript x(y). The following symbols are also used in (3.6a-d): κ_B (Boltzmann constant), T (temperature), n (density), E (electric field), v (velocity), ν_i (effective ion collision frequency), ν_{ei} (electron-ion collision frequency), and ν_{en} (electron-neutral collision frequency). The magnitude of the electron charge is represented by the symbol, e. In (3.6a-d) explicit forms for ν_i and ν_{ei} can be written in the following way [Braginskii, 1965; Kilb, 1977]:

$$\nu_i = \nu_{in} + k_\perp^2 \theta_v \quad ,$$

$$\theta_v = \frac{\kappa_B T_{io}}{m_i \nu_{ii}} \frac{1.2P^2 + 2.23}{P^4 + 4.03P^2 + 2.33} \quad , \quad P = \frac{2\Omega_i}{\nu_{ii}} \quad ,$$

3.2 DISPERSION RELATION

To derive the linear dispersion relation for E x B gradient drift and Rayleigh-Taylor eigenmodes along the geomagnetic field, it is sufficient to consider a low beta, slab-geometry plasma model with a z-directed constant magnetic field with strength, B_o, a density profile which depends on the x-coordinate, and a y-directed constant ambient electric field with strength, E_{oy}, in the neutral-wind frame of reference. In the neutral-wind frame of reference, electrons and ions have an x-directed E x B velocity of size cE_{oy}/B_o. Plasma parameters are permitted to vary in the z-direction. The collective oscillations are assumed to have the plane wave form, $\exp[i(k_\perp y - \omega t)]$, with $k_\perp$, ω, and t being the perpendicular wave number, frequency, and time, respectively. The z-dependence of the oscillations is determined self-consistently.

The plasma model includes neither ambipolar electric fields nor parallel electron currents as both these phenomena can be strongly coupled [Perkins et al., 1973] and undoubtedly have complicated three-dimensional dependences. For example, parallel variations in the perpendicular density gradient would imply that the perpendicular electrostatic potential, driven by ion-neutral diffusion, must be a function of the coordinate along the geomagnetic field and so parallel electric fields are present. Indeed, (1.21a-b) of Chapter 1 demonstrate that induced electric fields have strong spatial variations for even the relatively simple case of a uniform ellipsoidal, plasma cloud surrounded by a uniform plasma. Furthermore, plasma "equilibrium" is not an obvious nor proven requirement for the formation of striations [L. Wittwer, private communication, 1983]. An important unresolved issue is the understanding of how three-dimensional effects impact the basic plasma state upon which striations evolve.

Fluid modes with frequencies much smaller than the ion-gyrofrequency are considered. As usual with a fluid treatment, it is assumed that electron and ion mean free paths for collision are much smaller than the scale lengths for parallel spatial variations and electron- and ion-gyroradii are much smaller than the scale lengths for perpendicular spatial variations [Boyd and Sanderson, 1969].

ion-gravitational drifts are stabilizing. Under such a circumstance, the possibility for instability is confined to the ionosphere where the ion-Pedersen drift is finite. As indicated by entry 4 in Table 3.1, there is stability everywhere if both the ion-Pedersen drift and the combination of ion-centrifugal and ion-gravity drifts are stabilizing.

To determine the relative importance of collisionless and collisional instabilities in late-time phenomenology, a second-order linear differential equation is derived. The equation determines eigenvalues (i.e., temporal frequencies in complex space) and the associated eigenmode structure of the instabilities along geomagnetic field. The differential equation is solved for parameters and geometry appropriate to nuclear plumes.

It is demonstrated that for a specified late-time plasma configuration, striations tend to develop with larger scale sizes, perpendicular to the geomagnetic field, at higher altitudes than at lower altitudes. Electromagnetic effects are shown to be important for modes with smaller perpendicular wave numbers (i.e., $\lesssim 1$ km^{-1}) and ion-viscosity is important for modes with larger perpendicular wave numbers (i.e., $\gtrsim 4$ km^{-1}). Analytic criteria are given for the perpendicular wave numbers of the instability at which the real part of the frequency is equal to the growth rate and at which there is complete stabilization. It is argued that the equating of real part of the frequency and the growth rate gives a meaningful estimate of the perpendicular wave number at which striation "freezing" occurs. An appropriate algorithm, suitable for implementation in modeling codes, is given for the perpendicular wave number at "freezing." Simple empirical estimates for the parallel spatial extent of the striation density fluctuations are described.

This chapter is divided into five sections. Section 3.2 derives the differential equation which is the dispersion relation for the striation instabilities along the geomagnetic field. Section 3.3 gives applications for modeling the formation of striations in late-time HANE plasmas. Section 3.4 presents results appropriate to late-time HANE phenomenology. Section 3.5 is a summary and gives concluding remarks.

Table 3.1. The four possible combinations of $\vec{g}_{cg} \cdot \nabla n_{eo}$ and $\vec{g}_E \cdot \nabla n_{eo}$ as they relate to the possibility for instability. The case of $\vec{g}_{cg} \cdot \nabla n_{eo} < 0$ and $\vec{g}_E \cdot \nabla n_{eo} < 0$ is emphasized in this chapter.

	$\vec{g}_E \cdot \nabla n_{eo} < 0$ Destabilizing	$\vec{g}_E \cdot \nabla n_{eo} > 0$ Stabilizing
$\vec{g}_{cg} \cdot \nabla n_{eo} < 0$ destabilizing	1. Unstable at both high and low altitudes	2. Collisionless instability at high altitude
$\vec{g}_{cg} \cdot \nabla n_{eo} > 0$ stabilizing	3. Collisional instability at low altitude	4. Stable everywhere

$$\bar{\gamma} = \left(\frac{|\vec{g}_{cg}|}{L_\perp} \right)^{1/2} \quad . \tag{3.4}$$

In (3.4) $L_\perp$ is the scale length of the perpendicular density gradient. At lower altitudes within the ionosphere where the ion-neutral collision frequency is large compared to the growth rate, the characteristic growth rate of the instability has the form appropriate to collisional gradient-drift or collisional Rayleigh-Taylor modes [Völk and Haerendel, 1971; Perkins et al., 1973]:

$$\gamma_0 = \frac{|\vec{g}_e|}{\nu_{in} L_\perp} \quad . \tag{3.5}$$

For the present purpose, it is sufficient to note that $\bar{\gamma} \propto L_\perp^{-0.5}$ while $\gamma_0 \propto L_\perp^{-1}$. This suggests that the collisionless instability is favored by long perpendicular scale lengths in the density profile (i.e., large $L_\perp$) while the collisional mode is favored by short scale lengths in the density profile (i.e., small $L_\perp$). Now in general, the actual relative significance of collisionless and collisional modes depends on values for parameters and geometry. For example, consider $|\vec{g}_{cg}| = 5 \times 10^2$ cm/s^2 in (3.4) and $|\vec{g}_e|/\nu_{in} = 1 \times 10^4$ cm/s in (3.5). If $L_\perp = 2 \times 10^6$ cm then 1.6×10^{-2} s^{-1} $= \bar{\gamma} > \gamma_0 = 5 \times 10^{-3}$ s^{-1}, but if $L_\perp = 1 \times 10^5$ cm then 7.1×10^{-2} s^{-1} $= \bar{\gamma} < \gamma_0 = 1 \times 10^{-2}$ s^{-1}. Now consider $|\vec{g}_{cg}| = 1 \times 10^3$ cm/s^2 in (3.4) and $|\vec{g}_e|/\nu_{in} = 1 \times 10^4$ cm/s. It then follows that $\bar{\gamma} \geq \gamma_0$ for $L_\perp \geq 1 \times 10^5$ cm. These simple quantitative examples illustrate the potentially important role for collisionless instabilities in whatever structuring occurs in late-time nuclear plumes.

Examination of (3.2) indicates various possibilities for instability depending upon the sign of $\vec{g}_{cg} \cdot \nabla n_{eo}$ and $\vec{g}_E \cdot \nabla n_{eo}$. These possibilities are summarized in Table 3.1. The emphasis in this report is placed on the case when the ion-Pedersen drift and the combination of centrifugal acceleration and gravity permit the possibility for instability at both high and low altitudes. This case is specified as entry 1 in Table 3.1. Entry 2 of Table 3.1 illustrates that instability tends to be confined to higher altitudes if the ion-Pedersen drift is stabilizing. Conversely, entry 3 in Table 3.1 shows the case when the ion-Pedersen drift is destabilizing but the combination of ion-centrifugal and

In (3.1) the following symbols are used: R (distance from the center of the earth), $w_{\parallel}$ (plasma speed along the geomagnetic field), θ (geomagnetic colatitude), $\hat{e}_{\phi}$ (unit vector in the geomagnetic eastward direction), $\vec{B}_o$ (geomagnetic field), and B_o (magnitude of the geomagnetic field).

Away from the geomagnetic poles, the geomagnetic field has a component in the direction of the geomagnetic colatitude. Hence, the component of gravity perpendicular to the geomagnetic field can contribute to structuring by a collisionless Rayleigh-Taylor mechanism [Kadomtsev, 1965; Hudson and Kennel, 1975; Kilb, 1977].

The "effective gravity," $\vec{g}_e$, which drives striation growth at late times is permitted to consist of centrifugal, gravitational, and neutral wind contributions and so $\vec{g}_e$ has the following form,

$$\vec{g}_e = \vec{g}_{cg} + \vec{g}_E \tag{3.2}$$

with

$$\vec{g}_{cg} = \vec{g}_c + \vec{g}_{\perp} \quad , \quad \vec{g}_E = \nu_{in} \frac{\vec{B}_o}{B_o} \times \frac{c\vec{E}_o}{B_o} \quad . \tag{3.3}$$

In (3.2) and (3.3) the symbols are: ν_{in} (ion-neutral collision frequency), $\vec{E}_o$ (applied electric field), c (speed of light), and $\vec{g}_{\perp}$ (gravitational acceleration perpendicular to the geomagnetic field). Equation (3.3) is appropriate to a frame of reference in which a uniform neutral wind is stationary. Define the electron density to be n_{eo}. Since Rayleigh-Taylor instabilities require $\vec{g}_{cg} \cdot \nabla n_{eo} < 0$, gravity tends to destabilize the underside of nuclear plumes on lower L shells, while the centrifugal force, resulting from the curvature in the geomagnetic field, tends to promote stabilization. Conversely, on the upper side of a nuclear plume, on higher L shells, the centrifugal force is destabilizing while gravity is stabilizing.

At high altitudes where the ion-neutral collision frequency is small compared to the growth rate, the characteristic growth rate of the instability has the form appropriate to collisionless Rayleigh-Taylor modes [Kadomtsev, 1965; Hudson and Kennel, 1975]:

demonstrated that the form for k_t can be obtained by balancing the applied electric field (in the neutral-wind frame of reference) and the ion pressure gradient within a striation [see (G12) in Appendix G]. Under such a circumstance, it is not necessary for there to be induced electric fields in order for current-density fields to be nondivergent. In fact, the form for k_t suggests striation "freezing" represents the balance between two effects: (1) the tendency for bifurcation and (2) the tendency of ions to approach a state of thermodynamic equilibrium with applied electric fields. When ions are in thermodynamic equilibrium with applied electric fields, electrons are the primary current carriers in the frame of reference where the basic plasma state is stationary. Moreover, ion viscosity and ion thermal conductivity drive ions toward thermodynamic equilibrium and have no effect on ions when thermodynamic equilibrium is attained. Because the form and magnitude for k_t appears to be reasonable for barium clouds, it is assumed here that similar calculations for the high-altitude nuclear environment are also reasonable.

If $\Psi(z)$ can be approximated as having a plane-wave dependence on z, i.e., $\exp(ik_{\|}z)$, then by the replacement

$$\frac{d}{dz} \rightarrow ik_{\|} \tag{3.31}$$

the differential equation form of the non-local dispersion relation, equations (3.21) and (3.22), reduces to the local algebraic dispersion relation given by (16) of Glassman and Sperling [1983],

$$0 = \left[\frac{(\omega - \omega_o + i\nu_i)\lambda_i + \omega_i^*}{\omega - \omega_o + i\nu_c + i\nu_i\lambda_i} - \frac{\omega_i^*(\omega + i\delta)}{\omega(\omega + i\delta + i\nu_c)}\right]$$

$$\cdot\left[\frac{i\omega_e^2}{\omega\nu_e}\frac{(\omega + i\nu_c)}{(\omega + i\nu_c + i\delta)}\left(1 - \frac{\omega_e^*}{\omega}\right) - \frac{k_\perp^2c^2}{\omega^2}\right] + i\frac{T_{io}}{T_{eo}}\frac{\delta}{(\omega + i\nu_c + i\delta)}$$

$$\cdot\left(1 - \frac{\omega_e^*}{\omega}\right)\left[\frac{\omega_e^2\omega_e^*}{\nu_e\omega^2}\frac{c}{(\omega + i\nu_c + i\delta)} - \frac{k_\perp^2c^2}{\omega^2}\right] \tag{3.32}$$

where

$$\delta = \frac{k_{\parallel}^2 \kappa_B T_{eo}}{m_e \nu_e} \quad . \tag{3.33}$$

For spread-F and barium-cloud plasmas, Glassman and Sperling [1983] analyze the solution to the local dispersion relation, (3.32), while Sperling and Glassman [1983] compare the solution to the nonlocal dispersion relation, (3.21), with the solution to the local dispersion relation. A major conclusion is that the frequency becomes increasingly insensitive to the parallel wave number as $k_\perp$ increases. Hence, a local flute estimate for the frequency of the instability is very reasonable for sufficiently large $k_\perp$.

Although the eigenvalue ω can be well approximated using the flute approximation for large $k_\perp$, it does not mean that the eigenfunction, ψ, is independent of z. Quite to the contrary, ψ is strongly peaked in z and is confined to a spatial region where the background plasma parameters do not change too substantially [Sperling and Glassman, 1983]. In fact, a local flute estimate for the growth rate should be expected to be reasonable when $|k_{\parallel} L_z| \gtrsim 1$ where L_z is the characteristic length for parallel variations in background plasma parameters [Kadomtsev, 1965].

In the flute limit (i.e., $k_{\parallel} = 0$), (3.32) reduces to

$$0 = \frac{[\omega_f(k_\perp,z) - \omega_o + i\nu_i]\lambda_i + \omega_i^*}{\omega_f(k_\perp,z) - \omega_o + i\nu_c + i\nu_i\lambda_i} - \frac{\omega_i^*}{\omega_f(k_\perp,z) + i\nu_c} \tag{3.34}$$

which in turn can be written as a quadratic

$$0 = [\omega_f(k_\perp,z)]^2 + \xi_1\omega_f(k_\perp,z) + \xi_2 \quad . \tag{3.35}$$

In (3.34) and (3.35), $\omega_f(k_\perp,z)$ is the eigenvalue as determined from the flute approximation and is a function of $k_\perp$ and z. In (3.35)

$$\xi_1 = -\omega_o + i\nu_i + i\nu_c$$

$$\xi_2 = \frac{\omega_o\omega_i^*}{\lambda_i} - \nu_i\nu_c - i\nu_i\omega_i^* - i\omega_o\nu_c \quad . \tag{3.36}$$

The solution to (3.35) is

$$\omega_f(k_\perp,z) \equiv -\frac{\xi_1}{2} \pm \left(\frac{\xi_1^2}{4} - \xi_2\right)^{1/2} \quad . \tag{3.37}$$

Comparisons between (3.37) and numerical solution for ω using (3.21) verify that for a sufficiently large value of $k_\perp$

$$\omega \approx \omega_f(k_\perp,z_m) \quad . \tag{3.38}$$

In (3.38) z_m is the value of z which satisfies the condition that

$$R(k_\perp,z) \equiv \mathrm{Im}[\omega_f(k_\perp,z)] - \mathrm{Re}[\omega_f(k_\perp,z)] \tag{3.39}$$

is a maximum, i.e.,

$$0 = \frac{\partial R(k_\perp,z_m)}{\partial z_m} \quad , \quad 0 < \frac{\partial^2 R(k_\perp,z_m)}{\partial z_m^2} \quad . \tag{3.40}$$

The ability of $\omega_f(k_\perp,z_m)$ to closely approximate the actual eigenvalue ω suggests a simple algorithm for estimating an outer-scale wave number without actually having to solve the differential equation, (3.21). If it is hypothesized that appreciable striations require $\mathrm{Im}(\omega) \geq |\mathrm{Re}(\omega)|$, then k_t can be identified with the outer-scale wave number. Equations (3.39), (3.40), and the constraint

$$0 = R(k_t,z_m) \tag{3.41}$$

then completely determine k_t. The algorithm, used to determine k_t, is summarized in Figure 3.1.

In Appendix G explicit expressions are derived for not only k_t but also the perpendicular wave number appropriate to zero growth rate (i.e., k_s). Equation (3.37) is used in the evaluation of the various relevant expressions.

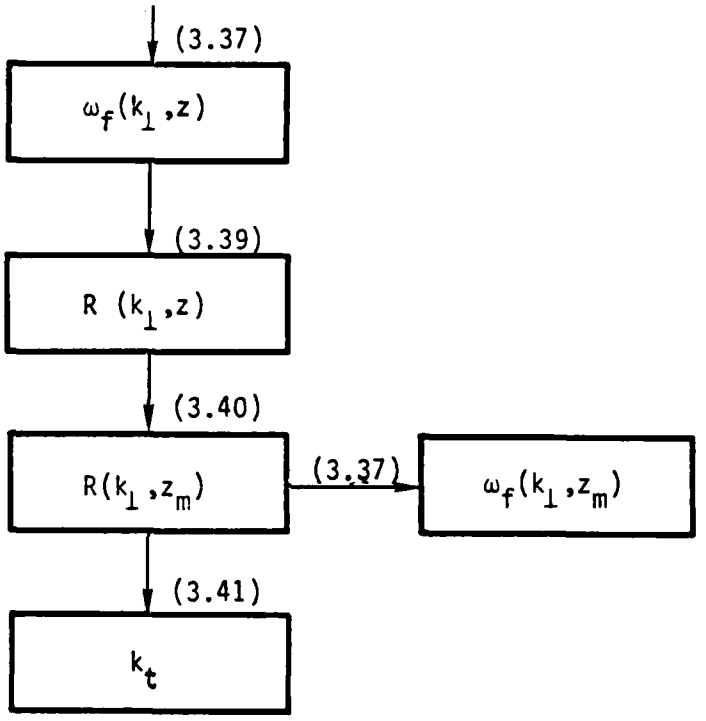

Figure 3.1. Algorithm for estimating the outer-scale wave number, k_t. The numbers designate equations in the text.

In addition to being able to make reasonable estimates of actual eigenvalues in the limit of large $k_\perp$, it is also possible to make good estimates for the spatial extent of the parallel density variations of linear striation eigenmodes (i.e., $|n_{e1}|$) when $k_\perp$ is large. When the region of growth is peaked at high altitude, above the ionosphere, then

$$|n_{e1}| \approx n_{f1} \equiv K|\alpha n_{eo}\omega_f(k_\perp,z)| \tag{3.42}$$

with α specified by (3.17b) and K a constant. However, if the region of growth is confined to lower altitudes, within the ionosphere, then

$$|n_{e1}| \approx n_{f2} \equiv n_{f1}\frac{\nu_{in}/|\omega_f(k_\perp,z)|}{1+\nu_{in}/|\omega_f(k_\perp,z)|} \quad . \tag{3.43}$$

The expressions for n_{f1} and n_{f2} are summarized in Table 3.2. If the formation of striations can be conceptualized as a mechanism for diffusing late-time nuclear plasmas then n_{f1} and n_{f2} provide estimates for the locations, along the geomagnetic field, where the diffusion occurs.

3.4 NUMERICAL RESULTS

In order to determine the eigenvalues and eigenmodes appropriate to late-time, high-altitude, nuclear plasmas, (3.21) has been explicitly solved using a hybrid collocation-Galerkin method [Sperling and Glassman, 1983] and plasma profiles appropriate to nuclear plumes [R. E. Stoeckly and R. W. Kilb, private communication, 1981; W. W. White, private communication, 1982]. The parameters and geometry for the five cases are summarized in Table 3.3. The first four cases differ only in the values of two parameters: the magnitude of the perpendicular density-gradient scale length, $L_\perp$, and the effective E x B velocity, $|\vec{g}_E|/\nu_{in}$. For Cases 1-4, ion-gravity and ion-curvature drifts contribute to instability (i.e., $\vec{g}_{cg} \neq 0$). Case 5 is identical to Case 1 except that both the ion-gravity and ion-curvature drifts are artificially set equal to zero (i.e., $\vec{g}_{cg} = 0$) and so instability can only be driven at lower altitudes, in the ionosphere where ion-Pedersen currents can be appreciable. Case 5 is

Table 3.2. Empirical estimates, n_{f1} and n_{f2}, for $|n_{e1}|$ as specified by (3.42) and (3.43). The estimates are algebraic and do not require solving the full second-order differential equation. The expression for n_{f1} is appropriate to the maximum value of $|\omega_f(k_\perp,z)|$ occurring above the ionosphere and the expression for n_{f2} is appropriate to the maximum value for $|\omega_f(k_\perp,z)|$ occurring well within the ionosphere.

Estimate	Criterion for Validity
$n_{f1} = Kn_{eo}\lvert\alpha\omega_f(k_\perp,z)\rvert$	$\dfrac{\nu_{in}}{\lvert\omega_f(k_\perp,z)\rvert} < 1$ at *maximum of* $\lvert\omega_f(k_\perp,z)\rvert$
$n_{f2} = Kn_{eo}\lvert\alpha\omega_f(k_\perp,z)\rvert \cdot \dfrac{\nu_{in}/\lvert\omega_f\rvert}{1+\nu_{in}/\lvert\omega_f\rvert}$	$\dfrac{\nu_{in}}{\lvert\omega_f(k_\perp,z)\rvert} > 1$ at maximum of $\lvert\omega_f(k_\perp,z)\rvert$

Table 3.3. Plasma parameters for the cases discussed in Section 3.4 and Appendix H. Subscripts 1 and 2 represent ions in the unstable and stable plasmas, respectively. For all cases $n_{1o}(z) = 0.5\ \bar{n}_{1o}\left\{1 + \tanh\left[(z - z_1)/L_1\right]\right\} + \bar{n}_{2o}$, $n_{no}(z) = \bar{n}_{no}\ (L_n/z)^{7.75}$, and $L_\perp(z) = \bar{L}_\perp \left\{1 + \exp\left[-2\ (z - z_1)/L_1\right]\right\}\left\{1 + \exp\left[2\ (z - z_2)/L_2\right]\right\}$. The atomic mass of the ions is assumed to be 20. The distance z is in kilometers. The entries for γ_o and $\bar{\gamma}$ assume that the perpendicular density-gradient scale length is $\bar{L}_\perp$. The altitude, h, can be related to z by h = 0.92 z.

	Case 1	Case 2	Case 3	Case 4	Case 5
$\bar{n}_{1o}$ (cm^{-3})	1×10^{7}	1×10^{7}	1×10^{7}	1×10^{7}	1×10^{7}
z_1 (km)	2.5×10^{2}	2.5×10^{2}	2.5×10^{2}	2.5×10^{2}	2.5×10^{2}
L_1 (km)	3.5×10^{1}	3.5×10^{1}	3.5×10^{1}	3.5×10^{1}	3.5×10^{1}
$\bar{n}_{2o}$ (cm^{-3})	1×10^{4}	1×10^{4}	1×10^{4}	1×10^{4}	1×10^{4}
$\bar{n}_{no}$ (cm^{-3})	4.18×10^{8}	4.18×10^{8}	4.18×10^{8}	4.18×10^{8}	4.18×10^{8}
L_n (km)	3×10^{2}	3×10^{2}	3×10^{2}	3×10^{2}	3×10^{2}
$\bar{L}_\perp$ (km)	1.5×10^{1}	1.5×10^{1}	1.0	1.0	1.5×10^{1}
z_2 (km)	2×10^{3}	2×10^{3}	2×10^{3}	2×10^{3}	2×10^{3}
L_2 (km)	1×10^{3}	1×10^{3}	1×10^{3}	1×10^{3}	1×10^{3}
B_o(G)	0.3	0.3	0.3	0.3	0.3
$\lvert\vec{g}_E\rvert/\nu_{in}$ (km/s)	0.1	1.0	0.1	1.0	0.1
γ_o (s^{-1})	6.7×10^{-3}	6.7×10^{-3}	6.7×10^{-3}	6.7×10^{-3}	6.7×10^{-3}
$\lvert\vec{g}_{cg}\rvert$ (km/s^2)	4.3×10^{-3}	4.3×10^{-3}	4.3×10^{-3}	4.3×10^{-3}	0
$\bar{\gamma}$ (s^{-1})	1.7×10^{-2}	1.7×10^{-2}	1.7×10^{-2}	1.7×10^{-2}	0
T_{1o} (eV) = T_{2o} (eV)	0.1	0.1	0.1	0.1	0.1
T_{eo} (eV)	0.1	0.1	0.1	0.1	0.1

discussed in Appendix H. The expressions and parameters shown in Table 3.3 are based upon information appropriate to altitudes above 100 km. The table indicates that the plasma density is largest (i.e., $\sim 1 \times 10^7$ cm^{-3}) for altitudes above $\sim 2.5 \times 10^2$ km and that the perpendicular density-gradient scale length is smallest (i.e., ~ 15 km for Cases 1, 2, and 5 and ~ 1 km for Cases 3 and 4) for altitudes between $\sim 2.5 \times 10^2$ km and 2×10^3 km.

Now for intermediate latitudes (e.g., $\theta = 46^0$) and an altitude of 1×10^3 km, $R \approx 7.4 \times 10^3$ km in (3.1). If in addition $w_{\parallel} \approx 5$ km/s and the inverse-square law for gravity is used [Kilb, 1977], (3.1) suggests that a reasonable value for $|\vec{g}_{cg}|$ is 4.3×10^{-3} km/s^2. This value of $|\vec{g}_{cg}|$ is specified in Table 3.3.

Figures 3.2a, 3.2b, 3.2c, and 3.2d are graphs of ω (s^{-1}) versus $k_{\perp}$ (km^{-1}) for Cases 1, 2, 3, and 4, respectively. The perpendicular wave number for maximum growth rate varies between 6 km^{-1} for Case 1, the most weakly driven of the four cases, to about 30 km^{-1} for Case 4, the most strongly driven of the four cases. The peak growth rate shifts to shorter perpendicular wavelengths as the strength of the driving currents increases relative to classical ambipolar diffusion.

As $k_{\perp}$ is decreased from the value for maximum growth, parallel currents act to reduce the striation growth rate. But as $k_{\perp}$ becomes still smaller, the growth rate levels off at a fraction of the maximum growth rate. This coincides with the electromagnetic effects becoming important. If only electrostatic terms are kept in the solution, the growth rate continues to decline with decreasing $k_{\perp}$, as shown in Appendix H.

As $k_{\perp}$ is increased from the value for maximum growth, the growth rate is decreased and stability is eventually attained because of the combination of ion-viscosity and classical ambipolar diffusion. The contribution of ion-viscosity to the growth rate is examined in Appendix H. As $k_{\perp}$ increases, the real part of ω grows rapidly and equals the growth rate for $k_{\perp} = k_t$. As discussed in section 3.3, k_t is hypothesized to be the effective outer scale wave number appropriate to the "freezing" of striations. In Appendix G, it is shown that k_t can be appreciably smaller than the perpendicular wave number appropriate to absolute stabilization, k_s, when $\omega_i^* \gg \nu_c$. Thus, it is in Cases 3 and 4

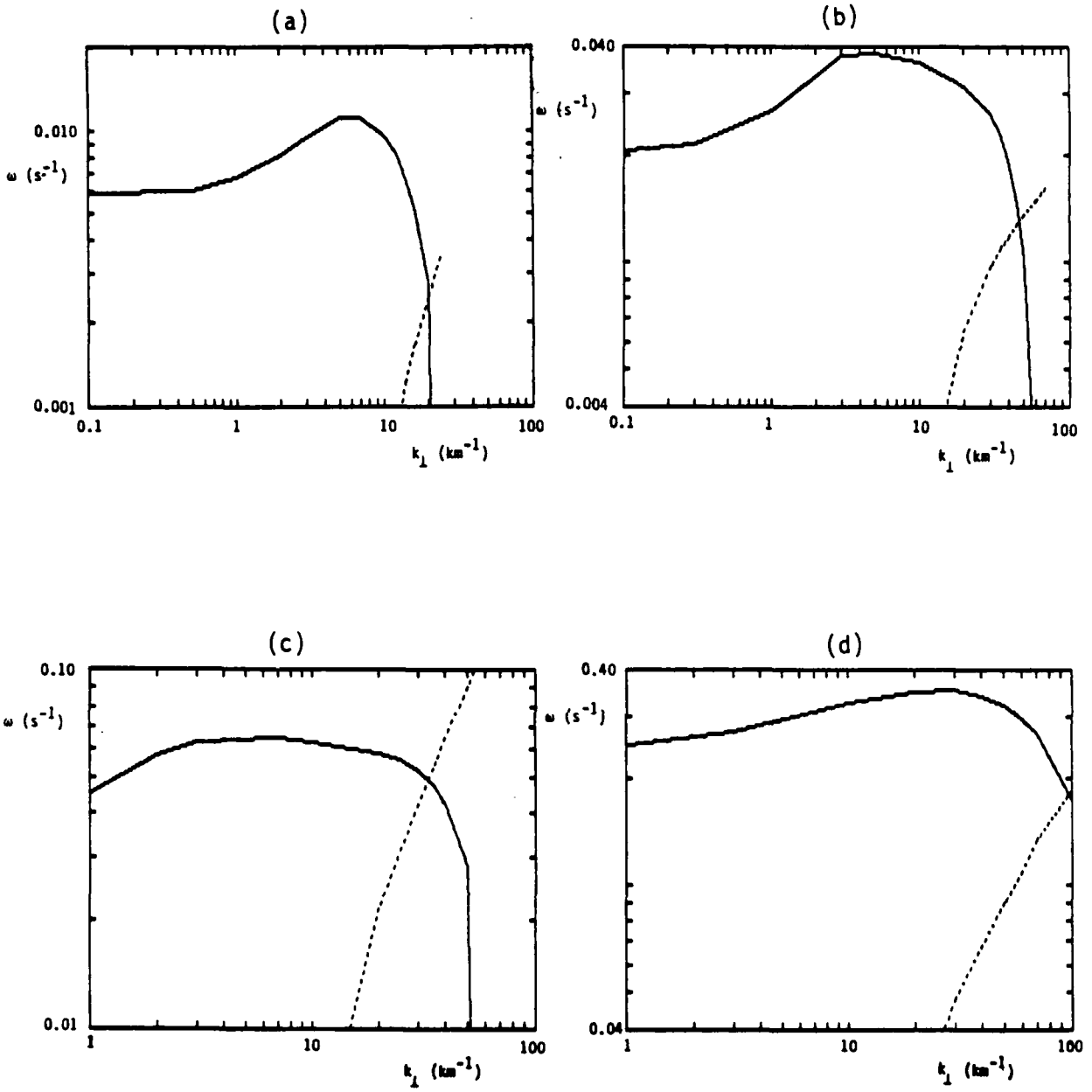

Figure 3.2. $\omega\ (s^{-1})$ versus $k_\perp\ (km^{-1})$ for (a) Case 1, (b) Case 2, (c) Case 3, and (d) Case 4. The solid and dashed lines designate the growth rate and real frequency, respectively.

(Figures 3.2c and 3.2d), where $L_\perp$ is the smallest and ω_i^* is largest for specified $k_\perp$, that the effect of $\mathrm{Re}(\omega)$ has the greatest effect on differentiating between k_t and k_s. The values for k_t generated using the flute approximation algorithm described in section 3.3 are 20, 60, 35, and 110 km^{-1} for Cases 1, 2, 3, and 4, respectively. This agrees well with the more exact results shown in Figure 3.2 (i.e., $k_t \approx$ 20, 50, 35, and 100 km^{-1} for Cases 1, 2, 3, and 4, respectively).

It was pointed out in section 3.3 that as $k_\perp$ becomes large, the solution of the local dispersion relation, (3.32), becomes increasingly insensitive to $k_\parallel$. The density of modes in the phase space of effective parallel wave numbers is high and so it is not surprising that the numerical determination of eigenmodes and eigenvalues becomes more difficult for larger values of $k_\perp$ (especially for $k_\perp \gtrsim k_t$). For $k_\perp \gtrsim k_t$, the eigenvalues are rather insensitive to the large-scale variation of plasma parameters along the geomagnetic field.

Figures 3.3a, 3.3b, 3.3c, and 3.3d are graphs of $|E_{1y}|/k_\perp$ versus z (km) for Cases 1, 2, 3, and 4, respectively. Curves for several different values of $k_\perp$ (km^{-1}) are plotted in each figure. As in the nonnuclear examples discussed by Sperling and Glassman [1983], the striation eigenmodes become more localized along the geomagnetic field as the perpendicular wave number becomes larger. Ion-polarization currents are essential to the localization at higher altitudes where ion-Pedersen currents are negligible [Sperling, 1983e]. Evidently in late-time HANE plasmas, localized disturbances along the geomagnetic field generally lead to a localized response and so the geomagnetic-field lines are not equipotentials. The peaks of the eigenmodes shift to lower altitudes as the perpendicular wave number increases. This effect is most evident in Figure 3.3a (Case 1) and in Figure 3.3c (Case 3), the two cases corresponding to the smaller values of $|\vec{g}_E|/\nu_{in}$ in Table 3.3. Cases 1 and 3 show a tendency for collisionless instabilities driven by ion-gravity and ion-curvature drifts at higher altitudes above the neutral atmosphere. For Case 1 (Figure 3.3a) the eigenmodes appear to be especially collisionless and peaked at higher altitudes for $k_\perp$ not too near stabilization. Now recall that the characteristic growth rates go as $L_\perp^{-1/2}$ and $L_\perp^{-1}$ for collisionless and collisional instabilities, respectively [cf, (3.4) and (3.5)]. In comparing Figures 3.3a and 3.3c, it is then reasonable that the modes in Case 1 (Figure 3.3a) with $L_\perp$ = 15 km tend to be more collisionless and extend to higher altitudes than in Case 3 (Figure 3.3c) with $L_\perp$ = 1 km. Similarly, the

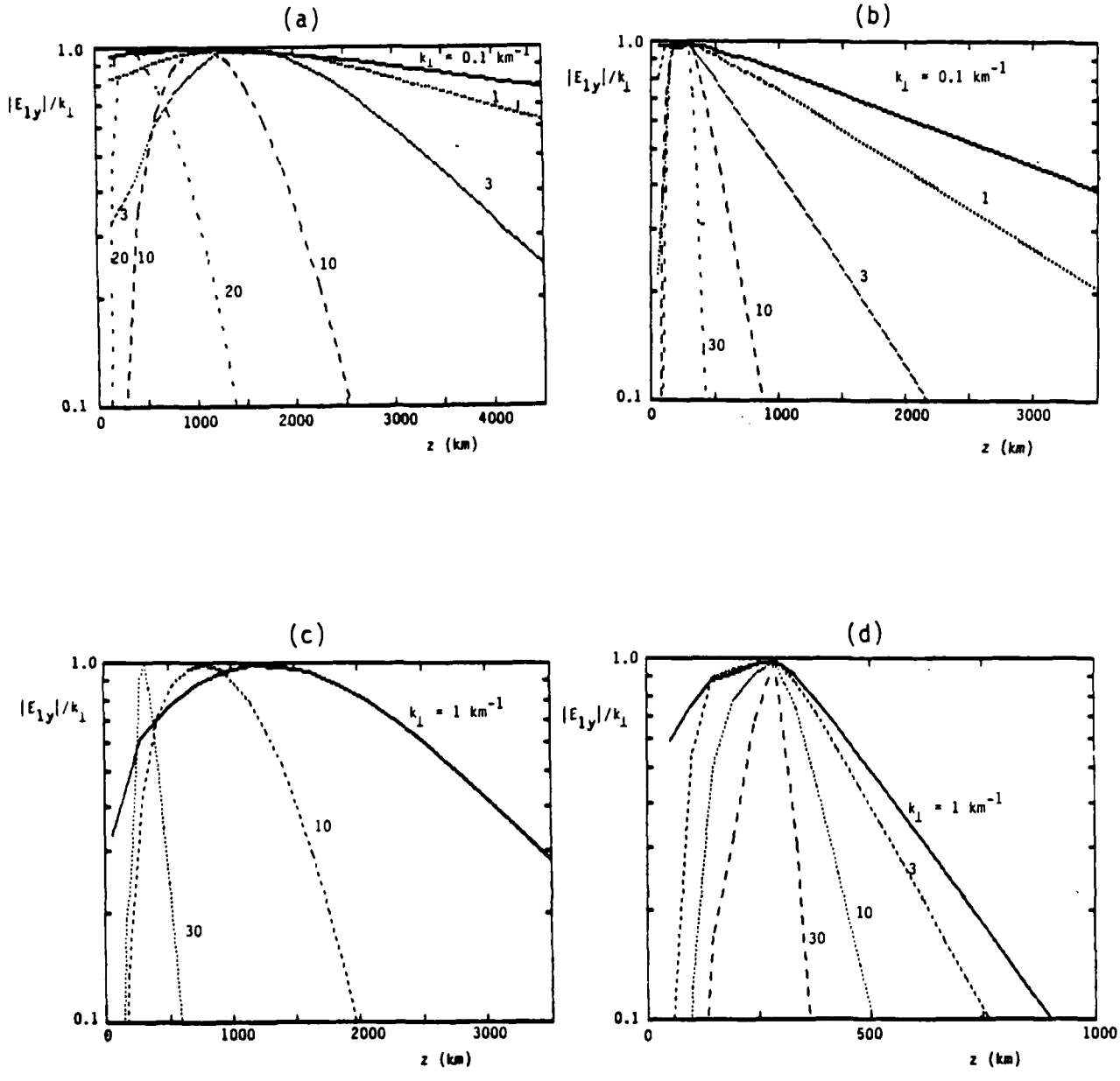

Figure 3.3. $|E_{1y}|/k_\perp$ versus z (km) for various $k_\perp$ (km^{-1}) and for (a) Case 1, (b) Case 2, (c) Case 3, and (d) Case 4. Each of the curves are in normalized dimensionless units.

eigenmodes shown in Figure 3.3b (Case 2) extend to higher altitudes than in Figure 3.3d (Case 4). The tendency for the peak of the eigenmodes to shift to lower altitudes as perpendicular wave number increases means that striations at higher altitudes will tend to have larger perpendicular scale sizes than striations at lower altitudes. It also means that for the case when both $\vec{g}_E$ and $\vec{g}_{cg}$ are both finite, the eigenmodes become more collisional and tend to peak at lower altitudes as $k_\perp$ increases and approaches k_t. Hence, in Appendix G, formulas for k_t are reasonably derived assuming the collisional limit when ion-neutral collisions are important. The high altitude peaking of Case 1 and its relation to ion-Pedersen versus ion-gravity and ion-curvature drifts is explored further in Appendix H.

The solutions to (3.35) [i.e., $\omega_f\ (k_\perp, z)\ (s^{-1})$] are plotted as a function of z (km) in Figures 3.4a, 3.4b, 3.4c, and 3.4d, for Cases 1, 2, 3, and 4, and $k_\perp$ values of 10, 30, 30, and 70 km^{-1}, respectively. The $k_\perp$ values are chosen to be larger than that appropriate to maximum growth but smaller than k_t. The values for z_m can be calculated from (3.39) and (3.40) and are approximately 690, 280, 280, and 260 km for Cases 1, 2, 3, and 4, respectively. The values of z_m roughly match the appropriate values for z where $|E_{1y}|/k_\perp$ are maximum in Figures 3.3a-d.

The approximate eigenvalues [i.e., $\omega_f\ (k_\perp, z_m)\ (s^{-1})$], deduced from (3.35), (3.39), and (3.40) are plotted as dashed lines versus $k_\perp\ (km^{-1})$ in Figures 3.5a, 3.5b, 3.5c, and 3.5d, for Cases 1, 2, 3, and 4, respectively. The solid lines in Figures 3.5a-d are $\omega(s^{-1})$ versus $k_\perp\ (km^{-1})$, replotted from Figures 3.2a-d. The curves for $\omega_f\ (k_\perp, z_m)$ and ω become especially close for $k_\perp \gtrsim k_t$. This demonstrates that the flute approximation yields accurate estimates for the eigenvalues when $k_\perp$ becomes large enough. For small values of $k_\perp$, eigenmodes sample large variations in background plasma parameters. $Im[\omega_f(k_\perp, z_m)]$ then overestimates the growth rate as parallel electron currents act to short-circuit the perpendicular electric fields in eigenmodes.

Figures 3.6a, 3.6b, 3.6c, and 3.6d are plots of $|n_{e1}|$, n_{f1}, and n_{f2} versus z (km) for Cases 1, 2, 3, and 4, respectively. Expressions for n_{f1} and n_{f2} are given by (3.42) and (3.43), respectively. The empirical estimates, n_{f1} for Case 1 and n_{f2} for Cases 2, 3, and 4, give reasonable approximations to $|n_{e1}|$ particularly at low altitudes where $|n_{e1}|$, n_{f1}, and n_{f2} mirror the spatial variation in n_{eo}.

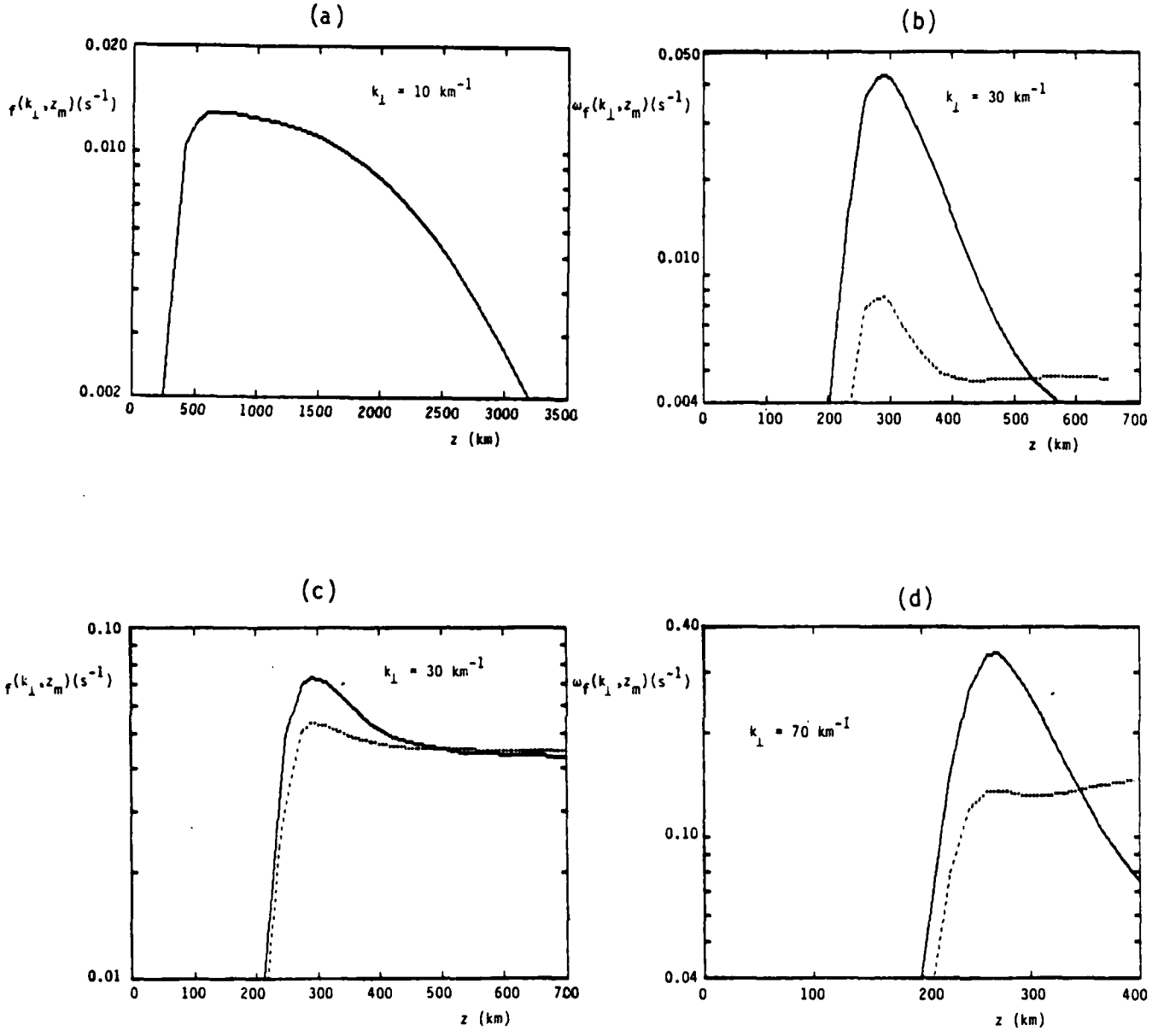

Figure 3.4. ω_f $(k_\perp, z_m)$ versus z (km) for (a) Case 1, (b) Case 2, (c) Case 3, and (d) Case 4. Specific values of $k_\perp$ (km^{-1}) are assumed. The solid and dashed lines designate the growth rate and real frequency, respectively.

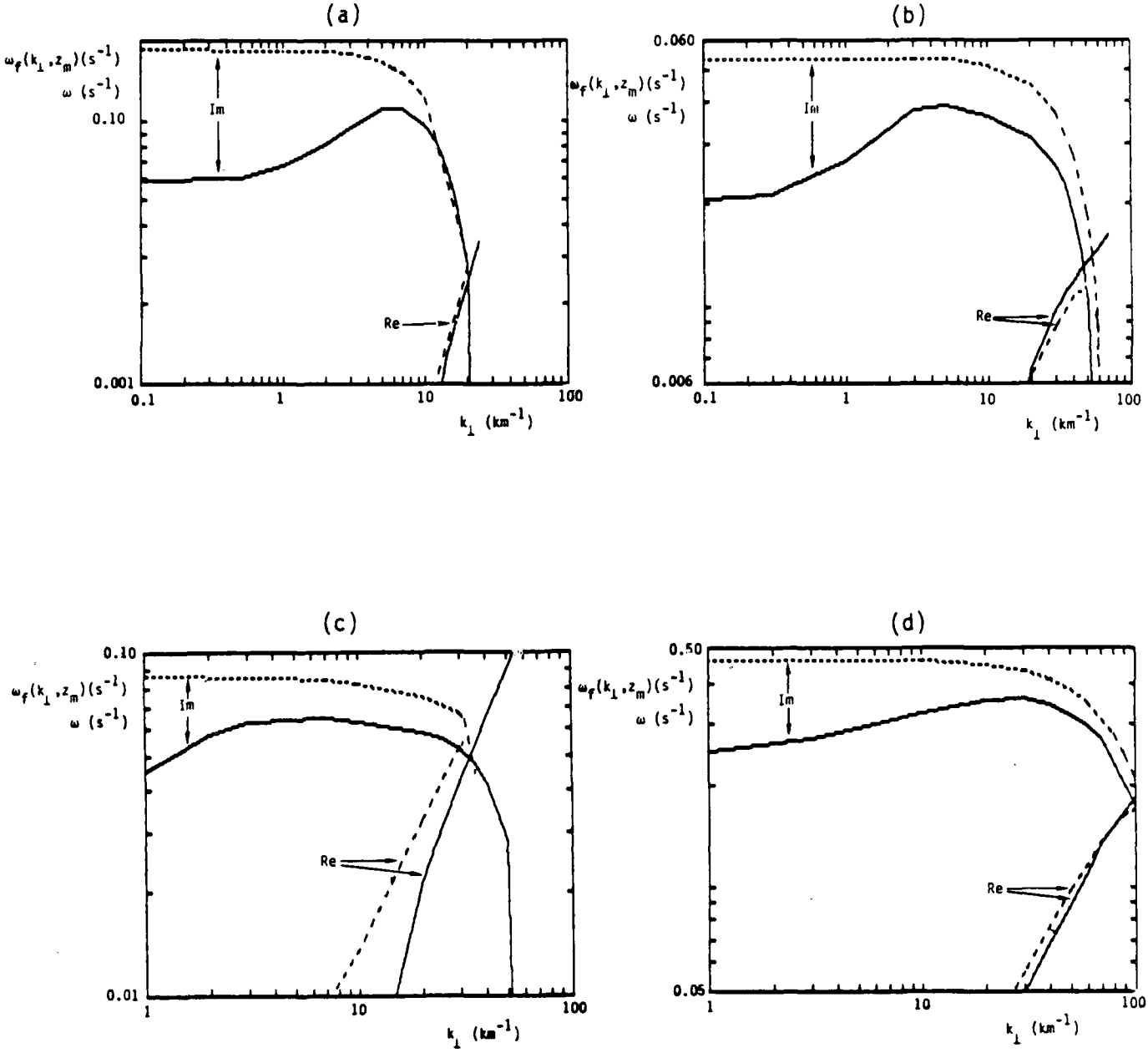

Figure 3.5. $\omega_f\ (k_\perp, z_m)\ (s^{-1})$ and $\omega\ (s^{-1})$ versus $k_\perp\ (km^{-1})$ for (a) Case 1, (b) Case 2, (c) Case 3, and (d) Case 4. The solid lines are ω and the dashed lines are $\omega_f\ (k_\perp, z_m)$. The imaginary and real parts of $\omega_f\ (k_\perp, z_m)$ and ω are appropriately designated by Im and Re.

AD-A155 973 THE ROLE OF FINITE PARALLEL CONDUCTIVITY AND OTHER CLASSICAL PROCESSES ON. (U) JAYCOR SAN DIEGO CA J L SPERLING ET AL. 26 MAY 84 JAYCOR-J530-84-207/2308 2/2

UNCLASSIFIED DNA-TR-84-196 DNA001-83-C-0150 F/G 20/3 NL

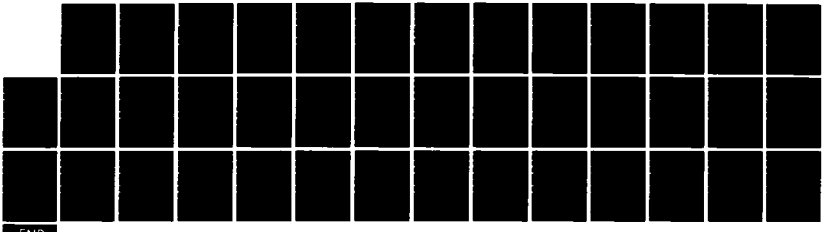

END

FILMED

DTIC

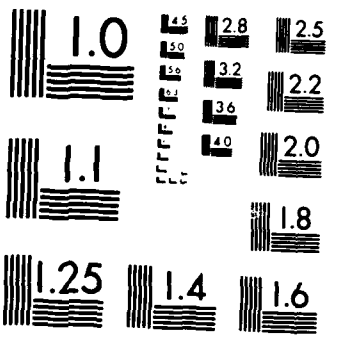

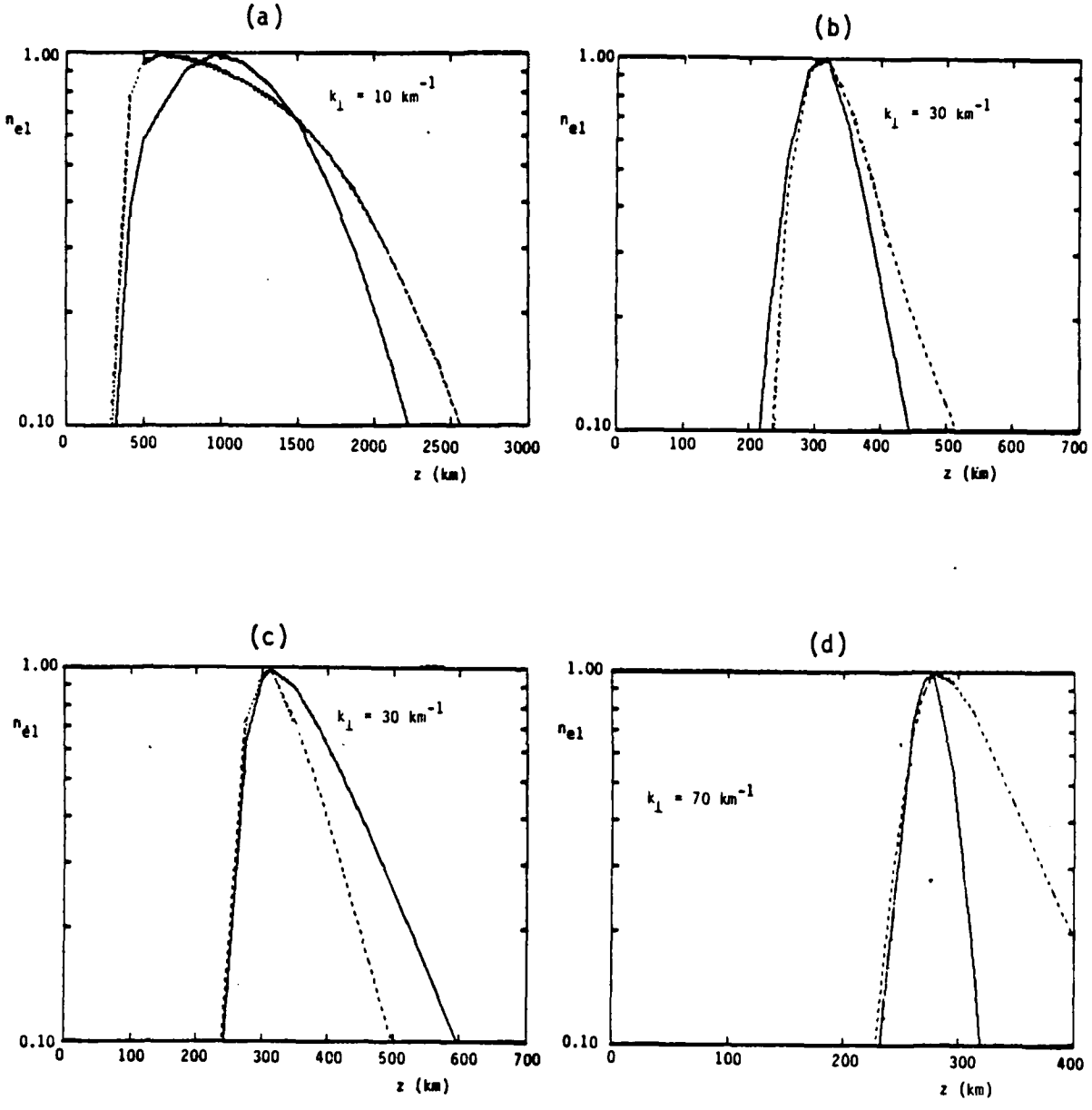

Figure 3.6. $|n_{el}|$, n_{f1}, and n_{f2} versus z (km) for (a) Case 1, (b) Case 2, (c) Case 3, and (d) Case 4. The solid line is $|n_{el}|$ as determined from (3.17a) and the solution of (3.21). The dashed line is (a) n_{f1} and (b)-(d) n_{f2}.

3.5 SUMMARY AND CONCLUDING REMARKS

A second-order linear differential equation has been derived for determining the linear eigenmodes of striation instabilities along the geomagnetic field and has been solved for parameters and geometry appropriate to late-time HANE plasmas, as described by MELT. Eigenvalues (i.e., frequencies) are determined along with the eigenmodes. The differential equation includes the contribution of two physical effects which are essential for correctly determining the eigenvalues and the localization of the eigenmodes. These effects are ion-polarization currents and inductive electric fields. Ion-polarization currents are especially important at higher altitudes where ion-Pedersen currents are negligible. Ion-polarization currents are a mechanism for short-circuiting voltage differences between adjacent geomagnetic-field lines. Inductive effects are required in order to properly take into account the fact that information is propagated along the geomagnetic field at a finite rate which depends upon the Alfven speed.

It is demonstrated that striations tend to develop with larger perpendicular scale sizes at higher altitudes than at lower altitudes. The results also demonstrate that, in late-time HANE plasmas, localized disturbances along the geomagnetic field generally lead to a localized response and so the geomagnetic-field lines are not necessarily equipotentials. Electromagnetic effects are shown to be important for modes with smaller perpendicular wave numbers (i.e., $\lesssim 1$ km^{-1}) and ion-viscosity is important for modes with larger perpendicular wave numbers (i.e., $\gtrsim 4$ km^{-1}). Analytic criteria are given for the perpendicular wave numbers of the instability at which the real part of the frequency is equal to the growth rate and at which there is complete stabilization. It is argued that the equating of real part of the frequency and the growth rate gives a meaningful estimate of the perpendicular wave number at which striation "freezing" occurs. An appropriate algorithm, suitable for implementation in modeling codes, is given for determining the perpendicular wave number at "freezing." Simple empirical estimates for the parallel spatial extent of the striation density fluctuations are also described.

REFERENCES

Alfven, H., Cosmic Plasma, D. Reidel, Boston, 1981.

Allis, W. P., S. J. Buchsbaum, and A. Bers, Waves in Anisotropic Plasmas, MIT Press, Cambridge, Massachusetts, 1963.

Block, L. P., Potential double layers in the ionosphere, Cosmic Electrodynam., 3, 349, 1972.

Boyd, T. J. M., and J. S. Sanderson, Plasma Dynamics, Barnes and Noble, New York, 1969, pp. 51-53.

Braginskii, S. I., Transport processes in plasmas, in Reviews of Plasma Physics, Vol. 1, edited by M. A. Leontovich, Consultants Bureau, New York, 1965.

Glassman, A. J., and J. L. Sperling, Electromagnetic theory of collisional interchange instabilities, J. Geophys. Res., 88, 10091, 1983.

Goldman, S. R., L. Baker, S. L. Ossakow, and A. J. Scannapieco, Striation formation associated with barium clouds in an inhomogeneous ionosphere, J. Geophys. Res., 81, 5097, 1976.

Goldman, S. R., and J. L. Sperling, Electric field limitations of drift dissipative wave generation in ionospheric structures, J. Geophys. Res., 87, 254, 1982.

Hudson, M. K., and C. F. Kennel, Linear theory of equatorial spread F, J. Geopnys. Res., 80, 4581, 1975.

Jackson, J. D., Classical Electrodynamics, John Wiley and Sons, New York, 1962, ch. 7.

Kadomtsev, B. B., Plasma Turbulence, Academic Press, New York, 1965.

Kilb, R. W., Striation formation, in Physics of High-Altitude Nuclear Bursts, Defense Nuclear Agency Rep. DNA 4501F, Defense Nuclear Agency, Washington, D.C., 1977.

Knapp, W. S., and K. Schwartz, Aids for the study of electromagnetic blackout, Defense Nuclear Agency Rep. DNA 3499H, Defense Nuclear Agency, Washington, D.C., 1975, p. 8-5.

Landau, L. D., and E. M. Lifshitz, Electrodynamics of Continuous Media, Pergamon, New York, 1960.

Linson, L. M., and J. B. Workman, Formation of striations in ionospheric clouds, J. Geophys. Res., 75, 3211, 1970.

Linson, L. M., and G. Meltz, Theory of ion cloud dynamics and morphology, in Analysis of Barium Clouds, Rep. RADC-TR-72-736, Ch. 5, Vol. 1, Avco Everett Research Laboratory, Everett, Massachusetts, 1972.

Linson, L. M., and D. C. Baxter, Ion cloud modelling, Defense Nuclear Agency Rep. DNA 4455F, Defense Nuclear Agency, Washington, D.C., 1977.

Longmire, C. L., Elementary Plasma Physics, Interscience, New York, 1963.

McDonald, B. E., M. J. Keskinen, S. L. Ossakow, and S. T. Zalesak, Computer simulation of gradient drift instability processes in Operation Avefria, J. Geophys. Res., 85, 2143, 1980.

McDonald, B. E., S. L. Ossakow, S. T. Zalesak, and N. J. Zabusky, Scale sizes and lifetimes of F region plasma cloud striations as determined by the condition of marginal stability, J. Geophys. Res., 86, 5775, 1981.

Mende, S. B., Morphology of the magnetospheric barium release, J. Geophys. Res., 78, 5751, 1973.

Ossakow, S. L., S. T. Zalesak, B. E. McDonald, and P. K. Chaturvedi, Nonlinear equatorial spread F: Dependence on altitude of the F peak and bottomside background density gradient scale length, J. Geophys. Res., 84, 17, 1979.

Ott, E., Theory of Rayleigh-Taylor bubbles in the equatorial ionosphere, J. Geophys. Res., 83, 2066, 1978.

Overman, E. A., II, N. J. Zabusky, and S. L. Ossakow, Ionospheric plasma cloud dynamics via regularized contour dynamics, I. Stability and nonlinear evolution of one-contour models, Phys. Fluids, 26, 1139, 1983.

Paoloni, F. J., Boundary effects on M = 0, ±1 Alfven waves in a cylindrical, collisionless plasma, Phys. Fluids, 18, 140, 1975.

Papadopoulos, K., A review of anomalous resistivity for the ionosphere, Rev. Geophys. Space Phys., 15, 113, 1977.

Perkins, F. W., N. J. Zabusky, and J. H. Doles, III, Deformation and striation of plasma clouds in the ionosphere, J. Geophys. Res., 78, 697, 1973.

Prettie, C. W., Results of Places data analysis, Defense Nuclear Agency Rep. DNA-TR-81-270, Defense Nuclear Agency, Washington, D.C., 1982.

Prettie, C. W., S. Y. F. Chu, and J. B. Workman, The microstructure theory for three-dimensional plasma transport, Defense Nuclear Agency Rep. DNA-TR-81-270, Defense Nuclear Agency, Washington, D.C., 1983.

Scannapieco, A. J., and S. L. Ossakow, Nonlinear equatorial spread F, Geophys. Res. Lett., 3, 451, 1976.

Scholer, M., On the motion of artificial ion clouds in the magnetosphere, Planet. Space Sci., 18, 977, 1970.

Simon, A., Instability of a partially ionized plasma in crossed electric and magnetic fields, Phys. Fluids, 6, 382, 1963.

Sperling, J. L., Inhomogeneity effects on wave properties in Elmo bumpy torus scale, Phys. Rev. A, 26, 1618, 1982a.

Sperling, J. L., Role of Rayleigh-Taylor instabilities on prompt striation evolution, J. Geophys. Res., 87, 10514, 1982b.

Sperling, J. L., and A. J. Glassman, Striation eigenmodes along the geomagnetic field and eigenvalues in the limit of strong ion-neutral collisions, JAYCOR Rep. J530-83-135, JAYCOR, San Diego, California, 1983.

Sperling, J. L., The role of ion-neutral diffusion on collisional structuring instabilities, JAYCOR Rep. J530-83-144, JAYCOR, San Diego, California, 1983a.

Sperling, J. L., Ion-Pedersen drift and parallel electric field effects on plasma jetting, J. Geophys. Res., 88, 7095, 1983b.

Sperling, J. L., On the effect of finite, field-aligned plasma length on a loss-cone instability, J. Geophys. Res., 88, 927, 1983c.

Sperling, J. L., Finite parallel wavelengths and ionospheric structuring, J. Geophys. Res., 88, 4075, 1983d.

Sperling, J. L., The parallel evanescence of striation parameters, JAYCOR Rep. J530-83-119, JAYCOR, San Diego, California, 1983e.

Spiegel, M. R., Schaum's Outline of Theory and Problems of Laplace Transforms, McGraw-Hill, New York, 1965.

Stix, T. H., The Theory of Plasma Waves, McGraw-Hill, New York, 1962.

Stratton, J. A., Electromagnetic Theory, McGraw-Hill, New York, 1941.

Vesecky, J., J. Chamberlain, J. Cornwall, D. Hammer, and F. W. Perkins, Irregularities in ionospheric plasma cloud: Their evaluation and effect on radio communications, JASON Tech. Rep., JSR-80-15, SRI International, Arlington, Virginia, 1980.

Völk, H. J., and G. Haerendel, Striations in ionospheric ion clouds, 1, J. Geophys. Res., 76, 4541, 1971.

Zalesak, S. T., and S. L. Ossakow, Nonlinear equatorial spread F: Spatially large bubbles resulting from horizontal scale initial perturbations, J. Geophys. Res., 85, 2131, 1980.

APPENDIX A
MATHEMATICAL DESCRIPTION OF CONDUCTIVITIES

This appendix specifies the mathematical forms for σ_x, σ_y, and σ_z in (1.3) and $\bar{\sigma}_x$, $\bar{\sigma}_y$, and $\bar{\sigma}_z$ in (1.6a-b).

The perpendicular currents, driven by the perpendicular electrostatic fields, are considered to be a consequence of ion-neutral collisions and temporal variations in the electrostatic fields. Hence, the perpendicular currents are of the Pedersen or polarization types. The parallel current is assumed to be controlled by the parallel electrostatic field and electron resistivity. Hence [Sperling, 1983b],

$$\vec{j}_\perp = -\sigma_\perp \nabla_\perp \phi \quad , \quad j_z = -\sigma_\parallel \frac{\partial \phi}{\partial z} \quad , \tag{A1}$$

with

$$\sigma_x = \sigma_y = \sigma_\perp = \frac{enc}{B\Omega_i}\left(\nu_{in} + \frac{\partial}{\partial t}\right) \quad , \quad \sigma_z = \frac{e^2 n}{m_e \nu_e} \quad . \tag{A2}$$

In (A2) the following symbols are used: e (proton charge), n (density), c (speed of light), B (magnetic field strength), ν_{in} (ion-neutral collision frequency), Ω_i (ion-gyrofrequency), m_e (electron mass), and ν_e (effective collision frequency for parallel electron motion). In writing (A2) it has been assumed that ν_{in}, $|\partial/\partial t| \ll \Omega_i, \nu_e$ and that ions have the proton charge. Relevant mathematical forms for ν_{in} and ν_e are [Braginskii, 1965; Kilb, 1977]

$$\nu_{in} = \begin{cases} 2.5 \times 10^{13}\, m_n n_n & \text{for air ions} \\ 2.5 \times 10^{12}\, m_n n_n & \text{for barium ions} \end{cases} ,$$

$$\nu_e = \nu_{en} + 0.51\, \nu_{ei}$$

$$\nu_{en} = 8.1 \times 10^{-8}\, T_e^{0.64} n_n \quad ,$$

$$\nu_{ei} = \frac{23.4 - 1.15 \log_{10}(n) + 3.45 \log_{10}(T_e)}{3.5 \times 10^{5}} \frac{n}{T_e^{3/2}} \quad . \tag{A3}$$

In (A3) the following symbols are used: m_i (ion mass), n_n (neutral density), and T_e (electron temperature). All parameters are in cgs units except for the electron temperature which is in units of eV.

It is evident from (A2) that $\sigma_\perp$ is affected by temporal variations in the electrostatic fields but σ_z is unaffected. The application of the Laplace transform (1.5a) to (1.4a-b) implies the following functional forms for $\bar{\sigma}_x$, $\bar{\sigma}_y$, and $\bar{\sigma}_z$ in (1.6a-b):

$$\bar{\sigma}_x = \bar{\sigma}_y = \bar{\sigma}_\perp = \alpha(\nu_{in} + s) \quad , \quad \bar{\sigma}_z = \sigma_z \quad , \tag{A4}$$

with

$$\alpha = \frac{enc}{B\Omega_i} \quad . \tag{A5}$$

The conductivity tensor remains diagonal with the Laplace transformation, i.e.,

$$\bar{\sigma} = \begin{pmatrix} \bar{\sigma}_x & 0 & 0 \\ 0 & \bar{\sigma}_y & 0 \\ 0 & 0 & \bar{\sigma}_z \end{pmatrix} \quad . \tag{A6}$$

APPENDIX B

TOTAL ELECTROSTATIC POTENTIAL FOR AN APPLIED ELECTROSTATIC FORCE

This appendix uses (1.21a-b) to derive the total electrostatic potential for the case when the external applied force is completely electrostatic. Specifically,

$$\vec{J}_{o\gtrless} = \bar{\sigma}_{\perp\gtrless}(E_{ox}\hat{x} + E_{oy}\hat{y}) + \bar{\sigma}_{z\gtrless}E_{oz}\hat{z} \quad . \tag{B1}$$

The electrostatic potential for the applied electrostatic field is

$$\phi_o = -E_{ox}\hat{x} - E_{oy}\hat{y} - E_{oz}\hat{z} \quad . \tag{B2}$$

Using the Laplace transformation, (1.5a), permits the total electrostatic potential to be written as

$$\bar{\phi}_{tot\gtrless} \equiv \bar{\phi}_o + \bar{\phi}_{\gtrless} \quad . \tag{B3}$$

The combination of (1.21a), (1.21b), (B1), and (B2) gives

$$\bar{\phi}_{tot<} = \frac{-E_{ox}x}{1 + \left(\frac{\sigma_{\perp<}}{\sigma_{\perp>}} - 1\right)\bar{h}_x(0)} - \frac{E_{oy}y}{1 + \left(\frac{\sigma_{\perp<}}{\sigma_{\perp>}} - 1\right)\bar{h}_y(0)}$$

$$- \frac{E_{oz}z}{1 + \left(\frac{\sigma_{z<}}{\sigma_{z>}} - 1\right)\bar{h}_z(0)} \quad , \tag{B4a}$$

$$\bar{\Phi}_{tot>} = -E_{ox}x \frac{1 + \left(\frac{\sigma_{\perp<}}{\sigma_{\perp>}} - 1\right)\left[\bar{h}_x(0) - \bar{h}_x(\xi)\right]}{1 + \left(\frac{\sigma_{\perp<}}{\sigma_{\perp>}} - 1\right)\bar{h}_x(0)}$$

$$- E_{oy}y \frac{1 + \left(\frac{\sigma_{\perp<}}{\sigma_{\perp>}} - 1\right)\left[\bar{h}_y(0) - \bar{h}_y(\xi)\right]}{1 + \left(\frac{\sigma_{\perp<}}{\sigma_{\perp>}} - 1\right)\bar{h}_y(0)}$$

$$- E_{oz}z \frac{1 + \left(\frac{\sigma_{z<}}{\sigma_{z>}} - 1\right)\left[\bar{h}_z(0) - \bar{h}_z(\xi)\right]}{1 + \left(\frac{\sigma_{z<}}{\sigma_{z>}} - 1\right)\bar{h}_z(0)} \quad . \qquad \text{(B4b)}$$

Equation (B4b) agrees with (35) and (38) on pages 212-213 of Stratton [1941] and the result of problem 6 on page 62 of Landau and Lifshitz [1960].

Equations (B2) and (B4a) indicate that the electric field strength in the interior of the ellipsoid is reduced (increased) relative to the value far from the ellipsoid if the appropriate conductivity inside the ellipsoid is larger (smaller) than the appropriate conductivity outside the ellipsoid. For example, $\bar{\sigma}_{\perp<} >(<) \bar{\sigma}_{\perp>}$ implies that the x-directed electric field is smaller (larger) inside the ellipsoid than far from the ellipsoid.

APPENDIX C

STEADY-STATE PARALLEL ELECTRON CURRENT ON THE SURFACE OF THE ELLIPSOIDAL PLASMA CLOUD

In this appendix, the expression, (1.45), for the maximum parallel current on the surface of the ellipsoidal plasma cloud is derived in the limit of $c_t^2 \ll a_t^2 = b_t^2$. For $j_{oy\gtrless} = j_{oz\gtrless} = 0$, the parallel electric field external to the ellipsoid is determined from the relation

$$\bar{E}_{z>} = - \frac{\partial w}{\partial z} \frac{\partial \xi}{\partial w} \frac{\partial \bar{\phi}_>}{\partial \xi} \quad . \tag{C1}$$

Equations (1.7), (1.12), (1.18), and (1.21b) give

$$\frac{\partial w}{\partial z} = \frac{1}{\sigma_{z>}^{0.5}} \, , \quad \frac{\partial \xi}{\partial w} = \frac{2w}{c_t^2 + \xi} \frac{1}{\dfrac{u^2 + v^2}{(a_t^2 + \xi)^2} + \dfrac{w^2}{(c_t^2 + \xi)^2}} \quad ,$$

$$\frac{\partial \phi_>}{\partial \xi} = - \frac{1}{2} \frac{x(\bar{j}_{ox<} - \bar{j}_{ox>})}{\bar{\sigma}_{\perp>} + (\bar{\sigma}_{\perp<} - \bar{\sigma}_{\perp>}) h_x(0)} \frac{a_t^2 c_t}{(\xi + a_t^2)^2 (\xi + c_t^2)^{0.5}} \quad . \tag{C2}$$

Hence, on the surface of the ellipsoid,

$$\bar{E}_{z>}(\xi=0) = \frac{zx}{a_0^2 c_0^2 s} \frac{\alpha_>(s + \nu_{in>})}{\alpha_> \dfrac{x^2 + y^2}{a_0^4} (s + \nu_{in>}) + \dfrac{z^2}{c_0^4} \sigma_{z>}}$$

$$\cdot \frac{j_{ox<} - j_{ox>}}{\alpha_>(s + \nu_{in>}) + [\alpha_>(s + \nu_{in<}) - \alpha_>(s + \nu_{in>})] k (s + \nu_{in>})^{0.5}} \, . \tag{C3}$$

The final-value theorem for Laplace transformations indicates that the steady-state value for the parallel electric field on the surface of the ellipsoid is

$$E_{z>}(\xi=0,\ t\to\infty) = \lim_{s\to 0}\left[s\,\bar{E}_{z>}(\xi=0)\right]$$

$$= \frac{j_{ox<} - j_{ox>}}{\sigma_{z>}} \frac{zx}{\frac{\alpha_{<}\nu_{in>}c_0^4}{\sigma_{z>}a_0^4}(x^2+y^2)+z^2}$$

$$\cdot \frac{c_0^2}{a_0^2}\frac{1}{1+\left(\frac{\alpha_{<}\nu_{in<}}{\alpha_{>}\nu_{in>}}-1\right)k\nu_{in>}^{0.5}} \quad . \tag{C4}$$

On the surface of the ellipsoid

$$x^2 + y^2 = a_0^2(1 - z^2/c_0^2) \quad . \tag{C5}$$

Hence, for $y = 0$ and $\alpha_{>}\nu_{in>}c_0^2/\sigma_{z>}a_0^2 \ll 1$,

$$E_{z>}(\xi=0,t\to\infty) \cong \pm \frac{j_{ox<} - j_{ox>}}{\sigma_{z>}} \frac{z(1 - z^2/c_0^2)^{1/2}}{\frac{\alpha_{>}\nu_{in>}c_0^4}{\sigma_{z>}a_0^2}+z^2} \frac{c_0^2}{a_0} \quad . \tag{C6}$$

The magnitude of the right-hand side has a maximum value for

$$z = \pm\left(\frac{\alpha_{>}\nu_{in>}}{\sigma_{z>}}\right)^{0.5}\frac{c_0^2}{a_0} \quad . \tag{C7}$$

or

$$E_x \simeq \frac{(j_{ox>} - j_{ox<})h_x}{\sigma_{\perp>} + (\sigma_{\perp<} - \sigma_{\perp>})h_x} \quad , \tag{F5}$$

if $E_{x<} \approx E_{x>} \approx E_x$. In (F5)

$$h_x \approx \pi \frac{c_0}{b_0} \left(\frac{\sigma_{\perp>}}{\sigma_{z>}}\right)^{0.5} \quad . \tag{F6}$$

To within a constant (F6) is in agreement with (1.21a) and the appropriate asymptotic form of entries 3 and 4 in Table 1.2.

If $b_0(\sigma_{z>})^{0.5} \gg c_0$, the field-line integrated Pedersen conductivities of the plasma cloud and the ambient plasma are determined from (F6) to be $c_0(\sigma_{\perp<})^{0.5}$ and $b_0(\sigma_{z>})^{0.5}\sigma_{\perp>}$, respectively. Hence, the concept of field-line integrated Pedersen conductivities appears to be approximately applicable, to within factors of order unity, for $a_t, c_t \ll b_t$ or $c_t \ll a_t = b_t$.

APPENDIX F

INDUCED ELECTRIC FIELDS AND FIELD-LINE INTEGRATION

It is evident from (1.18), (1.22a), (1.22b), and entries (3)-(5) of Table 1.2, that the depolarization factors are complicated functions of geometry when the semiprincipal axes (i.e., a_t, b_t, and c_t) are of comparable magnitude. Under such circumstances, field-line integration would appear to be inappropriate for determining induced electric fields inside plasma clouds.

Consider the situation of $j_{ox\gtrless} \neq 0$, $j_{oy\gtrless} = j_{oz\gtrless} = 0$, and c_t, $a_t \ll b_t$ or $c_t \ll a_t = b_t$. Overall quasineutrality requires that net current flow into and out of the ellipsoid be nondivergent. The total x-directed current inside the plasma cloud is

$$I_1 \approx \sigma_{\perp<} E_{x<} \pi b_0 c_0 + j_{ox<} \quad . \tag{F1}$$

Equation (F1) uses the fact that the total surface area presented to the x-directed current-density is $\sim \pi b_0 c_0$. The total x-directed current flowing from the external plasma directly into the plasma cloud is

$$I_2 \approx \sigma_{\perp>} E_{x>} \pi b_0 c_0 + j_{ox>} \quad . \tag{F2}$$

To maintain closed current loops, there is a return current in the external plasma which is present above and below the plasma cloud with respect to position along the geomagnetic field lines. Considerations similar to those leading to (1.29)-(1.31) indicate that the return current extends a distance $\sim b_t(\sigma_{z>})^{1/2}$ along the magnetic field line. Hence, the return current is

$$I_3 \approx - \sigma_{\perp>} E_{x>} b_0 b_t (\sigma_{z>})^{0.5} \quad . \tag{F3}$$

Total conservation of current requires

$$I_1 = I_2 + I_3 \quad , \tag{F4}$$

less likely to occur for plasma clouds with transverse scale size approaching L_n. When considering the formation of striations L_n can be equated with an inverse perpendicular wave number, k_y^{-1}. If $cE_{ox}/B = 1 \times 10^4$ cm/s, B = 0.3 G, and T_i = 0.1 eV, then $L_n \approx k_y^{-1} \approx 3.3 \times 10^3$ cm and the corresponding transverse wavelength is $\lambda_y = 2\pi/k_y \approx 2.1 \times 10^4$ cm. This value for λ_y is comparable to the observed scale size for "frozen" striations [Linson and Meltz, 1972].

Equation (E5) assumes that electric fields are not induced. The density profile implied by (E4) is

$$n_< = n_> + C \exp\left(\frac{v_{ox}}{\nu_{in<}\rho_{i<}^2}\, x\right) \quad , \tag{E6}$$

with C a constant of integration. If v_{ox} is an ion-Pedersen velocity then

$$v_{ox} = \frac{\nu_{in}}{\Omega_i}\,\frac{cE_{ox}}{B} \quad , \tag{E7}$$

and (E6) reduces to

$$n_< = n_> \exp\left(\frac{x}{L_n}\right) \quad . \tag{E8}$$

In (E8)

$$L_n = \frac{B\Omega_{i<}\rho_{i<}^2}{cE_{ox}} = \frac{k_B T_{i<}}{e\, E_{ox}} \quad . \tag{E9}$$

Equations (E8) and (E9) suggest that L_n is an important scale size in the dynamics of plasma clouds when ion-neutral collisions are important. If a plasma cloud has a much larger dimension than L_n across the magnetic field, then electric fields rather than ion-neutral diffusion can be expected to be the primary mechanism contributing to the maintenance of overall nondivergent current densities. However, as the perpendicular scale size approaches L_n, then ion-neutral diffusion can more likely be expected to contribute to the maintenance of overall nondivergent current densities.

Striations are observed to elongate outward from the backside of barium clouds. Electric fields are required for this bulk plasma motion, but it appears that when the perpendicular scale of a plasma cloud approaches L_n the tendency to induce electric fields can be lessened. Hence, the formation of striations is

APPENDIX E

DIVERGENT CURRENT DENSITIES AND ION-NEUTRAL DIFFUSION

Figure D1 shows a one-dimensional plasma cloud bounded at $x = \pm x_o$. There is a density gradient inside the plasma cloud. It is assumed that the plasma external to the cloud is uniform and symmetric about $x = 0$. An applied external force results in current densities, $j_{ox\gtrless}$.

The ion-diffusive current for the geometry of Figure D1 is

$$j_{ox} = -e\, D_{in<} \frac{dn_<}{dx} \quad , \tag{E1}$$

with the coefficient of ion-neutral diffusion given by

$$D_{in} = \nu_{in<} \rho_{i<}^2 \quad , \tag{E2}$$

with

$$\rho_{i<}^2 = \frac{k_B T_{i<}}{m_{i<} \Omega_{i<}^2} \tag{E3}$$

and k_B the Boltzmann constant.

Consider a drift velocity, v_{ox}, which is assumed to be independent of x. If

$$j_{ox} = env_{ox} \quad , \tag{E4}$$

and if $j_{ox>} \neq j_{ox<}$ then overall nondivergent current densities away from $|x| = x_o$ require

$$0 = (n_< - n_>)v_{ox} - D_{in<} \frac{dn_<}{dx} \quad . \tag{E5}$$

(Viscosity is not important if the time rate of change of E_x is larger than the ion-ion collision frequency.) When (D11) is satisfied, the polarization current density, rather than the viscous current density, is the main contributor to overall current flow within the bulk of the plasma cloud. If $n_< = 1 \times 10^6$ cm^{-3}, $T_{i<} = 0.1$ eV, $m_{i<} = 20\ m_p$, $B_o = 0.03$ G, and $x_o = 2 \times 10^5$ cm, then $|\bar{\kappa}_< x_o| \ll 1$ is satisfied for $|s| \gg 7.2 \times 10^{-4}$ s^{-1}. Provided $\delta_\gtrless > 1$, the viscous force increases with altitude if all other parameters are kept the same and so the parameter s must be correspondingly larger for (D11) to be satisfied. At sufficiently high altitudes $\delta_< < 1$ and the viscous force does not depend upon the magnetic field strength within the plasma cloud.

As a quantitative example, consider a barium cloud, at an altitude of 200 km, with $n_< = 1 \times 10^7$ cm^{-3}, $n_> = 1.2 \times 10^4$ cm^{-3}, $T_{i\gtrless} = 0.1$ eV, $n_n = 8.3 \times 10^9$ cm^{-3}, and $m_{i>} = 20\ m_p$, $B = 0.4$ G, and $x_o = 2 \times 10^5$ cm. At steady state, (D8) and (D9) indicate that $\kappa_< \approx 4.5 \times 10^{-4}$ cm^{-1} and $\kappa_> = 5.5 \times 10^{-2}$ cm^{-1} and so the boundary layer extends $\sim 2.2 \times 10^3$ cm into the plasma cloud. The values of $\kappa_<$ and $\kappa_>$ are sufficiently large (i.e., $k_< \rho_{i<} \sim 1$ and $\kappa_> \rho_{i>} \gg 1$ with ρ_i the ion-gyroradius) so that finite gyroradius effects, not included in the present analysis, would likely impact actual boundary layers. In any case, it appears that viscosity permits the existence of plasma structures with large perpendicular gradients at an altitude of 200 km. However, since E_x varies near the edge of the plasma it follows that the E x B velocity must also vary. Hence, viscosity is an additional mechanism, besides diffusion and Pedersen convection [Linson and Meltz, 1972; Prettie, 1982], for ablating plasma clouds and thereby transforming plasma rods into plasma sheets [Linson and Meltz, 1972].

As altitude increases, (D9) indicates that $\kappa_{\gtrless} \to 0$ since $\nu_{in} \to 0$, and so the boundary layers become thick at sufficiently high altitudes and steady state. If $m_{i>} = m_{i<}$, $T_{i>} = T_{i<}$, $\delta_{\gtrless} \gg 1$, and $n_< \gg n_>$, then (D2) and (D10) indicate that $\kappa_< \ll \kappa_>$ and the viscous current density specified by (D3) is a main contributor to current flow throughout the plasma cloud, not only at the edge of the cloud. Since ablation would appear to act over a large distance inside a plasma cloud if $\kappa_< x_o \lesssim 1$, it appears that large perpendicular gradients are then not permitted.

Viscosity allows large perpendicular gradients at the boundaries of plasma clouds if

$$|\bar{\kappa}_< x_o| \ , \ |\bar{\kappa}_> x_o| \gg 1 \quad . \tag{D10}$$

If the parameter s in (D6) is considered to be representative of the time rate of change of E_x, then even if $\nu_{in} \to 0$ sharp perpendicular gradients are possible if

$$\left| \frac{s\nu_{ii<} m_{i<}}{d_< k_B T_{i<}} x_o \right| \ , \ \left| \frac{s\nu_{ii>} m_i}{d_> k_B T_{i>}} x_o \right| \gg 1 \quad . \tag{D11}$$

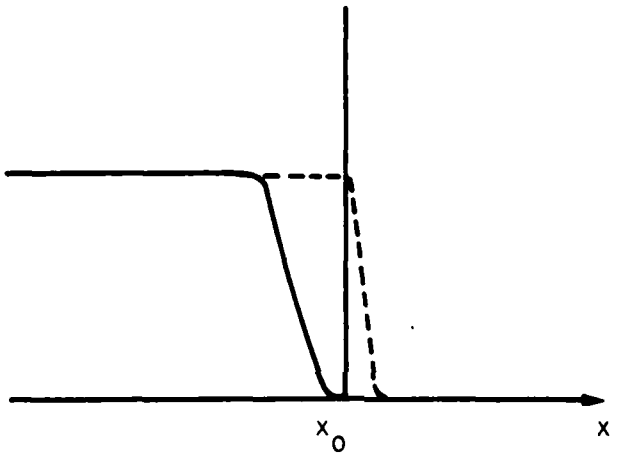

Figure D2. Schematic illustration of viscous boundary layers near $x \approx x_0$ for $|\kappa_<| \ll |\kappa_>|$ (———) and $|\kappa_>| \gg |\kappa_<|$ (-----). The location of the plasma cloud is $|x| < x_0$ as shown in Figure D1.

For both $\nu_{ii} \to 0$ and ∞, the viscous force goes to zero. Equations (D5a) and (D5b) then reduce to

$$\bar{E}_x = \begin{cases} 0 & \text{for } |x| \geq x_o \quad \text{(D7a)} \\ \bar{K}_1 & \text{for } |x| \leq x_o \quad . \quad \text{(D7b)} \end{cases}$$

Evidently, the transition of $\bar{E}_x$ across $x = \pm x_o$ appropriately occurs over an infinitesimal distance.

For finite values of ν_{ii}, (D5a) and (D5b) indicate the existence of viscous boundary layers with finite thickness at $x = \pm x_o$. These boundary layers are illustrated in Figure D2. Two different situations arise depending on the relative magnitudes of $\bar{\kappa}_<$ and $\bar{\kappa}_>$. When $|\bar{\kappa}_<| \ll |\bar{\kappa}_>|$ the electric field appropriate to $|x| \gg x_o$ extends a distance of approximately $[\mathrm{Re}(\bar{\kappa}_<)]^{-1}$ into the plasma cloud. Conversely, when $|\bar{\kappa}_<| \ll |\bar{\kappa}_>|$ the electric field appropriate to $|x| \ll x_o$ extends a distance of approximately $[\mathrm{Re}(\bar{\kappa}_>)]^{-1}$ outside the plasma cloud.

In general, the temporal variation of E_x can be determined by using the inverse Laplace transformation, (1.5b). Steady-state values of E_x are determined from $\lim_{s \to 0} (s\bar{E}_x)$. If $j_{ox\gtrless}$ are both independent of time then

$$\lim_{t \to \infty} E_x = \begin{cases} \dfrac{K_1}{K_2} \dfrac{\kappa_<}{\kappa_>} \sinh(\kappa_< x_o) \exp[\kappa_>(x_o - |x|)] & \text{for } |x| \geq x_o \quad \text{(D8a)} \\ K_1 \left[1 - \dfrac{\cosh(\kappa_< x)}{K_2} \right] & \text{for } |x| \leq x_o \quad \text{(D8b)} \end{cases}$$

with

$$K_1 = \frac{B}{c} \frac{\Omega_{i<}(j_{ox>} - j_{ox<})}{en_< \nu_{in<}} \quad , \quad K_2 = \frac{\kappa_\leq}{\kappa_>} \sinh(\kappa_< x_o) + \cosh(\kappa_< x_o) \quad ,$$

$$\kappa_{\gtrless} = \left(\frac{\nu_{in} \nu_{ii} m_i}{d\, k_B\, T_i} \right)^{1/2}_{\gtrless} \quad . \quad \text{(D9)}$$

Using the Laplace transformation, (1.5a), and the perpendicular conductivity specified by (A4), the requirement, that total current be free of divergence, can be written as

$$\bar{K} = \bar{j}_{ox} - \left[\frac{c^2}{B^2}\frac{d}{dx}\left(\eta_1 \frac{d}{dx}\right) - \frac{enc}{B\Omega_i}(\nu_{in} + s)\right] \bar{E}_x \quad . \tag{D4}$$

In (D4), $\bar{K}$ does not depend upon x but may depend upon the Laplace transform variable, s.

A physically reasonable solution to (D4) is obtained by requiring both $\bar{E}_x$ and $d\bar{E}_x/dx$ to be continuous across $x = \pm x_o$. This implies that the viscous forces and the related current are finite at the boundaries of the cloud. Furthermore, if $\bar{E}_x \to 0$ for $|x| \to \infty$, then it follows that $\bar{K} = \bar{j}_{ox>}$.

The appropriate solution to (D4) is

$$\bar{E}_x = \begin{cases} \dfrac{\bar{K}_1}{\bar{K}_2}\dfrac{\bar{\kappa}_<}{\bar{\kappa}_>}\sinh(\bar{\kappa}_< x_o)\exp\left[\bar{\kappa}_>(x_o - |x|)\right] & \text{for } |x| \geq x_o \quad \text{(D5a)} \\ \bar{K}_1\left[1 - \dfrac{\cosh(\bar{\kappa}_< x)}{\bar{K}_2}\right] & \text{for } |x| \leq x_o \quad \text{(D5b)} \end{cases}$$

with

$$\bar{K}_1 = \frac{B}{c}\frac{\Omega_{i<}(\bar{j}_{ox>} - \bar{j}_{ox<})}{en_<(\nu_{in<} + s)} \quad , \quad \bar{K}_2 = \frac{\bar{\kappa}_<}{\bar{\kappa}_>}\sinh(\bar{\kappa}_< x_o) + \cosh(\bar{\kappa}_< x_o) \quad ,$$

$$\bar{\kappa}_{\gtrless} = \left[\frac{(\nu_{in} + s)\nu_{ii} m_i}{d\, k_B\, T_i}\right]^{1/2}_{\gtrless} \quad . \tag{D6}$$

The real part of $\kappa_>$ is chosen to be greater than zero.

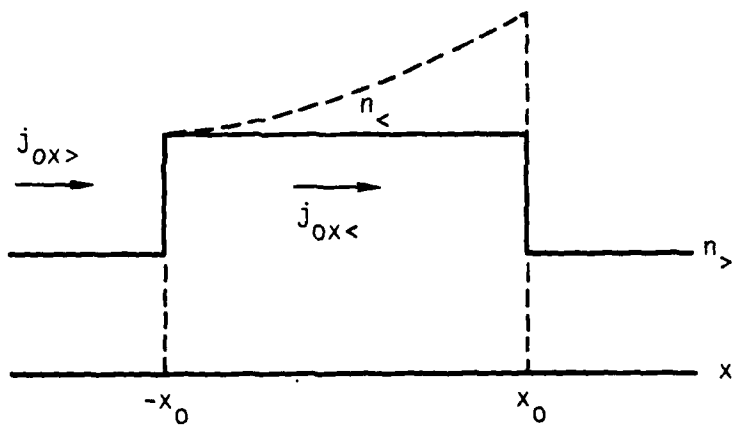

Figure D1. The one-dimensional plasma cloud used to calculate the effect of viscosity and ion-neutral diffusion on the creation of induced electric fields resulting from currents traversing through an inhomogeneous plasma. For the calculation of ion-viscous effects the density profile is flat inside the plasma cloud (——), but for the calculation of ion-neutral-diffusive effects a density gradient is permitted inside the plasma cloud (-----).

APPENDIX D

INDUCED ELECTROSTATIC FIELDS IN A VISCOUS MEDIUM

To illustrate the impact of ion viscosity on the formation of induced electrostatic fields, the simplified one-dimensional geometry of Figure D1 is used. The geometry is symmetric about $x = 0$. A uniform plasma cloud is present for $0 \leq |x| \leq x_0$. The plasma external to the cloud is also uniform. An applied external force results in current densities, $j_{ox\gtrless}$.

If $j_{ox>} \neq j_{ox<}$ an x-directed electric field, E_x, is created. This electric field results in a y-directed plasma velocity, $v_y = -cE_x/B$, and a y-directed viscous force per unit volume, i.e.,

$$F_{vy} = -\frac{c}{B}\left(\frac{d}{dx}\,\eta_1\,\frac{d}{dx}\right)E_x \quad , \tag{D1}$$

with [Braginskii, 1965]

$$\eta_1 = \frac{nk_BT_id}{\nu_{ii}} \quad , \quad d = \frac{1.2\delta + 2.23}{\delta^2 + 4.03\delta + 2.33} \quad , \quad \delta = \left(\frac{2\Omega_i}{\nu_{ii}}\right)^2 \quad ,$$

$$\nu_{ii} = \frac{23.4 - 1.15\log_{10}(n) + 3.45\log_{10}(T_e)}{3 \times 10^7}\left(\frac{2m_p}{m_i}\right)^{1/2}\frac{n}{T_i^{3/2}} \quad . \tag{D2}$$

In (D2), the following symbols are used: T_i (ion temperature), ν_{ii} (ion-ion collision frequency), and m_p (proton mass). All quantities in (1.3) are in cgs units except for temperature which is in units of eV. The Boltzmann constant k_B has the value 1.6×10^{-12} ergs/eV. The force specified by (D1) implies an x-directed current density,

$$j_{vx} = -\frac{c^2}{B^2}\left(\frac{d}{dx}\,\eta_1\,\frac{d}{dx}\right)E_x \quad . \tag{D3}$$

The maximum value of the parallel electric field on the surface of the ellipsoid, $|E_{z>,max}|$ is determined from (C6) and (C7) to be

$$|E_{z>,max}| \cong \frac{1}{2} \frac{|j_{ox<} - j_{ox>}|}{(\alpha_{>}\nu_{in>}\sigma_{z>})^{0.5}} \quad . \tag{C8}$$

Equation (1.45) follows directly from (C8) by recognizing that the maximum parallel current on the surface of the ellipsoid, $|j_{z>,max}|$, is determined by

$$|j_{z>,max}| = \sigma_{z>}|E_{z>,max}| \quad . \tag{C9}$$

It is evident from (C8) and (C9) that for $\sigma_{z>} \to \infty$, $|E_{z>,max}| \to 0$ but $|j_{z>,max}| \to \infty$. For $\nu_{in>} \to 0$, both $|E_{z>,max}| \to \infty$ and $|j_{z>,max}| \to \infty$.

APPENDIX G

ASYMPTOTIC FORMS OF THE FLUTE SOLUTION AND APPLICATIONS

The quantitative solution of (3.21) indicates that the flute approximation can provide accurate estimates for the eigenvalues (i.e., frequencies) for large perpendicular wave numbers. In this appendix (3.36) and (3.37) are used to derive relevant expressions for the perpendicular wave number where the real part of the frequency is equal to the growth rate (i.e., k_t) and the perpendicular wave number appropriate to zero growth rate (i.e., k_s). Hence, k_t is determined by the condition

$$\mathrm{Re}(\omega_f) = \mathrm{Im}(\omega_f) \tag{G1}$$

while k_s is determined by the condition

$$0 = \mathrm{Im}(\omega_f) \quad . \tag{G2}$$

Throughout this appendix, the dependence of ω_f on $k_\perp$ and z is suppressed for brevity of notation.

In the strongly driven limit,

$$\omega_o, \omega_i^* \gg \nu_i, \nu_c \quad . \tag{G3}$$

Equation (G3) is most likely to be satisfied in early or intermediate times following a high-altitude nuclear explosion. The combination of (3.36), (3.37), and (G3) gives

$$\mathrm{Re}(\omega_f) \approx \frac{\omega_o}{2} \tag{G4a}$$

$$\mathrm{Im}(\omega_f) \approx \left(\frac{\omega_o \omega_i^*}{\lambda_i} - \frac{\omega_o^2}{4} \right)^{1/2} \quad . \tag{G4b}$$

From (G1) and (G2), it follows that

$$k_t \approx \left(\frac{2\Omega_i}{L_\perp u_{ioy}}\right)^{1/2} \tag{G5a}$$

$$k_s \approx (2)^{1/2} k_t \quad . \tag{G5b}$$

Hence, k_s is a factor of $(2)^{1/2}$ larger than k_t, irrespective of plasma parameters.

The limit, when ion-neutral collisional effects and ion-viscous effects are significant, is important for late-time phenomenology. If

$$\nu_i \gg |\omega_f| \, , \, |\omega_o| \, , \, |\omega_i^*| \, , \, \nu_c \tag{G6}$$

then (3.36) and (3.37) give

$$\mathrm{Re}(\omega_f) \approx \omega_i^* + \frac{\omega_o^2 \omega_i^*}{\nu_i^2 \lambda_i} \tag{G7a}$$

$$\mathrm{Im}(\omega_f) \approx \frac{\omega_o \omega_i^*}{\lambda_i \nu_i} - \nu_c \quad . \tag{G7b}$$

The first and second terms on the right-hand side of (G7a) require the appropriate consideration of ion-neutral diffusion and ion inertia, respectively. The first term on the right-hand side of (G7b) is the maximum growth rate in the collisional limit [cf. (3.5)]. The second term is a result of the stabilizing role played by ambipolar diffusion.

If the contribution of ion-viscosity to ν_i is small relative to the contribution of ion-neutral collisions, i.e.,

$$\nu_i \approx \nu_{in} \gg k_\perp^2 \theta_v \tag{G8}$$

then

$$k_t = -\zeta_1 + (\zeta_1^2 + \zeta_2^2)^{1/2} \tag{G9a}$$

$$k_s = \zeta_2 \quad . \tag{G9b}$$

In (G9a)

$$\zeta_1 = \frac{1}{2}\left(\frac{\kappa_B T_{io}}{m_i \Omega_i L_\perp D_c} + \frac{\Omega_i u_{ioy}^2}{L_\perp \nu_{in}^2 D_c}\right) \quad , \quad \zeta_2^2 = \frac{\Omega_i u_{ioy}}{L_\perp \nu_{in} D_c} \tag{G10}$$

If $\zeta_1^2 \ll \zeta_2^2$ then (G9a) reduces to

$$k_t \approx k_s \quad . \tag{G11}$$

Equation (G11) implies that the real part of the frequency tends to be small compared to the maximum growth rate, $\omega_o \omega_i^*/\lambda_i \nu_{in}$. If $\zeta_1^2 \gg \zeta_2^2$, then (G9a) reduces to

$$k_t = \frac{e|\vec{g}_e|}{\nu_{in} \kappa_B T_{io}} \quad . \tag{G12}$$

This value for k_t is much smaller than k_s and indicates that the real part of the frequency can be comparable to or larger than the maximum growth rate, $\omega_o \omega_i^*/\lambda_i \nu_{in}$. Equation (G12) is precisely what would be obtained in a static situation if an ambipolar electric field of strength, $|\vec{g}_e|/\nu_{in}$, were to be balanced by an ion-pressure gradient. Sperling and Glassman [1983] show that (G12) provides a better estimate for k_t than (G11) for spread-F and barium clouds.

If the major contribution to the effective ion-collision frequency is from ion viscosity rather than from ion-neutral collisions, then

$$\nu_i \approx k_\perp^2 \theta_v \gg \nu_{in} \quad . \tag{G13}$$

Sufficiently large values for $k_\perp$ are required for (G13) to be valid. From (G2) and (G7b) it then follows that

$$k_s \approx \left(\frac{\Omega_i u_{ioy}}{L_\perp \theta_v D_c}\right)^{1/4} \quad . \tag{G14}$$

If $\nu_c \gg \omega_i^*$, then (G1) and (G7a-b) give

$$k_t \approx \left(\frac{\Omega_i u_{ioy}}{L_\perp \theta_v D_c}\right)^{1/4} \quad . \tag{G15}$$

The expressions for k_s and k_t in (G14) and (G15) are equal because the characteristic growth rate, $\omega_o \omega_i^*/\lambda_i \nu_i$, is much larger than $\mathrm{Re}(\omega)$ ($\cong \omega_i^*$). If $\nu_c \ll \omega_i^*$, then (G1) and (G7a-b) give

$$k_t \approx \left(\frac{m_i \Omega_i^2 u_{ioy}}{\kappa_B T_{io} \theta_v}\right)^{1/3} \quad . \tag{G16}$$

When (G16) is appropriate, k_s is substantially smaller than k_t and $\mathrm{Re}(\omega)$ ($\cong \omega_i^*$) can be much larger than the characteristic growth rate, $\omega_o \omega_i^*/\lambda_i \nu_i$.

In general, $k_t \approx k_s$ when $\nu_c \gg \omega_i^*$ and the real part of the frequency is unimportant. However, $k_t \ll k_s$ when $\nu_c \ll \omega_i^*$. The real part of ω then gives a significant contribution to k_t.

The various approximate expressions described in this appendix (for ω, k_t, and k_s) are summarized in Tables G1, G2, and G3.

Table G1. Various asymptotic expressions for ω_f as deduced from (3.36) and (3.37).

Expression	Criteria for Validity
Strongly Driven $\omega_f = \frac{k_\perp u_{ioy}}{2} + i\left[\frac{\Omega_i u_{ioy}}{L_\perp} - \left(\frac{k_\perp u_{ioy}}{2}\right)^2\right]^{1/2}$	$k_\perp \gg \frac{\nu_{in}}{u_{ioy}}$, $\frac{\nu_{in}\Omega_i L_\perp}{v_i^2}$ $k_\perp \ll \frac{u_{ioy}}{\theta_v}$, $\frac{u_{ioy}}{D_c}$, $\frac{v_i^2}{\Omega_i L_\perp \theta_v}$, $\frac{v_i^2}{\Omega_i L_\perp D_c}$
Collisional $\omega_f = k_\perp\left(\frac{v_i^2}{\Omega_i L_\perp} + \frac{u_{ioy}^2 \Omega_i}{L_\perp \nu_{in}^2}\right) + i\left(\frac{\Omega_i u_{ioy}}{L_\perp \nu_{in}} - k_\perp^2 D_c\right)$	$\nu_{in}^2 \gg \frac{\Omega_i u_{ioy}}{L_\perp}$ $\nu_{in} \gg k_\perp^2 \theta_v$
Ion Viscosity Dominated $\omega_f = k_\perp \frac{v_i^2}{\Omega_i L_\perp} + k_\perp^{-3} \frac{u_{ioy}^2 \Omega_i}{L_\perp \theta_v^2} + i\left(\frac{\Omega_i u_{ioy}}{L_\perp \theta_v k^2} - k_\perp^2 D_c\right)$	$k_\perp \gg \left(\frac{\Omega_i u_{ioy}}{L_\perp \theta_v^2}\right)^{1/4}$ $\nu_{in} \ll k_\perp^2 \theta_v$

Table G2. Asymptotic expressions for k_t as determined from (G1) in Appendix G. Expressions (2a) and (2b) are appropriate asymptotic forms of Expression (2).

Expression	Criteria for Validity
1. $k_t = \left(\frac{2\Omega_i}{L_\perp u_{ioy}}\right)^{1/2}$	$k_t \gg \frac{\nu_{in}}{u_{ioy}}$, $\frac{\nu_{in}\Omega_i L_\perp}{v_i^2}$ $k_t \ll \frac{u_{ioy}}{\theta_v}$, $\frac{u_{ioy}}{D_c}$, $\frac{v_i^2}{\Omega_i L_\perp \theta_v}$, $\frac{v_i^2}{\Omega_i L_\perp D_c}$
2. $k_t = -d + \left[d^2 + \frac{\Omega_i u_{ioy}}{L_\perp \nu_{in} D_c}\right]^{1/2}$ where $d = \frac{v_i^2}{\Omega_i L_\perp D_c} + \frac{\Omega_i u_{ioy}^2}{L_\perp D_c \nu_{in}^2}$	$\nu_{in}^2 \gg \frac{\Omega_i u_{ioy}}{L_\perp}$ $\nu_{in} \gg k_t^2 \theta_v$
2a. $k_t = \left(\frac{\Omega_i u_{ioy}}{L_\perp \nu_{in} D_c}\right)^{1/2}$	if $k_t \gg \frac{v_i^2}{\Omega_i L_\perp D_c}$
2b. $k_t = \left[\frac{v_i^2 \nu_{in}}{\Omega_i^2 u_{ioy}} + \frac{u_{ioy}}{\nu_{in}}\right]^{-1}$	if $k_t \ll \frac{v_i^2}{\Omega_i L_\perp D_c}$

Table G2. -(Continued)

Expression	Criteria for Validity
3. $k_t = \left(\frac{\Omega_i u_{ioy}}{L_\perp D_c \theta_v}\right)^{1/4}$	$\nu_{in} \ll k_t^2 \theta_v$ $k_t \gg \frac{\nu_i^2}{\Omega_i L_\perp D_c}$, $\left(\frac{\Omega_i u_{ioy}}{L_\perp \theta_v^2}\right)^{1/4}$
4. $k_t = \left(\frac{\Omega_i^2 u_{ioy}}{\nu_i^2 \theta_v}\right)^{1/3}$	$\nu_{in} \ll k_t^2 \theta_v$ $\left(\frac{\Omega_i u_{ioy}}{L_\perp \theta_v^2}\right)^{1/4} \ll k_t \ll \frac{\nu_i^2}{\Omega_i L_\perp D_c}$

Table G3. Asymptotic expressions for k_s as determined from (G2) in Appendix G.

Expression	Criteria for Validity
1. $k_s = 2\left(\frac{\Omega_i}{L_\perp u_{ioy}}\right)^{1/2}$	$k_s \gg \frac{\nu_{in}}{u_{ioy}}$, $\frac{\nu_{in}\Omega_i L_\perp}{v_i^2}$ $k_s \ll \frac{u_{ioy}}{\theta_v}$, $\frac{u_{ioy}}{D_c}$, $\frac{v_i^2}{\Omega_i L_\perp \theta_v}$, $\frac{v_i^2}{\Omega_i L_\perp D_c}$
2. $k_s = \left(\frac{\Omega_i u_{ioy}}{L_\perp \nu_{in} D_c}\right)^{1/2}$	$\nu_{in}^2 \gg \frac{\Omega_i u_{ioy}}{L_\perp}$ $\nu_{in} \gg k_s^2 \theta_v$
3. $k_s = \left(\frac{\Omega_i u_{ioy}}{L_\perp \theta_v D_c}\right)^{1/4}$	$k_s \gg \left(\frac{\Omega_i u_{ioy}}{L_\perp \theta_v^2}\right)^{1/4}$ $\nu_{in} \ll k_s^2 \theta_v$

APPENDIX H

NUMERICAL INVESTIGATION OF THE RELATIVE IMPORTANCE OF VARIOUS ION DRIFTS ON STRUCTURING

To evaluate the relative importance of ion-Pedersen drifts and the combination of ion-gravity and ion-curvature drifts on possible structuring during late-times following a high-altitude nuclear burst, a fifth case is specified in Table 3.2. The table shows that Case 5 differs from Case 1 in that Case 5 neglects ion-gravity and ion-curvature drifts and so only ion-Pedersen drifts in the ionosphere can cause structuring instabilities. Case 1 includes ion-gravity, ion-curvature, and ion-Pedersen drifts. For Case 1, instability can be driven at high as well as low altitude. Of the two cases, Case 1 is clearly more realistic than Case 5.

Figures 3.3a and H1a are plots of $|E_{1y}|/k_\perp$ versus z (km) for Cases 1 and 5, respectively. Curves are shown in the figures for different $k_\perp$ (km^{-1}). As in the nonnuclear examples of Sperling and Glassman [1983], the striation eigenmodes become more localized along the geomagnetic field as the perpendicular wave number becomes larger. Ion-polarization currents are essential to the localization at higher altitudes where ion-Pedersen currents are negligible [Sperling, 1983e]. Evidently, in late-time HANE plasmas, localized disturbances along the geomagnetic field generally lead to a localized response and so the geomagnetic-field lines are not equipotentials. The major qualitative difference between Figures 3.3a and H1a is the tendency for the maximum value of $|E_{1y}|/k_\perp$ to occur at lower altitudes in Figure H1a and at higher altitudes in Figure 3.3a. This suggests that ion-Pedersen drifts are not always the primary drivers of instability in nuclear plumes. Rather, the ion-gravity and ion-curvature drifts at altitudes above the neutral atmosphere can be the major drivers of instability. This is verified by Figure H1b which is a plot of ω (s^{-1}) versus $k_\perp$ (km^{-1}) for both Cases 1 and 5. Figure H1b shows that growth rates for Case 1 are larger than those for Case 5 for all perpendicular wave numbers except right near stability. Indeed the growth rates for Case 1 are larger than the maximum possible growth rate for Case 5 (i.e., γ_0 in Table 3.2), for $1\ km^{-1} < k_\perp < 14\ km^{-1}$.

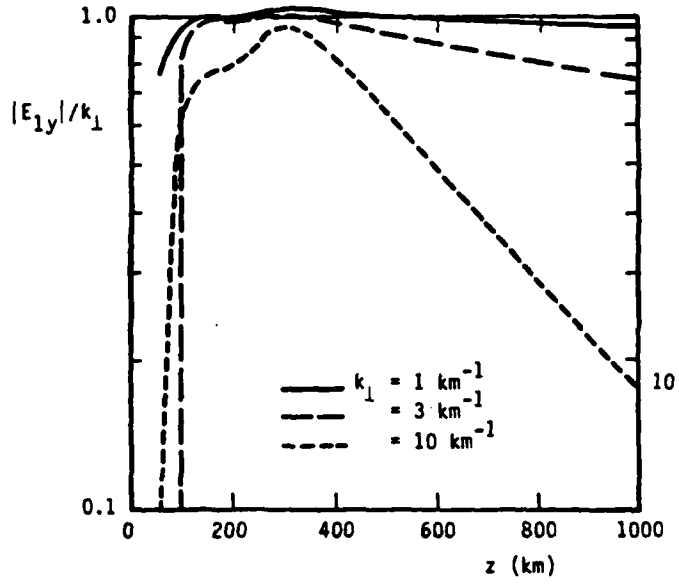

Figure H1a. $|E_{1y}|/k_\perp$ versus z (km) for various $k_\perp$ (km^{-1}) and Case 5. Each of the curves are in normalized dimensionless units.

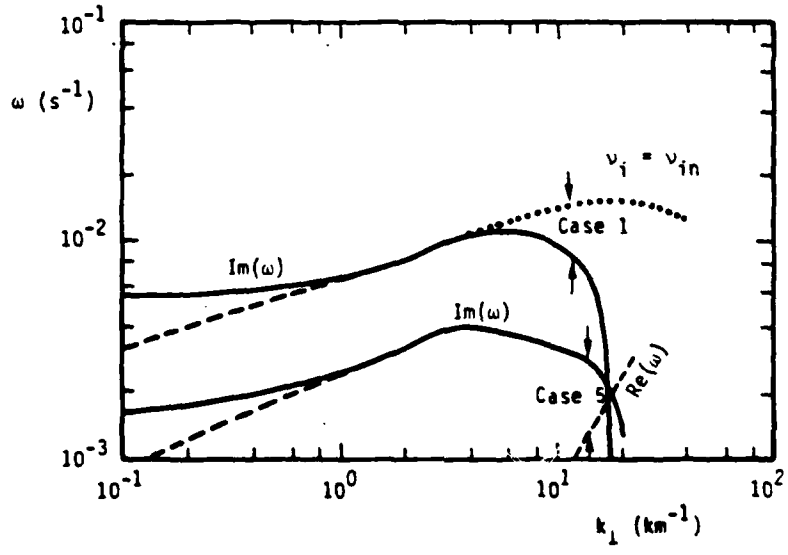

Figure H1b. ω(s^{-1}) versus $k_\perp$ (km^{-1}) for Cases 1 and 5. The dashed line shows the appropriate eigenvalues with the neglect of electromagnetic effects. The dotted line shows the eigenvalues for Case 1 neglecting viscosity.

The dashed lines in Figure H1b are the growth rates obtained when electromagnetic effects are neglected. In agreement with the nonnuclear examples of Sperling and Glassman [1983], the neglect of electromagnetic effects results in reduced growth rates for smaller values of $k_\perp$. Evidently, electromagnetic effects hinder electrostatic short-circuiting of the instability [Sperling, 1983e]. When electromagnetic effects are important, the growth rate is a relatively weak function of $k_\perp$. Indeed, our numerical results also indicate that $|E_{1y}|/k_\perp$ is a weak function of $k_\perp$ when electromagnetic effects are important (see Figures 3.3a and H1a).

For both cases, ion viscosity is considered and contributes to the curves indicated by the solid and dashed lines in Figure H1b. For Case 1, eigenvalues have also been calculated neglecting ion viscosity. The results are indicated by the dotted line in Figure H1b. It is clear that ion viscosity plays a vital role in structuring for larger values of $k_\perp$. Equations (G14) and (G15) in Appendix G are the relevant asymptotic expressions for k_s and k_t, respectively. Figure H1b verifies that $k_t \approx k_s$.

DISTRIBUTION LIST

DEPARTMENT OF DEFENSE

Defense Nuclear Agency
ATTN: NATF
ATTN: NAWE
ATTN: RAAE, P. Lunn
ATTN: RAAE, K. Schwartz
ATTN: RAEE
ATTN: STNA
3 cy ATTN: RAAE
4 cy ATTN: STTI-CA

Defense Technical Information Ctr
12 cy ATTN: DD

DEPARTMENT OF THE ARMY

BMD Advanced Technology Ctr
ATTN: ATC-O, W. Davies
ATTN: ATC-R, D. Russ
ATTN: ATC-R, W. Dickinson
ATTN: ATC-T, M. Capps

BMD Systems Command
ATTN: BMDSC-LEE, R. Webb
2 cy ATTN: BMDSC-HW

DEPARTMENT OF THE NAVY

Naval Research Laboratory
ATTN: Code 4700, S. Ossakow
ATTN: Code 7500, B. Wald
ATTN: 4720, J. Davis
ATTN: 4108, E. Szuszewicz
ATTN: Code 6700
ATTN: Code 4700
ATTN: Code 4780
ATTN: Code 4187
ATTN: Code 7950, J. Goodman

DEPARTMENT OF THE AIR FORCE

Air Force Geophysics Lab
ATTN: CA, A. Stair
ATTN: LIS, J. Buchau
ATTN: LYD, K. Champion
ATTN: OPR, H. Gardiner
ATTN: OPR-1
ATTN: R. Babcock
ATTN: R. O'Neil

Air Force Weapons Laboratory
ATTN: NTN
ATTN: SUL

Air Force Wright Aeronautical Lab
ATTN: A. Johnson
ATTN: W. Hunt

DEPARTMENT OF ENERGY CONTRACTORS

Sandia National Laboratories
ATTN: D. Dahlgren
ATTN: D. Thornbrough
ATTN: Org 1231, R. Backstrom
ATTN: Org 1250, W. Brown
ATTN: Org 4231, T. Wright
ATTN: Space Project Div
ATTN: Tech Lib 3141

DEPARTMENT OF ENERGY CONTRACTORS (Continued)

Los Alamos National Laboratories
ATTN: D. Sappenfield
ATTN: D. Simons
ATTN: G-6, E. Jones
ATTN: J. Hopkins
ATTN: J. Wolcott
ATTN: MS 664, J. Zinn
ATTN: R. Jeffries
ATTN: T. Kunkle, ESS-5

DEPARTMENT OF DEFENSE CONTRACTORS

Berkeley Rsch Associates, Inc
ATTN: C. Prettie
ATTN: J. Workman
ATTN: S. Brecht

EOS Technologies, Inc
ATTN: B. Gabbard
ATTN: W. Lelevier

JAYCOR
2 cy ATTN: A. Glassman
2 cy ATTN: J. Sperling

Kaman Tempo
ATTN: B. Gambill
ATTN: DASIAC
ATTN: W. McNamara

Kaman Tempo
ATTN: DASIAC

Maxim Technologies, Inc
ATTN: E. Tsui
ATTN: J. Marshall
ATTN: R. Morganstern

Mission Research Corp
ATTN: C. Lauer
ATTN: D. Knepp
ATTN: F. Fajen
ATTN: F. Guigliano
ATTN: G. McCartor
ATTN: R. Bigonj
ATTN: R. Bogusch
ATTN: R. Dana
ATTN: R. Hendrick
ATTN: R. Kilb
ATTN: S. Gutsche
ATTN: Tech Library

Pacific-Sierra Research Corp
ATTN: H. Brode, Chairman SAGE

Physical Dynamics, Inc
ATTN: E. Fremouw
ATTN: J. Secan

Physical Research, Inc
ATTN: K. Schueter
ATTN: R. Deliberis
ATTN: T. Stephens

R&D Associates
ATTN: B. Yoon

DEPARTMENT OF DEFENSE CONTRACTORS (Continued)

Physical Research, Inc
ATTN: J. Devore
ATTN: J. Thompson

R&D Associates
ATTN: C. Greifinger
ATTN: F. Gilmore
ATTN: G. St. Cyr
ATTN: H. Ory
ATTN: M. Gantsweg
ATTN: R. Turco
ATTN: W. Karzas
ATTN: W. Wright
ATTN: P. Haas

R&D Associates
ATTN: G. Ganong

Rand Corp
ATTN: E. Bedrozian

Science Applications, Inc
ATTN: C. Smith
ATTN: D. Hamlin
ATTN: D. Sachs
ATTN: E. Straker
ATTN: L. Linson

TRW Electronics & Defense Sector
ATTN: R. Plebuch

DEPARTMENT OF DEFENSE CONTRACTORS (Continued)

SRI International
ATTN: A. Burns
ATTN: C. Rino
ATTN: D. McDaniels
ATTN: D. Neilson
ATTN: G. Price
ATTN: G. Smith
ATTN: J. Petrickes
ATTN: J. Vickrey
ATTN: M. Baron
ATTN: R. Leadabrand
ATTN: R. Livingston
ATTN: R. Tsunoda
ATTN: V. Gonzales
ATTN: W. Chesnut
ATTN: W. Jaye

Toyon Research Corp
ATTN: J. Garbarino
ATTN: J. Ise

Visidyne, Inc
ATTN: C. Humphrey
ATTN: H. Smith
ATTN: J. Carpenter
ATTN: O. Shepard
ATTN: W. Reidy

END

FILMED

8-85

DTIC